LASER EXCITED FLUORESCENCE AND IONIZATION FOR FLAME DIAGNOSTICS

BY

MICHAEL JAMES RUTLEDGE

A DISSERTATION PRESENTED TO THE GRADUATE SCHOOL
OF THE UNIVERSITY OF FLORIDA IN
PARTIAL FULFILLMENT OF THE REQUIREMENTS
FOR THE DEGREE OF DOCTOR OF PHILOSOPHY

UNIVERSITY OF FLORIDA

1987

To my parents and family,

whose unending support made all this possible.

ACKNOWLEDGMENTS

I gratefully acknowledge the support of Dr. Benjamin Smith, Dr. Edward Voigtman, and Dr. Nicolo Omenetto whose knowledge, enthusiasm, and helpful suggestions were a continuing source of inspiration.

I thank Dr. James D. Winefordner for the privilege of working with him for the past four years and with the best spectroscopy group in the world. His concern and encouragement during my four years have made my work more pleasurable and an invaluable learning experience.

My sincerest thanks go to Jeanne Karably and the secretaries of J.D. Winefordner. They have been my constant friends for the past 4 years.

I also thank the members of other research groups in the analytical department especially Ken Matuszak, Paul McCaslin, and David Berberich whose help with my golf game may prove invaluable.

TABLE OF CONTENTS

Page

ACKNOWLEDGMENTS.....iii

LIST OF TABLES.....vi

LIST OF FIGURES.....vii

ABSTRACT.....ix

CHAPTERS

1 INTRODUCTION.....1

2 MEASUREMENT APPROACHES FOR ATOMIC FLUORESCENCE AND IONIZATION SPECTROSCOPIES.....4

Introduction to Laser Atomic Fluorescence Spectroscopy and Laser Enhanced Ionization Spectroscopy Systems.....4
Measurement Approaches and Instrumentation.....10
Results and Discussion.....17
Conclusions.....25

3 ESTIMATION OF ABSOLUTE NUMBER DENSITIES.....27

General Curve of Growth Introduction and Evaluation.....27
Calculated Curves of Growth.....33
Experimental Verification of Curves of Growth.....43
Saturation and Collisional Effects.....46
Conclusions.....62

4 SPATIAL DISTRIBUTIONS OF ATOMS IN INHOMOGENEOUS FLAMES.....63

Concentration Modulated Absorption Spectroscopy.....63
Two-Wavelength Laser Enhanced Ionization and Fluorescence: Spatial Distributions.....76
Experimental Setup and Discussion.....78
Conclusions.....89

5 FINAL COMMENTS AND FURTHER STUDIES.....91

APPENDICES

A GLOSSARY OF TERMS AND SYMBOLS.....94

B COMPUTER PROGRAM LISTING FOR CALCULATION OF FLUORESCENCE CURVES OF GROWTH INCLUDING SATURATION, COLLISIONAL AND PREFILTER AND POSTFILTER EFFECTS.....96

REFERENCES.....109

BIOGRAPHICAL SKETCH.....113

LIST OF TABLES

Table		Page
2-1	Limits of Detection (ng/mL)	18
3-1	Broadening Effects on the a-Parameter for Self-Broadening	50
4-1	Ionization Processes, Optical Arrangements, Signals and Noises for Two-Wavelength Laser Enhanced Ionization Spectroscopy	85

LIST OF FIGURES

Figure		Page
2-1	Lasing Diagram for Copper Vapor Laser	5
2-2	Experimental Setup	8
2-3	Boxcar Plus Lock-In Amplifier Signal Processing Layout	11
2-4	Boxcar-Active Baseline Subtraction Signal Processing Layout	14
2-5	Bandwidth Limitation and Conventional Signal Processing Layout	16
2-6	Bandwidth Limitation Effects	21
2-7	Noise Power Spectrum at 588.9 nm	24
3-1	Diagram for Right Angle Fluorescence	28
3-2	Expression for Right Angle Fluorescence	29
3-3	Curves of Growth for Line Source Excitation	34
3-4	Curves of Growth for Continuum Source Excitation	35
3-5	Curves of Growth for Two Pseudocontinuum Sources	37
3-6	Curves of Growth for Mild, Medium, and Severe Prefiltering--Line Source, Dark = prefilter region	38
3-7	Curves of Growth for Mild, Medium, and Severe Prefiltering--Continuum Source, Dark = prefilter region	39
3-8	Curves of Growth for Mild, Medium, and Severe Postfiltering--Line Source, Dark = prefilter region	41
3-9	Curves of Growth for Mild, Medium, and Severe Postfiltering--Continuum Source, Dark = prefilter region	42

3-10 Calculated and Experimental Curves of Growth for Na.....44

3-11 Calculated and Experimental Curves of Growth for Pb.....46

3-12 Expression for Collisional Broadening.....48

3-13 Curves of Growth with Added Collisional Broadening.....52

3-14 Curves of Growth for Several Intensities for a Line Source.....55

3-15 Curves of Growth for Several Intensities for a Continuum Source.....56

3-16 Curves of Growth for Pb Direct-Line (----) and Resonance (——) Fluorescence for Several Source Intensities.....57

3-17 Equations for Curves of Growth Equalities for Saturating Irradiances.....58

3-18 Prefilter Removal by a Saturating Source, Resonance (——) and Direct-Line (----).....60

3-19 Postfilter Effects with Saturation Effects Added, Resonance (——) and Direct-Line (----).....61

4-1 Concentration Modulated Absorption Experimental Setup: Co-linear Beams.....67

4-2 Experimental Setup for Spatial Diagnostics for COMAS.....69

4-3 Results for Perpendicular and Parallel Burners for COMAS.....71

4-4 Design of Surface Burner Used.....72

4-5 Simple Absorption Results for Perpendicular and Parallel Burners.....75

4-6 Experimental Setup for Two-Wavelength LEIS and LAFS.....79

4-7 Spatial Profile Result for LEIS.....82

4-8 Spatial Profile Result for LAFS.....88

4-9 Three-Dimensional Spatial Profile for LEIS.....90

Abstract of Dissertation Presented to the Graduate School
of the University of Florida in Partial Fulfillment of the
Requirements for the Degree of Doctor of Philosophy

LASER EXCITED FLUORESCENCE AND IONIZATION
FOR FLAME DIAGNOSTICS

BY

MICHAEL JAMES RUTLEDGE

May, 1987

Chairman: James D. Winefordner
Major Department: Chemistry

Measurement approaches involving electrical signal manipulation and signal processing are investigated for a copper vapor laser pumped dye laser system. Correction methods used involve modulation of a pulsed laser output and subtraction of noise. Bandwidth limitation of signals to reduce radio-frequency noise is also discussed. A general purpose computer program for calculation of the absolute number density of an atomic species present in an analytical volume is presented. The program is written in FORTRAN with a high-speed, high-precision approximation of the Voigt profile to incorporate atomic broadening effects. Comparison to experimentally measured fluorescence results is included.

A discussion of saturation and collisional broadening effects is included. Calculated results are found to agree with experimental results within an order of magnitude in all experimental cases. Spatial profiling results are presented for two-wavelength excitation

of atomic species with detection via fluorescence and ionization of the species of interest. A new form of absorption spectroscopy, termed concentration modulated absorption spectroscopy, is investigated for spatial profiling applications. These methods are investigated for detection power, as well as spatial information obtainable. Comparison to other methods of determining absolute number densities and spatial information is included.

CHAPTER 1
INTRODUCTION

Laser excited atomic fluorescence and laser enhanced ionization spectroscopies have been used for many different types of applications. The extreme sensitivity of these techniques has been shown many times.[1-3] Some of the best limits of detection are obtained using these methods. These sensitive techniques are applied here to the investigation of absolute number densities and spatial profiles in inhomogeneous flames.

A copper vapor laser is used for all investigations throughout these studies. This laser has found limited application in chemistry[4,5] but has found many applications outside this field.[6] This laser system consists of a pulsed laser plus the dye laser(s) for tunability to the wavelength(s) of interest. This is a pulsed laser which operates at a 6 kHz repetition rate with an average power of 25 W. Measurement approaches for atomic fluorescence and ionization are presented as preliminary investigations using this laser system in Chapter 2. These measurement approaches rely on bandwidth limitation and/or removal of correlated background noises. A more complete discussion of the use of correlation functions to increase signal-to-noise ratios is given by Doerffel et al.[7] The extension of these methods to measurement of atomic

fluorescence for determination of absolute number densities is discussed in Chapter 3.

Determination of absolute number densities is accomplished using a computer program to model the expected relationship between concentration of a species of interest and fluorescence signal detected. The relationship between fluorescence intensity and concentration, expressed in a log-log graph, is called a fluorescence curve of growth (COG). The point of departure from linearity allows determination of absolute number densities. Many methods have been presented for determination of absolute number densities in flames, plasmas and vapor cells. These methods range from the classical approaches of the absolute intensity method[8] and the integral absorption method[9,10] to some more recently introduced methods such as laser induced fluorescence saturation spectroscopy[11] and anomalous dispersion.[12] Several methods have also been presented which allow absolute number density evaluation from the absolute magnitude of the signal detected and the experimental detection efficiency.[13] Several COG methods have been presented which allow determination of absolute number densities with a minimal knowledge of the atomic and geometric parameters.[14] Other methods include determination of number densities from vapor pressure measurements of Na and Pb in laser excited fluorescence experiments.[15,16] Some of the simplest methods for evaluation of number density rely on the supply of and atomization efficiency of the analyte of interest. Experimentally, many of the above mentioned methods are quite difficult or time-consuming to implement. Many rely on an absolute calibration of the

detection optics and photodetector, while some require an additional calibrated source. Some methods require a detailed knowledge of the source characteristics including the source intensity and the spectral profile (Gaussian or otherwise). A general overview of many of these methods is given in two excellent works by Alkemade and coworkers.[13,17]

Atomic fluorescence with two-wavelength excitation and a multichannel image detector has been used for spatial imaging of OH and for flow visualization.[18-20] No research has been presented which utilizes two-wavelength excitation of atomic species for spatial resolution with direct detection using laser atomic fluorescence (LAFS) or laser enhanced ionization (LEIS) spectrometry. This topic and some related areas are the focus of Chapter 4. In a recent study by Turk et al.,[21] two-wavelength atomic spectra were measured with detection via ionization. In that study, only the wavelengths are scanned and the three-dimensional spectra are presented with axes of one wavelength (λ_1) and the other wavelength (λ_2) versus intensity. Here, the spatial distributions of atoms using two-wavelength LEIS and LAFS and single-wavelength absorption are investigated. An initial investigation into absorption spectroscopy with a modulated pulsed laser is included.

The absorption technique, termed concentration modulated absorption spectroscopy (COMAS), is investigated for increased sensitivity and spatial profiling applications. The highly sensitive techniques of LEIS and LAFS are applied to probing small volumes in inhomogeneous flames as a final study.

CHAPTER 2
MEASUREMENT APPROACHES FOR ATOMIC FLUORESCENCE AND IONIZATION SPECTROSCOPIES

Introduction to Laser Atomic Fluorescence Spectroscopy and Laser Enhanced Ionization Spectroscopy Systems

In these experiments, a 20 W copper vapor laser (Cooper Lasersonics model 251) and a flowing dye cell were used. This is a pulsed laser system operating at ~6 kHz with moderate peak powers of ~160 kW. Laser action in a cell containing copper vapor was first reported by Walter et al. in 1966.[22] Lasing action is accomplished via the thermal production of ground state copper atoms and electrical pumping of the ground state (^2S) to the lowest resonance levels (^2P) resulting in spectral output at 510 and 578 nm (see Figure 2-1). Repetition rates of between 800 and 10,000 pulses per second have been obtained in our laboratory. This high repetition rate is accomplished using a thyratron-switched power supply using ~4000 W of electrical power. This high-power, high-frequency switching produces a large amount of radio-frequency (RF) interference which was found to be a major noise source in all analytical experiments. From oscilloscope measurements and gate-scanned boxcar averager outputs, it was determined that the radio-frequency has a high degree of pulse-to-pulse correlation. Shielding of the detection electronics was attempted but was inefficient in the reduction of RF interference.

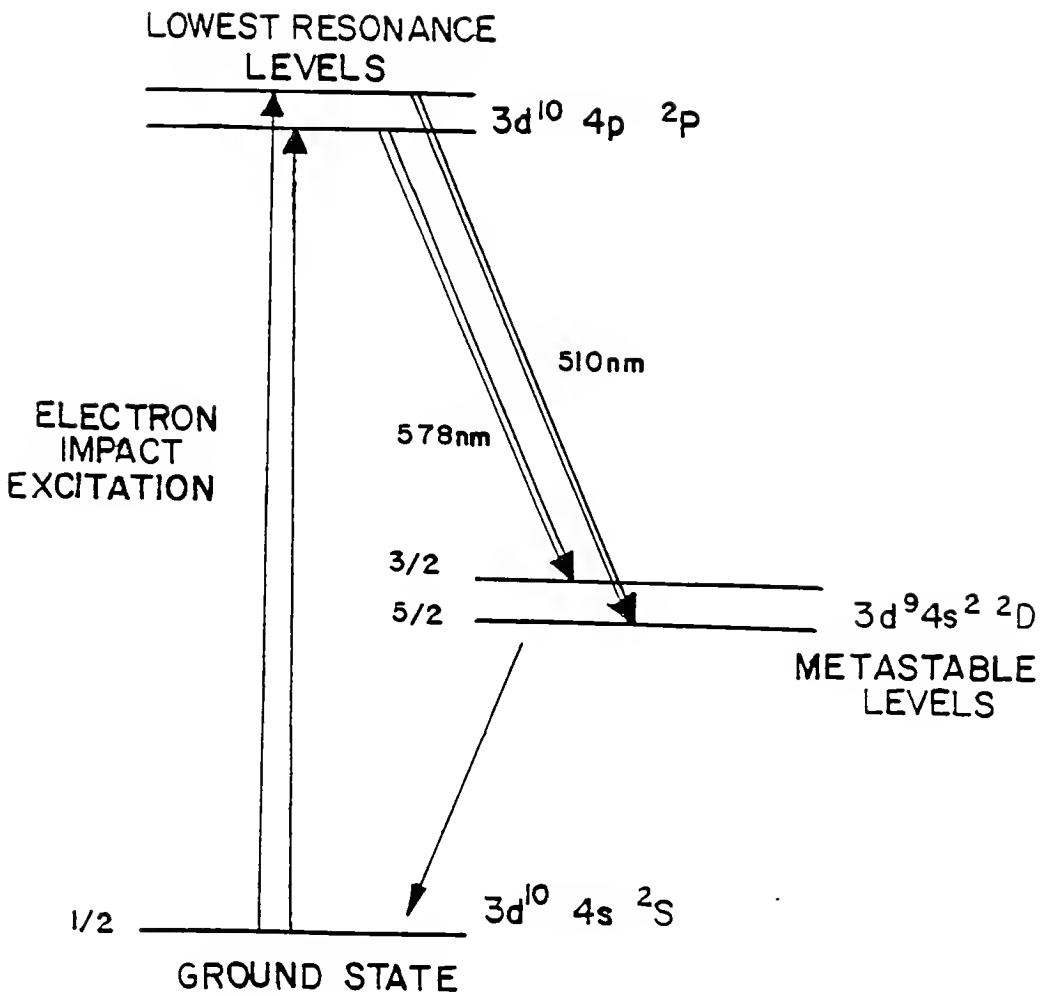

Figure 2-1. Lasing Diagram for Copper Vapor Laser

Three models were used to correct for and/or reduce background radio-frequency and other noise sources. Two methods rely on synchronization of the laser with a high-speed chopper to block alternate laser pulses. One of these methods involved the use of a gated integrator and boxcar averager equipped with an active baseline subtraction circuit. Another used a gated integrator and boxcar averager plus lock-in amplifier to accomplish the same background subtraction. The third method used a bandwidth limited amplifier to reduce high frequency noise components present in the signal. For comparison purposes, the conventional method of measuring pulsed laser signals is also included. Analysis for several elements is included to show consistency of the results.

Chemicals

Stock solutions of all elements were prepared from analytical grade LiCl, NaCl, Fe wire, and In_2O_3 to give 1000 µg/mL solutions. Standard solutions were prepared by serial dilution of the stock solutions. Laser dyes (Exciton Corporation) used included oxazine 720 (Li), and mixtures of Rhodamine 6G and Kiton Red 620 (In, Na, and Fe).

Instrumentation

The frequency-doubled dye laser output (Molectron model DLII pumped by a Cooper Lasersonics model 251 copper vapor laser with an Inrad Autotracker II frequency doubler) was used to illuminate a 1 cm^3 region of the flame. A flat mirror was mounted 5 cm from the flame to allow for a second pass of the laser. For frequency-doubled experiments, the laser had a pulse width of ~20 ns, a pulse energy of

5-35 μJ, and a spectral bandwidth of 0.02 nm. For experiments involving the fundamental wavelength of the dye laser, the frequency doubler was removed from the optical path. The fundamental wavelength experiments are characterized by a pulse width of 30 ns, a pulse energy of ~100-500 μJ, and a spectral line width of 0.03 nm. Pulse temporal widths were measured using a gate-scanned boxcar averager with a 2 ns risetime photomultiplier tube and a 2 ns boxcar gate. Additionally, line widths were measured by slowly scanning the dye laser across an atomic transition and measuring the fluorescence of a 1 μg/mL solution of the element aspirated into the flame. The flame was produced on a laboratory-constructed, brass capillary burner[23] (1 cm^2) mounted on a commercial atomic absorption spray chamber (Perkin Elmer model 303-0110). An approximately stoichiometric air-acetylene flame was used for all studies. Commercial-grade gases were pressure-regulated and flow controlled using rotometers with needle valves. The experimental setup is shown in Figure 2-2. Symbols are defined in Appendix A.

The fluorescence was produced in a flame volume of approximately 1 cm^3 and detected using a small monochromator (SPEX 1670 Minimate, f/4.0, 220 mm focal length) and RCA model 1414 photomultiplier tube. The monochromator optical axis was 90° to the laser beam. No additional optics were used since the acceptance angle of the monochromator was filled. With the 1.25 mm slits used, this monochromator had a 10 nm bandpass. The photocurrent pulse was stretched slightly by a 1000 Ω load resistor and connected directly to the input of the gated integrator and boxcar averager

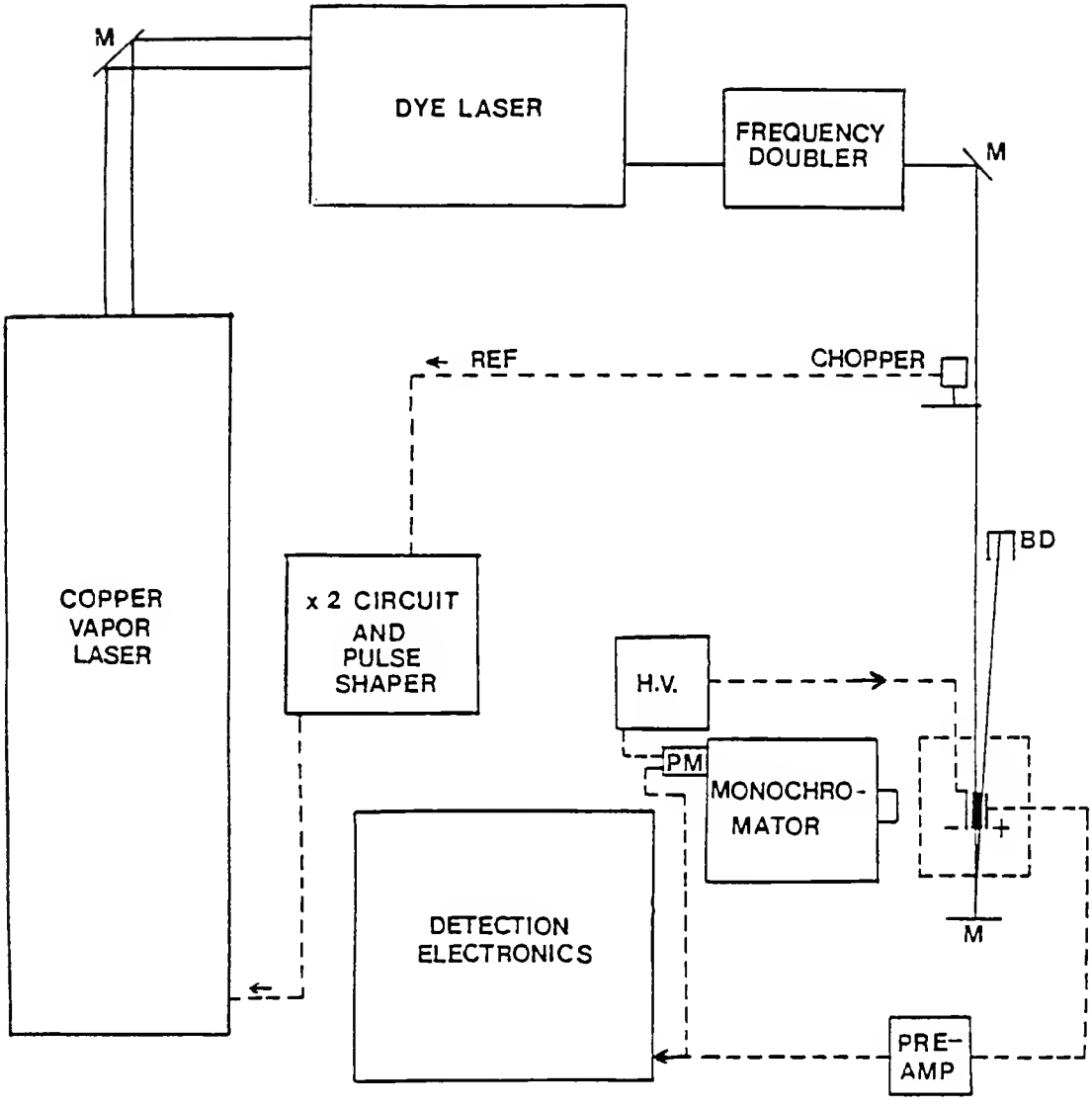

Figure 2-2. Experimental Setup

(Stanford Research Systems model 250). The boxcar was triggered using a photodiode positioned to receive a portion of the copper vapor 510 and 578 nm output.

The laser enhanced ionization experiments were performed similarly with the following exceptions. A 5 cm stainless steel slot burner (Perkin-Elmer model 0040-0277) was used and served as the detecting electrode. A -1500 V bias potential was applied to a water-cooled stainless steel electrode placed ~1 cm above the burner surface. The laser beam was positioned to pass parallel to and ~0.3 cm below the bias electrode. The entire assembly was placed inside a shielded and grounded housing. This experimental arrangement is a modification of that presented by Travis et al.[24] Ionization currents were capacitively coupled to reduce flame background leakage currents and then converted to voltages using a current-to-voltage converter (Princeton Applied Research model 181). Gains of 10^6 V/A were typically used. This signal was connected directly into the input of the gated integrator. For the boxcar plus lock-in amplifier portion of the experiments, the signals from the boxcar were connected directly into the input of the lock-in amplifier (Keithley model 840). Signals obtained in all experiments were integrated using a voltage-to-frequency converter (Analog Devices model 650) and counted for a 10 s integration period.[25] This method of signal integration was found to give an unambiguous result. Limits of detection were determined using the IUPAC convention,[26] namely, a signal-to-noise ratio equal to three. Noise levels were determined as the standard deviation of 16 blank

measurements. A more complete discussion of this and other methods for calculating limits of detection is covered by Long and Winefordner.[27]

Measurement Approaches and Instrumentation

Gated Integrator and Boxcar Averager Plus Lock-In Amplifier (BLIA)

This method of background correction is similar to background correction methods in flame absorption or fluorescence using a continuous wave (cw) laser or conventional source employing modulation of the source intensity. For a complete discussion of background correction methods, the reader is referred to the excellent works of Alkemade et al.[28] and Kirkbright and Sargent.[29]

In this experiment, a high speed chopper (Photon Technology) was used free-running at 3 kHz, and the reference output of the chopper was used to control the laser repetition rate. The reference from the chopper was connected to a multiply-by-two circuit constructed from a monostable multivibrator (74LS123) and an OR gate (74LS32). This circuit was set up to give a single pulse output from both the rising and falling edges of the chopper reference waveform. This signal was used to trigger the laser externally at a 6 kHz repetition rate. Initial attempts to control the high speed chopper from the laser reference output failed due to the momentum and drift of the chopper blade. Synchronization of the chopper had to be absolute since any drift resulted in a complete reversal of the signal polarity for at least a portion of the integration period. The electrical signal processing system is shown in Figure 2-3.

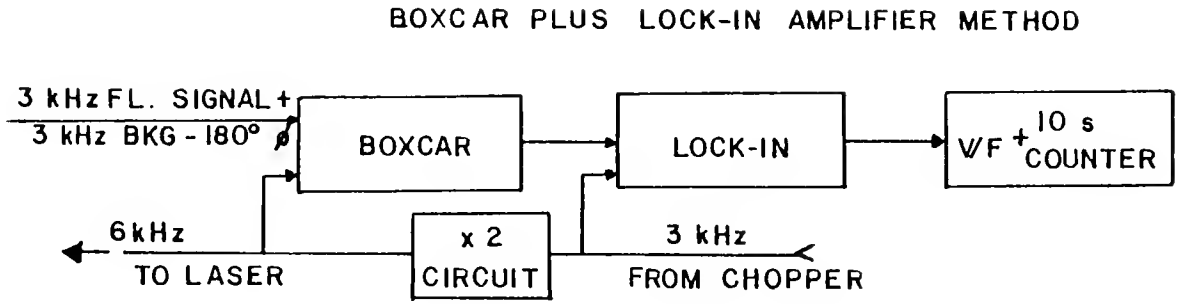

Figure 2-3. Boxcar Plus Lock-In Amplifier Signal Processing Layout

Signals obtained from the fluorescence or the photoionization were fed directly to the input of the gated integrator. The Stanford boxcar averager has two output signals, a last sample and an average sample. The average sample is useful for reduction of signal fluctuation and employs a gated resistor-capacitor low-pass (RC) filter to average a variable number of samples. The last-sample output is the most recent signal detected by the boxcar averager. The last-sample output was used in this instance because the signal varies between signal plus noise on one pulse and noise only on the following pulse, and the demodulation of this signal was accomplished in the lock-in amplifier. The last-sample output was connected directly to the input of the lock-in amplifier. The reference output of the high speed chopper was connected to the reference channel of the lock-in amplifier which was triggered at the 3 kHz repetition rate. Synchronization of the lock-in reference waveform and the boxcar signal is obtained using the phase adjustment on the reference channel of the lock-in amplifier. The output from the boxcar, which consisted of signal plus noise during one half-period and noise only during the following half-period, was demodulated and background was subtracted by the phase-sensitive detector in the lock-in amplifier. Output signal ripple of the phase-sensitive detector was smoothed using a 1 s time constant output filter. Signals output from the lock-in were connected directly to the voltage-to-frequency converter and then counted for a 10 s integration period.

Gated Integrator and Boxcar Averager: Active Baseline Subtraction (ABS)

This technique was a special method applicable only to the Stanford Research Systems boxcar used here or similar systems with an active baseline subtraction method. In this method, the same signals were connected to the boxcar, but the boxcar was placed in the active baseline subtraction mode (ABS). This mode caused the electronics in the boxcar to switch the polarity of alternating samples before adding each one to a moving average. The moving average circuit was implemented using a gated RC filter[30] with varying resistors and capacitors depending on the number of samples to be averaged. This method of correction is significantly different from the true phase-sensitive detection methods employed in lock-in amplifiers. The moving average switch was set at 3000 samples to keep an effective 1 s time constant, consistent with the lock-in amplifier case (BLIA). Blocking alternating laser pulses resulted in a subtraction of noise produced during each laser pulse. Signal output from the boxcar averager was connected directly to a frequency-to-voltage converter and counted for a 10 s integration period. This is shown diagrammatically in Figure 2-4.

Bandwidth Limited Signal Processing (BLSP)

Another method of diminishing the effect of high frequency noise was investigated using a form of low-pass filtering. This "low-pass filtering" was implemented using a bandwidth-limited amplifier. Fluorescence photocurrents (~25 ns) were stretched and converted to voltages using a 1 kΩ resistor giving a signal of approximately

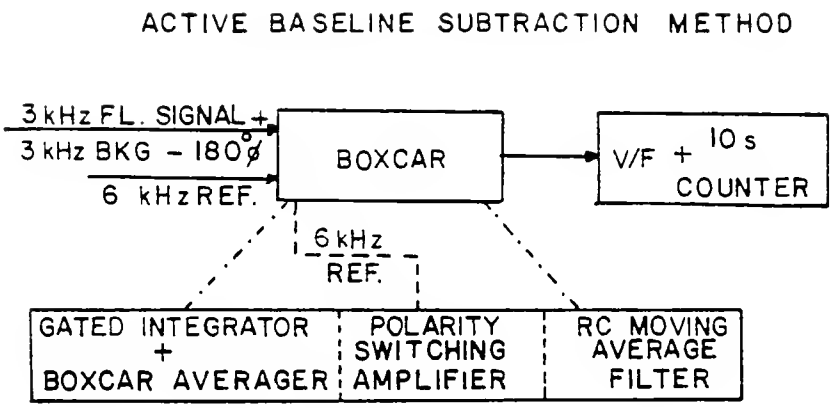

Figure 2-4. Boxcar-Active Baseline Subtraction Signal Processing Layout

100 ns full width at half maximum (FWHM), i.e., a bandwidth of ~10 MHz. Stretching occurred due to the RC time constant of the photomultipler tube and connecting cables, due to the load resistor and the stray capacitance in the system. The fluorescence signals obtained were input to the bandwidth-limited amplifier and then connected directly to the gated integrator and boxcar averager. The amplifier used, an Evans model 4131, has a 3 dB bandwidth of 10 MHz at a gain of 10 times. Signals were stretched to approximately 120 ns (FWHM) by the Evans amplifier. The decreased response of the amplifier in the high frequency region resulted in a significant reduction of high frequency noise components. Actual low-pass filtering would be difficult to implement since a time constant on the order of 10 ns would be necessary to avoid significant signal distortion. Stray capacitance and resistance make this low time constant difficult to obtain. Signals from the Evans amplifier were connected directly to the gated integrator and boxcar averager. Signals from the boxcar were connected to a voltage-to-frequency converter and counted for a 10 s integration period as in all other cases. The electrical system is shown in Figure 2-5 along with the conventional method for measuring signals.

Conventional Method (CONV)

Signals obtained from fluorescence and photoionization were input directly into the gated integrator with no modifications. This method is included for comparison purposes as a reference.[31] The signal output from the boxcar averager was connected to the voltage-to-frequency converter and the signal was counted for a 10 s

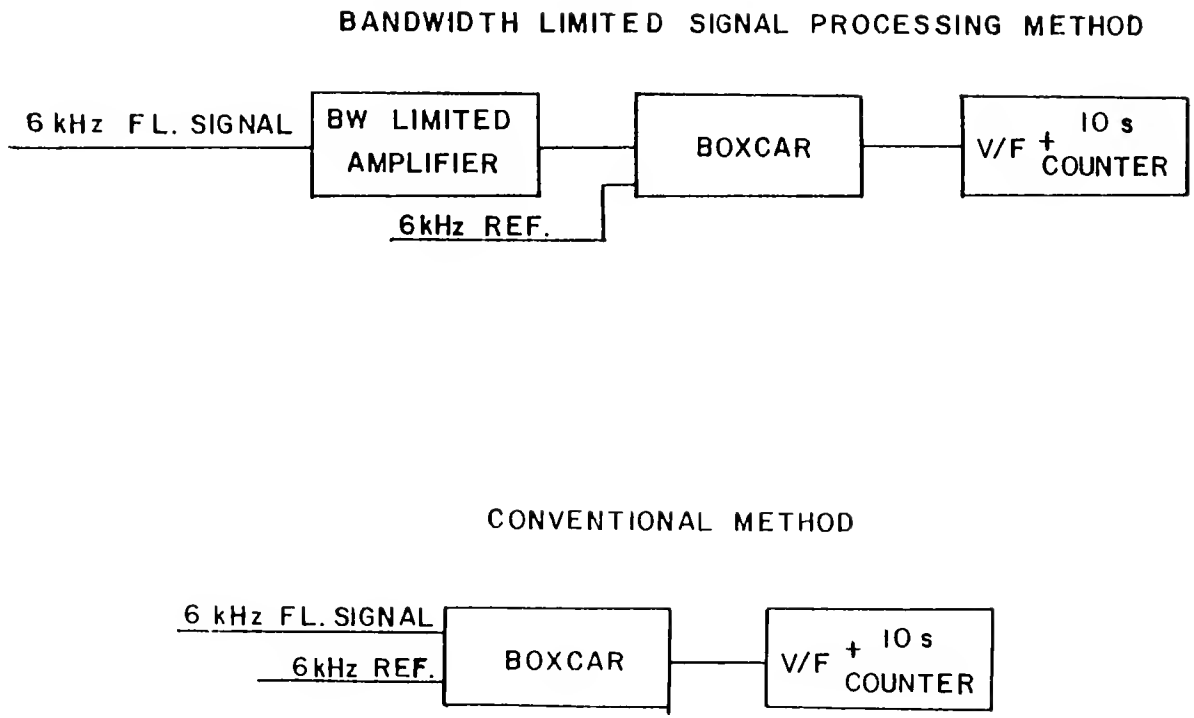

Figure 2-5. Bandwidth Limitation and Conventional Signal Processing Layout

period. In all four measurement methods, the boxcar averager was operated with a 10 kHz first-order cutoff filter on the input to help remove unwanted low frequency components.

Results and Discussion

All correction methods used show a significant improvement over the conventional method (Table 2-1). While no attempt was made to optimize fully system components or operating conditions, the limits of detection obtained are very good and demonstrate the improvements expected. Laser power was found to present a severe problem when frequency doubling the copper vapor laser (CVL) dye laser output. The relatively low peak power and squared dependence of frequency doubling on input power[32] resulted in low power outputs for In and Fe. The low laser power is partially compensated for (in limits of detection) by the lack of laser scatter and the associated shot noise in the direct-line fluorescence of Fe and In. Compromises concerning excitation wavelengths had to be made since the CVL fundamental output is in the visible region at 510 and 578 nm. Additionally, RF interference from this laser was and has been found to limit severely its analytical applicability for laser enhanced ionization and fluorescence.[33]

The simplicity and nearly equivalent results obtained using the bandwidth limitation scheme (BW) for signal processing make this the processing method of choice for most applications. As seen in Table 2-1, results obtained using the bandwidth limited approach for fluorescence are nearly equivalent to those obtained using

Table 2-1. Limits of Detection (ng/mL).

	CONV[a]	ABS[b]	BLIA[c]
Copper Vapor Dye Laser			
Laser Enhanced Ionization Detection			
Li	2.0	0.3	0.1
Fe	30	5.0	2.0
In	4.0	0.6	0.2
Laser Excited Fluorescence Detection			
Li	14	0.8	0.4
Fe	98	18	5.0
In	43	8.0	5.0
Na	14	3.0	1.0
Excimer Dye Laser			
Laser Enhanced Ionization Detection			
Li	0.7	0.3	0.5
Na	4.0	1.0	2.0
In	0.2	0.2	0.4

	BW[d]	BW+ABS[e]	BW+BLIA[f]
Copper Vapor Dye Laser			
Bandwidth Limited Signal Processing--Fluorescence Detection			
Li	2.0	0.6	0.3
Na	2.0	1.1	1.0
In	3.0		
Fe	15		

[a] CONV = Conventional method of measuring pulsed laser signals using a boxcar averager and gated integrator.

[b] ABS = Active baseline subtraction method using a modulated pulsed laser. Subtraction of background noise is done by the boxcar special electronics.

Table 2-1--continued.

[c] BLIA = Boxcar averager plus lock-in amplifier using a modulated pulsed laser. Subtraction of background noise is accomplished in the lock-in amplifier.

[d] BW = Bandwidth limited signal processing in which high frequency laser noise is not amplified while the signal is amplified to increase signal-to-noise ratio of fluorescence signals.

[e] BW+ABS = Bandwidth limitation as discussed above followed by active baseline subtraction.

[f] BW+BLIA = Bandwidth limitation followed by the boxcar averager plus lock-in amplifier.

more complicated schemes. No correction for the total number of laser pulses per second has been made. In the BLSP scheme and the CONV method, 6000 pulses per second pass through the flame and are detected. In the ABS and BLIA experiments, there are only 3000 pulses passing through and being detected in the flame each second. The remaining 3000 pulses were blocked by the chopper and the noises detected in laser enhanced fluorescence and ionization were subtracted out.

The background subtraction methods (ABS and BLIA) provide an additional advantage over the BLSP scheme and the CONV method, namely the removal of low frequency changes in the laser conditions. The CVL operates in a continuous flow mode with a constant addition of neon and a constant removal of neon and a small amount of copper vapor. Conditions within the laser cavity are changing at a very slow rate (relative to the 6 kHz repetition rate) due to changes in the neon pressure, partial pressure of the copper vapor, and position of the electrical arc within the laser tube. These changing conditions result in small changes in the dye laser power output but, more importantly, changes in the magnitude of the radio-frequency signal detected within the boxcar gate. No correction for dye laser power fluctuations could be obtained, since the fluctuations were in the source prior to modulation. Correction for flame and analyte background flicker was accomplished in both the ABS and BLIA methods.

The effect of bandwidth limited signal processing (BLSP) on fluorescence signals is demonstrated in Figure 2-6. The fluorescence signals in Figure 2-6 prior to bandwidth limitation demonstrate the

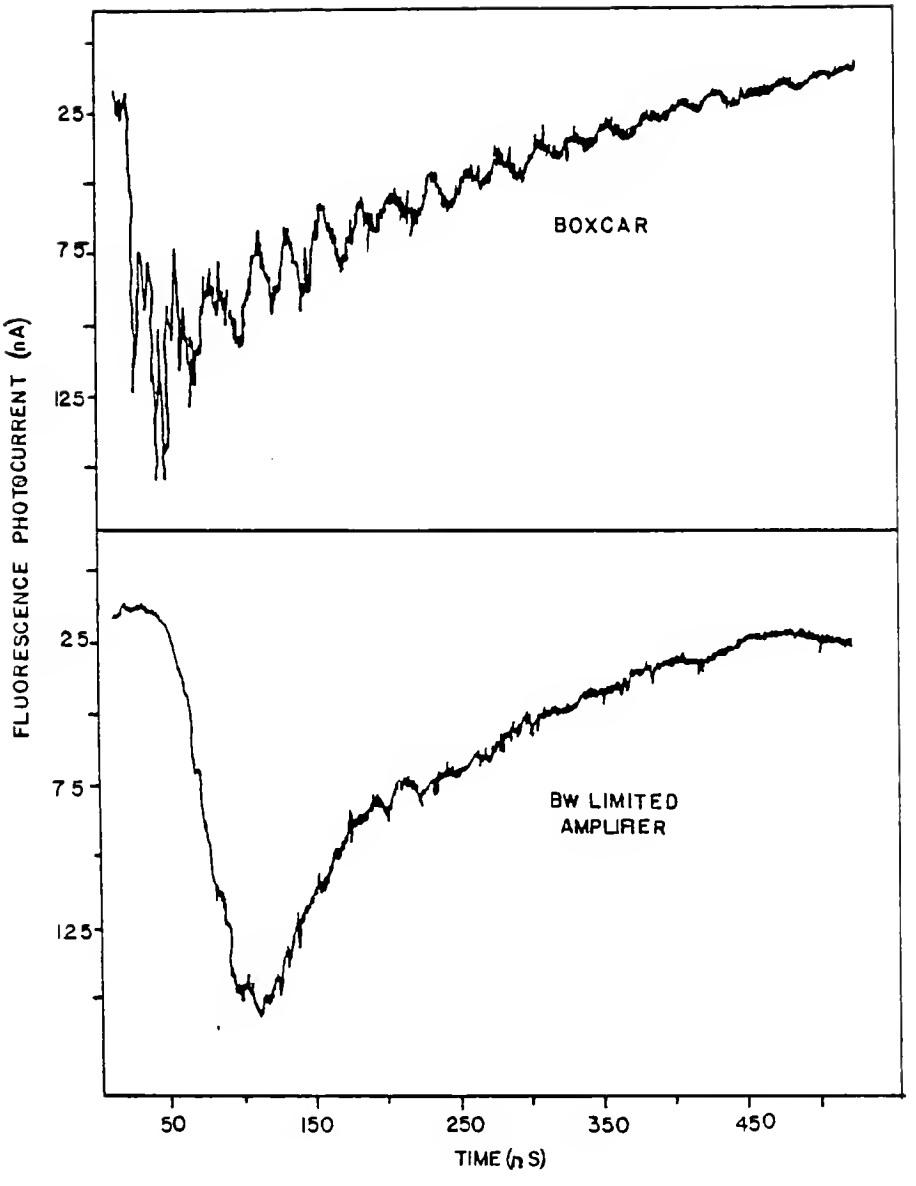

Figure 2-6. Bandwidth Limitation Effects

high frequency noise which is the limiting noise source for this type of laser. The temporal effect of bandwidth limitation on fluorescence signals is also shown in Figure 2-6.

The BLIA results show a marked improvement over CONV results in all cases. The BLIA results are felt to be slightly better than the ABS results because a true phase-sensitive detection method was employed in this scheme. The ABS method used a gated RC filter to add capacitively signals of alternating polarity to remove background and was susceptible to capacitor leakage, noise added by the polarity switching amplifier, and signal fluctuation when a low number of samples is averaged.

The experiments with active baseline subtraction (ABS and BLIA) provide some unique opportunities for signal manipulation due to the extremely high repetition rate of CVL. At the 6 kHz repetition rate used, signals obtained are well above the low frequency flicker noise region of the flame (or a plasma) and analyte background flicker. Additionally based on laser repetition rate, beam diameter, and flame gas flow rate, it is possible to irradiate each atom present within the flame with 3 to 10 laser pulses of moderate intensity as the atoms pass through the flame volume. Indeed, the high repetition rate of the CVL should make it possible to detect virtually every atom passing through a flame (or any plasma).

For comparison purposes, results obtained using our excimer laser (Lumonics model TE-861) are included for laser enhanced ionization. This laser is capable of providing peak energies of up to 3 mJ per pulse of fundamental power from the dye laser much higher

than the CVL system. Typical energies obtained at 25 Hz repetition rate were in the range of ~80-250 μJ per pulse of frequency doubled energy in a bandwidth of 0.0015 nm. The inferior performance of the two methods employing background correction (BLIA and ABS) should be noted for results obtained using the excimer laser. These results may be explained in one of two ways: diminished performance of our lock-in amplifier at the 25 Hz repetition rate (where a larger amount of flame background flicker and analyte flicker is present); and/or lower correlation of the interfering noise from the excimer laser compared to the copper vapor laser. Both effects are felt to contribute to some extent. At 25 Hz, a much larger flicker component is present than at the 6 kHz CVL repetition rate. The low frequency analyte and background flicker component at the sodium wavelength 588.9 nm is shown in Figure 2-7. These signals were measured with only the flame on and no laser present. Signals were measured using a cross channel spectrum analyzer (Wavetek, model 5890B) and represent the total signal present across the frequency range shown. Several trends are apparent from this figure. Flame background flicker noises are small and become very small above approximately 1.0 kHz. Analyte flicker is much higher at low frequency and decreases at higher frequency. The much higher flicker noise of the analyte can be attributed to nebulizer noise while the higher overall signal magnitude is due to analyte emission.

The other contribution to flicker noise is the pulse-to-pulse fluctuation of the laser. The lower correlation of the pulse-to-pulse noise from the excimer laser is felt to be a limiting factor in

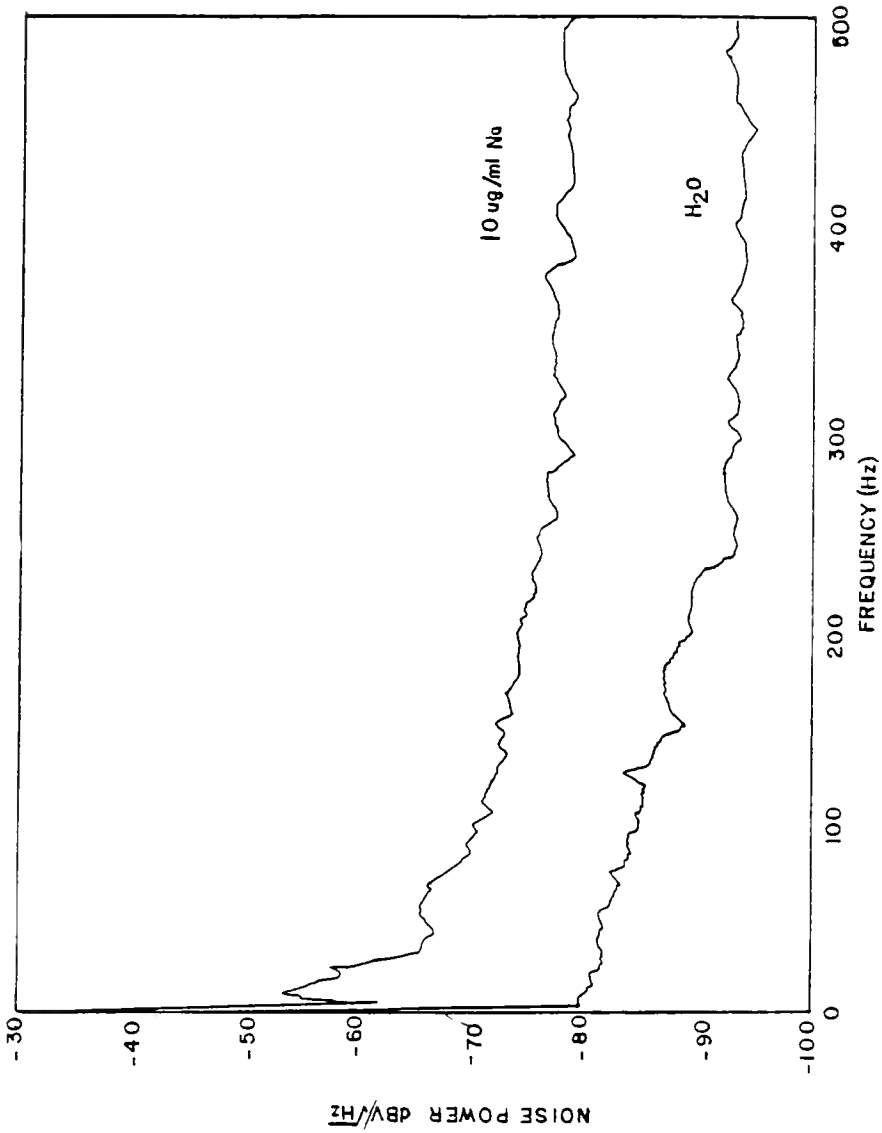

Figure 2-7. Noise Power Spectra at 588.9 nm

the improvements obtained with the excimer laser. The excimer discharge voltage, ~32,000 V, is less easily regulated than the 7,000 V used in the copper vapor laser. Oscilloscope comparisons of the noise from the two lasers confirmed the much higher noise fluctuations for the excimer laser. No correction for laser noise could be obtained unless the noise component was present on successive laser pulses.

The two noise correction methods (BLIA and ABS) were combined with the noise reduction method, bandwidth limitation (BW) to determine the individual contributions to noise reduction, and signal-to-noise enhancement. It was found that the combination of these techniques results in minimal improvement beyond that obtained with bandwidth limitation alone. This indicates that the major improvement is due to bandwidth limitation and thus the major noise source is RF interference from the laser system.

Conclusions

The methods presented are shown to provide a significant increase in the detection power for LAFS and LEIS. For active baseline subtraction, improvements of up to 6 times were obtained while with the combined bandwidth limitation and boxcar plus lock-in amplifier (BW+BLIA) improvements of up to 40 times were obtained. While these improvements may be possible for other laser systems, it is to be emphasized that many of these methods rely on a certain stability in the noise levels associated with a given laser system. Application of these correction methods to a poorly correlated noise

source may yield little or no improvement in the detection power (see excimer laser results). A more highly correlated noise source should yield correspondingly better results. Additionally, modulation of a pulsed laser and subsequent loss of one-half of the laser pulses may be more harmful than the gain in detection power allowed by subtraction of any noises.

CHAPTER 3
ESTIMATION OF ABSOLUTE NUMBER DENSITIES

General Curve of Growth Introduction and Evaluation

A general overview of methods for determination of the absolute number density of a species is presented in Chapter 1. In this chapter, general expressions and a computer program are presented for evaluation of the fluorescence curve of growth and the absolute number density determination. The computer program for these calculations was written in FORTRAN-77 and was approximately 500 lines long. FORTRAN-77 was chosen for the programming language as a compromise of speed, flexibility, and scientific compatability.

The computer program for evaluation of the absolute number density calculates the fluorescence intensity vs the concentration of the species of interest. A log-log plot of these terms is referred to as a curve of growth (COG). The expression for right angle fluorescence (diagrammed in Figure 3-1) is shown in Figure 3-2. The expression for fluorescence may be divided into several parts: a primary absorption term, a self-absorption term, and a term for the optical collection efficiency. (The prefilter and postfilter terms are considered separately below.) The primary absorption term is derived from the Beer-Lambert law and can be used for an absorption curve of growth in conjunction with an optical collection efficiency term. The primary absorption term is responsible for some of the

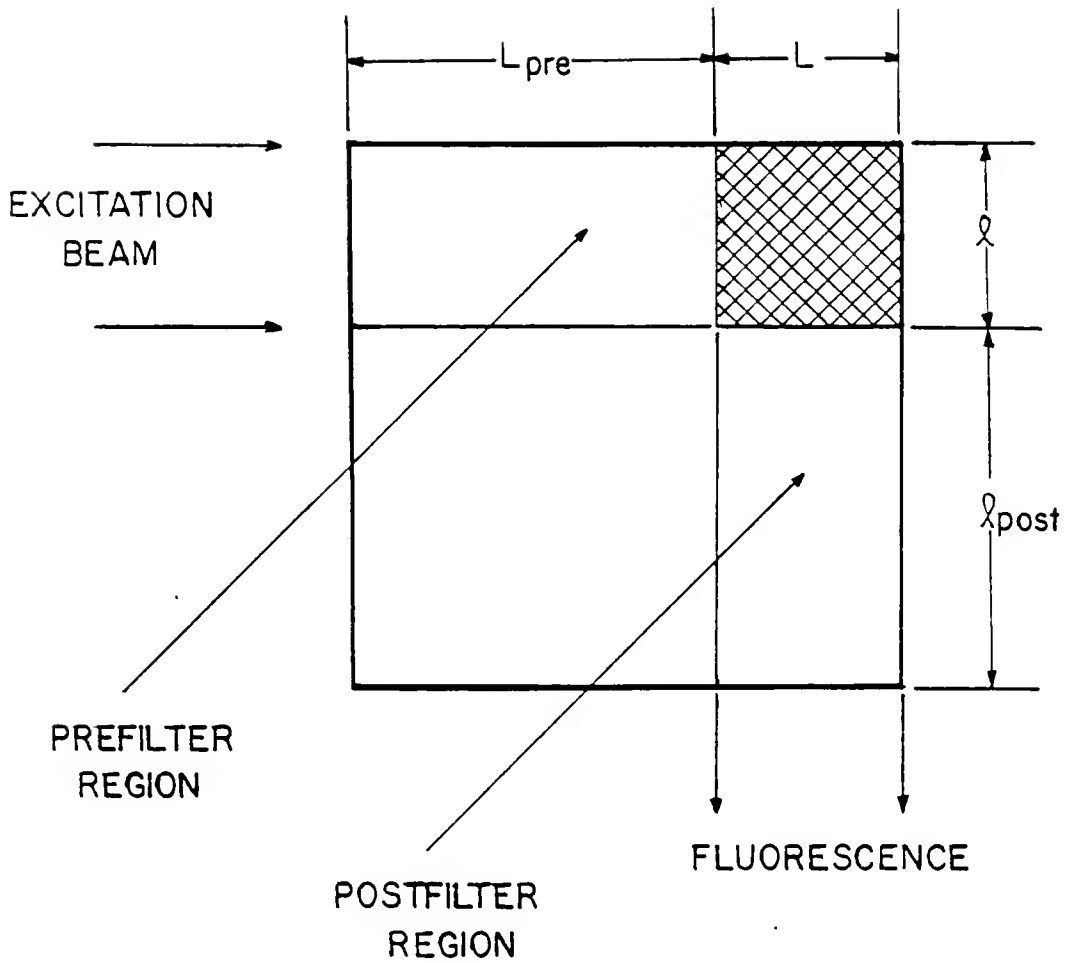

Figure 3-1. Diagram for Right Angle Fluorescence

$$\Delta \Phi = F_{pr} F_{po} \frac{\Omega}{4\pi} \frac{\Delta h \Delta \ell \Delta L T_e}{u^2 m_L m_H} Y_p \frac{\sqrt{4 \ln 2}}{\sqrt{\pi} k_0 L \Delta \lambda_D} \int_{-\infty}^{+\infty} (1 - e^{-k(\lambda) \frac{E^s_\lambda}{E_\lambda + E^s_\lambda} L}) d\lambda \; \frac{1}{\Delta \lambda_s} \int_{-\infty}^{+\infty} E_\lambda (1 - e^{-k(\lambda) L \frac{E^s_\lambda}{E_\lambda + E^s_\lambda}}) d\lambda$$

Optical collection term Self-absorption term Primary absorption term

$$F_{pr} = \frac{\int_{-\infty}^{+\infty} 1 - EXP\left[-k(\lambda) L \frac{E^s_\lambda}{E_\lambda + E^s_\lambda} \left(1 + \frac{L_{pr}}{L}\right)\right] d\lambda - \int_{-\infty}^{+\infty} 1 - EXP\left[-k(\lambda) \frac{E^s_\lambda}{E_\lambda + E^s_\lambda} L \frac{L_{pr}}{L}\right] d\lambda}{\int_{-\infty}^{+\infty} 1 - EXP\left[-k(\lambda) \frac{E^s_\lambda}{E_\lambda + E^s_\lambda} L\right] d\lambda}$$

$$F_{po} = \frac{\int_{-\infty}^{+\infty} 1 - EXP\left[-k(\lambda) \ell \left(1 + \frac{\ell_{po}}{\ell}\right)\right] d\lambda - \int_{-\infty}^{+\infty} 1 - EXP\left[-k(\lambda) \ell \frac{\ell_{po}}{\ell}\right] d\lambda}{\int_{-\infty}^{+\infty} 1 - EXP\left[-k(\lambda) \ell\right] d\lambda}$$

Figure 3-2. Expression for Right Angle Fluorescence

curvature in a curve of growth at higher number density. The source irradiance becomes increasingly absorbed at high number densities until the entire source irradiance is absorbed at extremely high number densities. The self-absorption term is a dimensionless factor accounting for reabsorption of fluorescence photons, within the excitation volume, as they traverse the atom reservoir. The self-absorption term also contributes to the curvature of the curve of growth and continues to increase with increasing number density. This term may or may not be important depending on whether resonance or direct-line fluorescence is measured. The remaining term to account for the optical collection efficiency includes T_E, the transmittance of the collection optics; m_L and m_H, magnifications of the length and height dimensions of the source on the atom cell; and n, the refractive index of the medium (to account for the change of solid angle of collection due to medium to air transfer of radiation). The term $\Delta h \Delta \ell \Delta L$ is used to give the observed radiant fluorescence flux, $\Delta \phi$.

Shown in Figure 3-1 (with expressions in Figure 3-2) are regions for prefiltering of the excitation source and postfiltering of the fluorescence radiation. A prefilter region is one in which the analyte of interest is present and is illuminated by the excitation beam but the resulting fluorescence is not viewed by the detector. A postfilter region is one in which the analyte of interest is present but the region is not illuminated by the excitation source. These terms become important in some analytical situations where it may not be possible to avoid prefiltering and/or postfiltering.

Some simplifying considerations used in the development and evaluation of the expressions are as follows:

(i) a single atomic transition is considered for the atomic emission and absorption methods while results are included for both direct-line and resonance fluorescence;

(ii) for the absorption and fluorescence cases, the excitation beam is of rectangular cross section (ℓ x H) and is spatially, as well as temporally, homogeneous;

(iii) the atom reservoir consists of a uniform ground state number density distribution at a uniform temperature in the absence of the excitation beam;

(iv) the absorption and fluorescence spectral line profiles may be described by a Voigt function;

(v) no restrictions are made as to source intensity, but it should be noted that saturation of a transition by an apparent line source may result in saturation broadening of the spectral excitation profile until the source no longer may be considered effectively a line source. The validity and applicability of many of these considerations are discussed by Zeegers et al.[34]

Definitions of all terms used in the fluorescence expression (and other equations used in this text) are included in Appendix A. The computer program used for evaluation of the fluorescence expressions is included in Appendix B.

In this research, no simplifying assumptions were made other than those noted above. Assumptions of line or continuum source

excitation would greatly simplify the equations and calculations involved, but the much more difficult case of an intermediate source is considered here. The shapes of curves for line or continuum excitation have been studied thoroughly.[35-37] A more complete development of the curve of growth equation is given in these sources.

The program for curve of growth calculation uses some approximations to enable the calculation to be performed. The first of these approximations is the substitution of a large polynomial approximation for the Voigt profile. The Voigt profile is the spectral convolution of a Doppler profile with added collisional broadening and is used in calculating the atomic absorption profile $k(\nu)$ where

$$k(\nu) = k_o V(a,v)$$

and

$$V(a,v) = \frac{a}{\pi} \int_{-\infty}^{+\infty} \frac{\exp(-y^2)dy}{a^2+(v-y)^2} .$$

The Voigt integral cannot be solved in closed form and a substitution proposed by Hui et al.[38] is used. This approximation is extremely accurate (one part in 10^6) and evaluation is fast with no loss in overall accuracy of the COG. The limiting accuracy of the COG is determined by the accuracy of the integration limits used in the evaluation of the other integrals of the fluorescence expression and the accuracy of the experimental parameters used. The other major approximation involved in the COG calculation is in the evaluation of the primary, self-absorption, prefilter, and postfilter integrals.

The integrals should be evaluated from minus infinity to infinity. Obviously, this integration is not possible and a tolerance for the convergence of the integral must be chosen. In most cases, a convergence tolerance of a maximum of 0.001 percent of the value of interest was used. In some cases where a tighter convergence was desired, an even smaller tolerance was used, although a greater accuracy was not generally available.

Calculated Curves of Growth

The general COG in atomic spectroscopy is described by a linear low concentration (or low number density) region and a noticeable curvature at higher number densities. The degree of curvature and the final slope of the COG at high number densities depends on the source spectral width and the atomic parameters used in evaluation of the fluorescence intensity expression. The curves of growth for line and continuum sources are presented in Figures 3-3 and 3-4, respectively. These curves are shown for several a values. The a value or a-parameter is a measure of the ratios of the collisional width to the Doppler width:

$$a = \sqrt{\ln 2}\left(\frac{\Delta\lambda_C}{\Delta\lambda_D}\right) .$$

The collisional width, $\Delta\lambda_C$, is largely dependent upon the mass and number of collisional species present and the temperature of the atoms. The Doppler width, $\Delta\lambda_D$, depends upon the mass and temperature

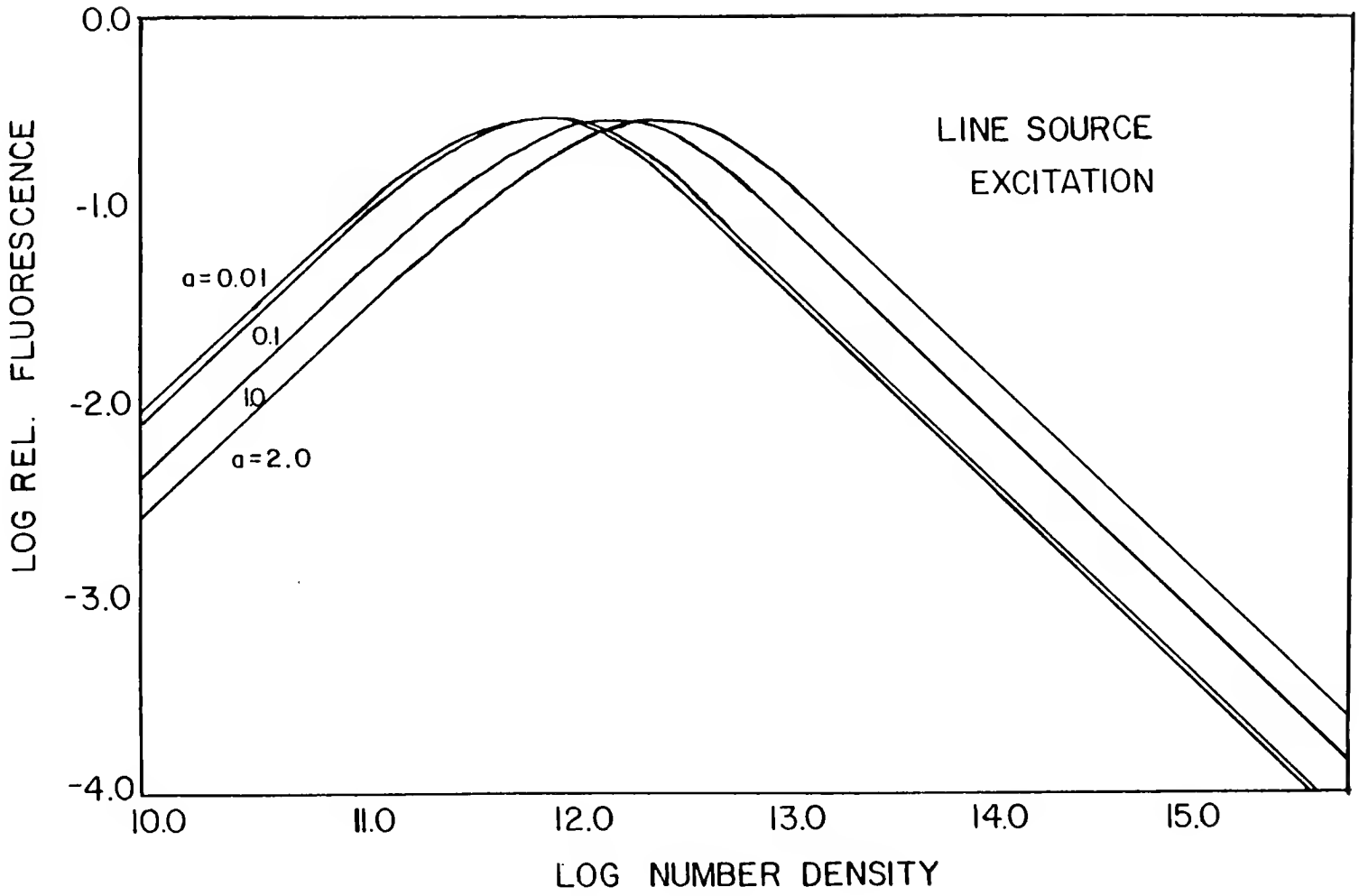

Figure 3-3. Curves of Growth for Line Source Excitation

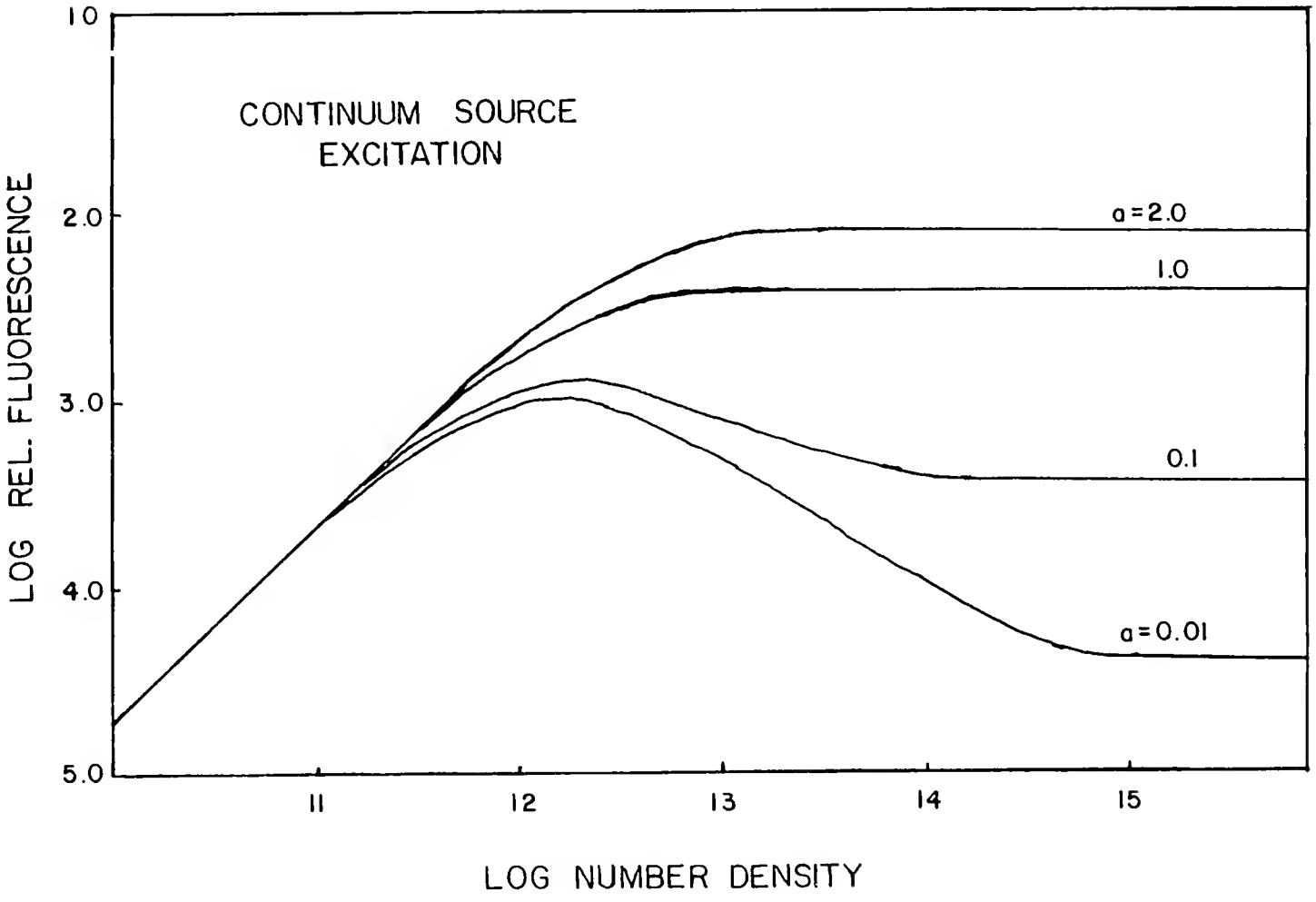

Figure 3-4. Curves of Growth for Continuum Source Excitation

of the atom. The expression for $\Delta\lambda_D$ is presented below with expressions for collisional broadening widths presented later.

$$\Delta\lambda_D = 4\pi\lambda/C \sqrt{2\ RT\ \ln\ 2/M}\ .$$

The curves presented for line and continuum sources agree well with the other literature and experimental results presented previously. The abscissa in all curves is shown in relative units since we are not concerned with the absolute signal magnitude but rather the shape of the COG. Here, we are more concerned with the intermediate case of a pseudocontinuum source, i.e., a laser.

The spatial line widths of dye lasers (measured as the full width at one-half maximum (FWHM)) typically are on the order of ~0.01 to 0.05 nm when only a grating is used as a tuning element. Atomic spectroscopy line widths in analytical flames vary from about 0.0005 nm to 0.02 nm.[39] Thus, the laser will vary from approximately equal to, to approximately 100 times the line width of the atom of interest. This can be considered a pseudocontinuum source for most applications. The curves of growth for pseudocontinuum sources of equal laser and atom line atomic width and a laser which is 10 times the atomic absorption profile (FWHM) are shown in Figure 3-5.

Curves of growth are shown for prefilter and postfilter effects in the next series of figures. These curves are presented for an a-parameter value of 1.0, which is used as an average value of approximately 40 elements in an air-acetylene flame.[40-41] Shown in Figures 3-6 and 3-7 are prefilter effects for mild, medium, and

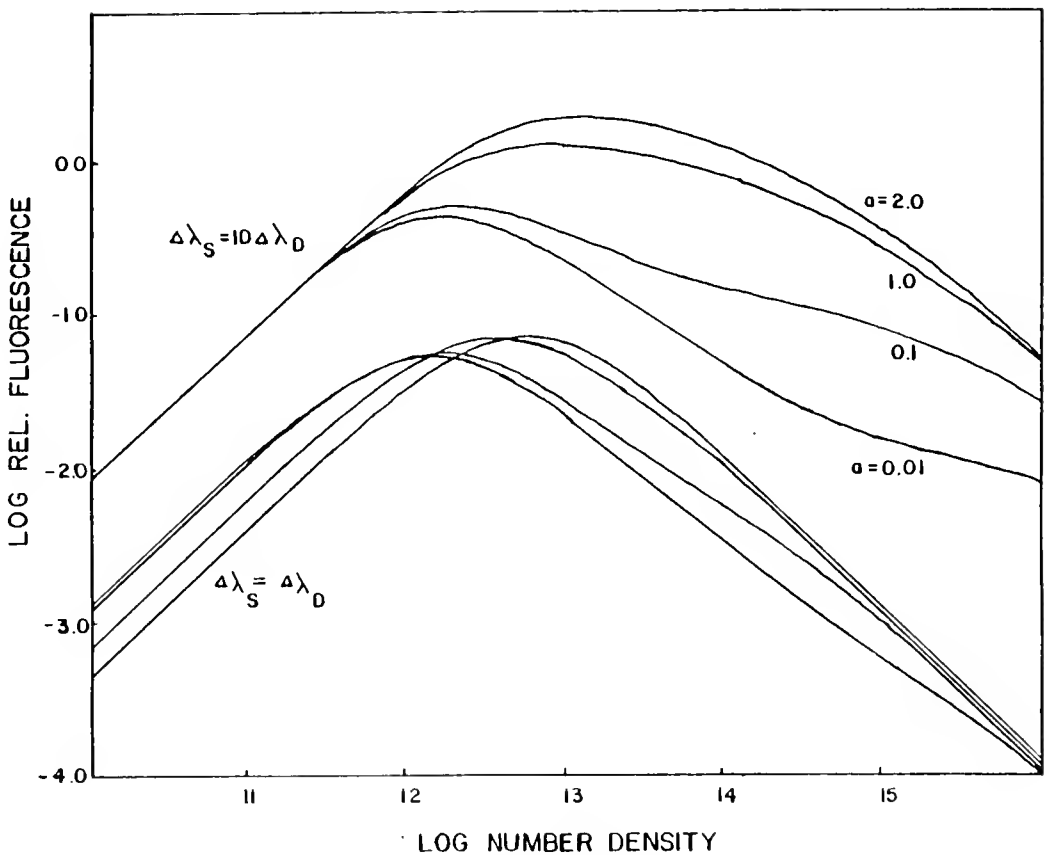

Figure 3-5. Curves of Growth for Two Pseudocontinuum Sources

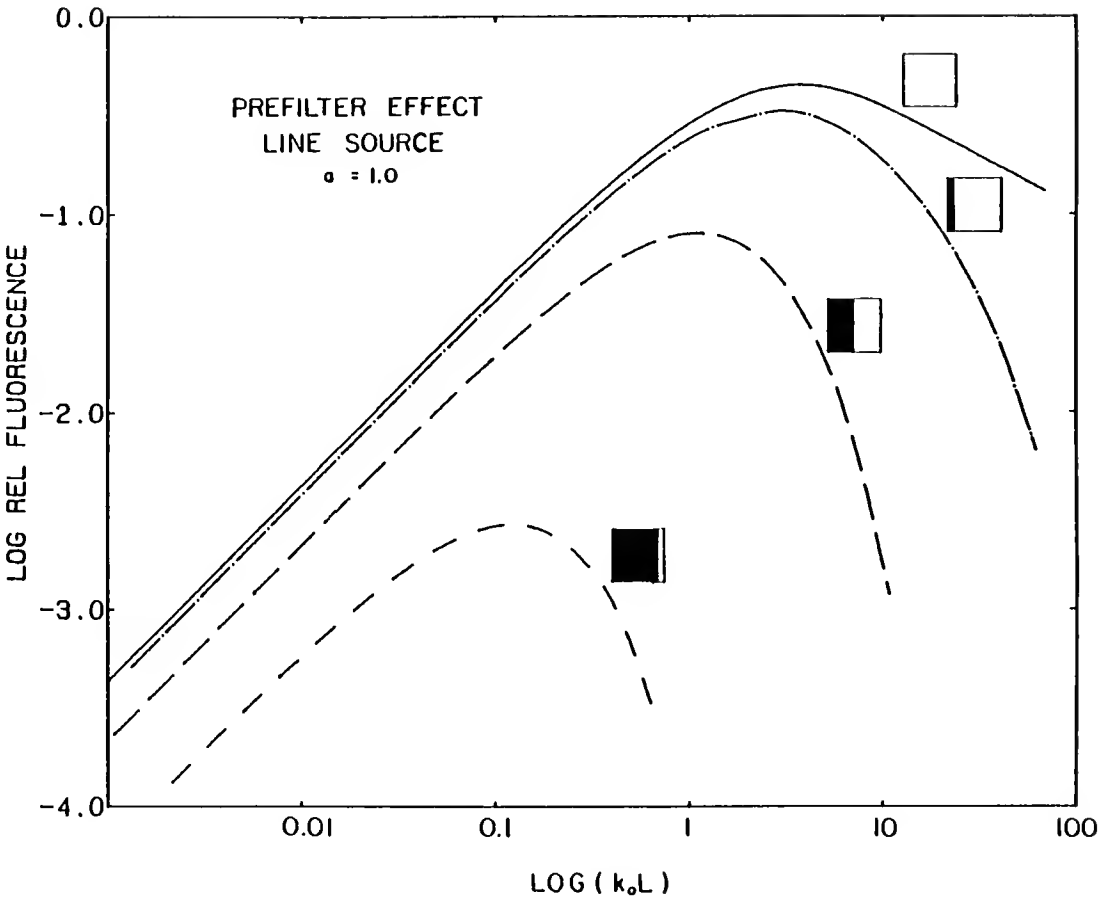

Figure 3-6. Curves of Growth for Mild, Medium, and Severe Prefiltering--Line Source, Dark = prefilter region

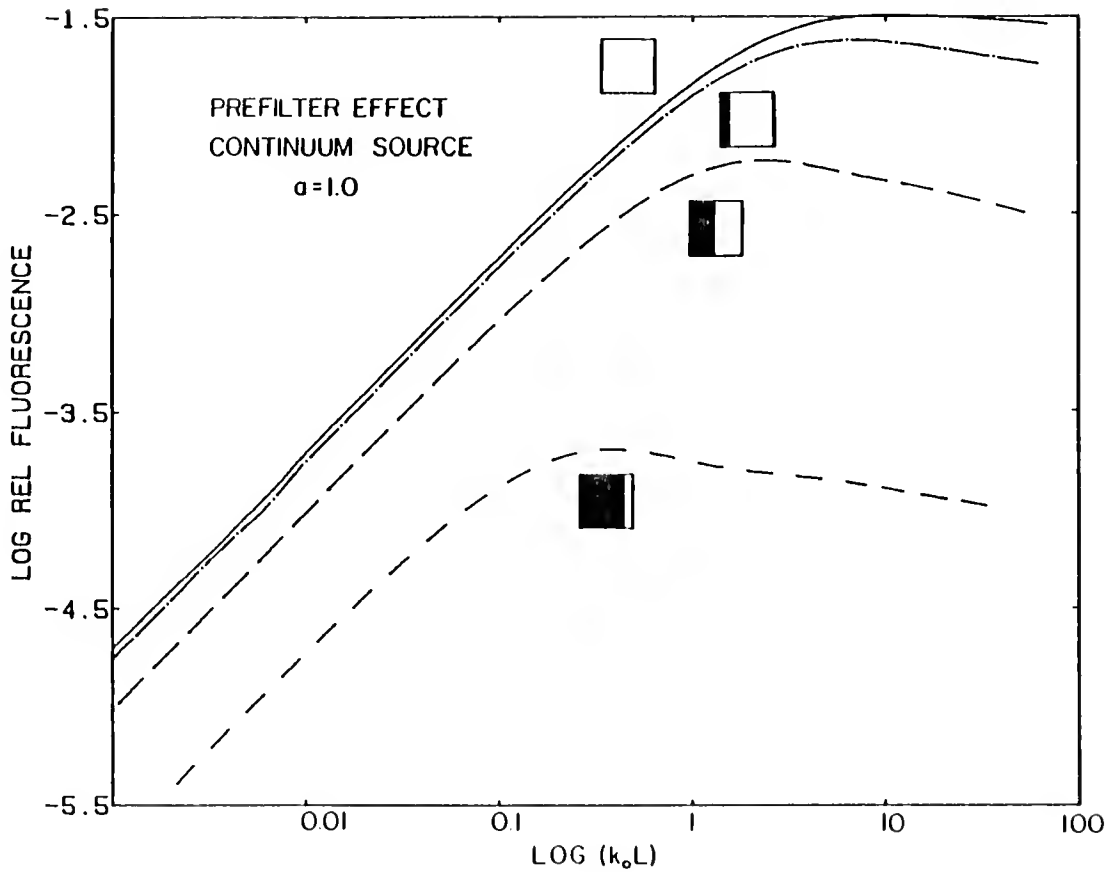

Figure 3-7. Curves of Growth for Mild, Medium, and Severe Prefiltering--Continuum Source, Dark = prefilter region

severe prefiltering for line and continuum sources, respectively. The equivalent curves of growth for line and continuum sources are shown for postfiltering in Figures 3-8 and 3-9, respectively.

The COGs for all prefilter and postfilter calculations are shown with log (k_oL) as the abscissa. This is used, instead of the log number density, to partially compensate for the reduced absorption pathlength involved. The relationship between the peak absorption coefficient (for pure Doppler broadening), k_o, and the number density, n, is presented below.

$$k_o = \frac{\sqrt{4\pi \ln 2}\, e^2 \lambda_o^2 nf}{mc^2 \Delta\lambda_D}$$

This relationship is developed in Mitchell and Zemansky[10] and is based on the absorption oscillator strength, f, and the central wavelength, λ_o, and Doppler width, $\Delta\lambda_D$, (FWHM) of the atom of interest (other terms are defined in Appendix A).

General trends which may be noted for these curves are relatively simple. Prefiltering of the source results in an increase in the rate of curvature for line and continuum sources. This increase in curvature is accompanied by a general decrease in the signal strength. This is due primarily to the decreased fluorescence volume observed. The postfilter effect results in a general decrease in the overall fluorescence intensity. A more complete discussion of the prefilter and postfilter effects is included in a later section on collision broadening and saturation effects. From the figures and

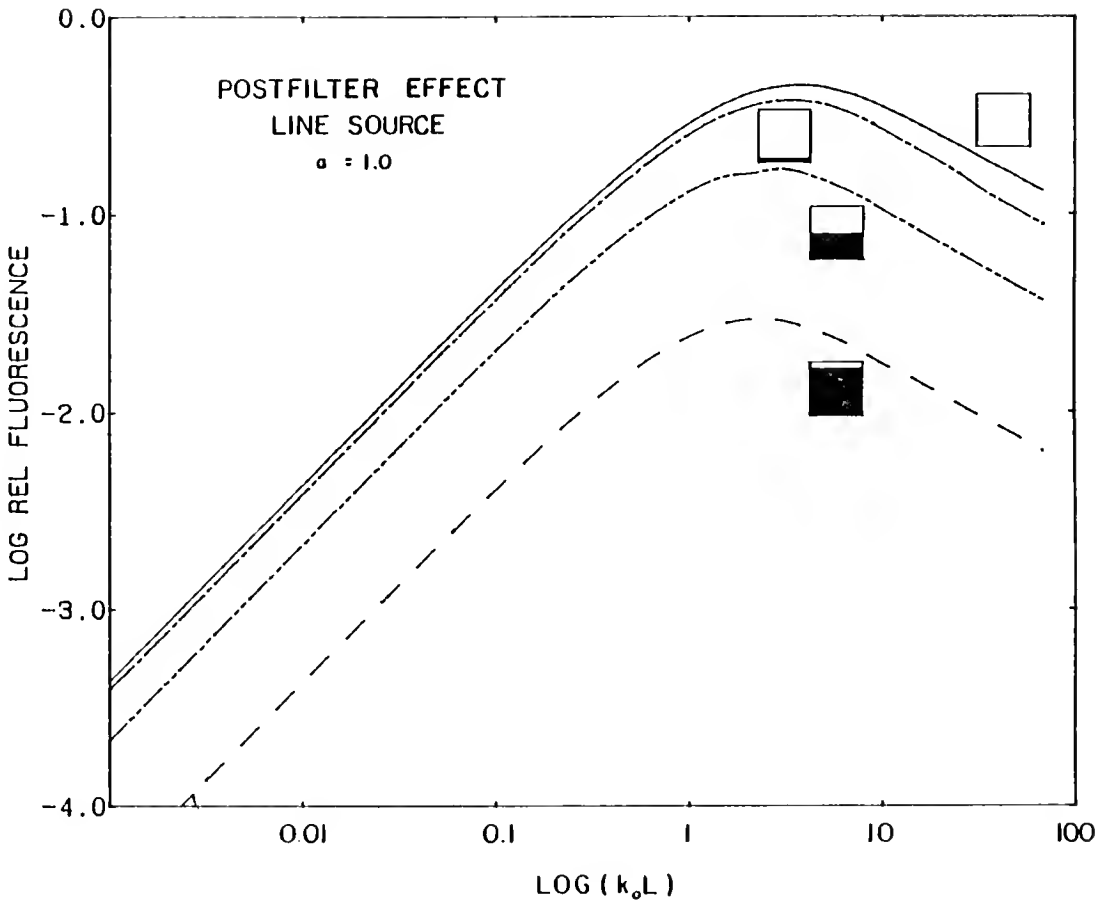

Figure 3-8. Curves of Growth for Mild, Medium, and Severe Postfiltering--Line Source, Dark = postfilter region

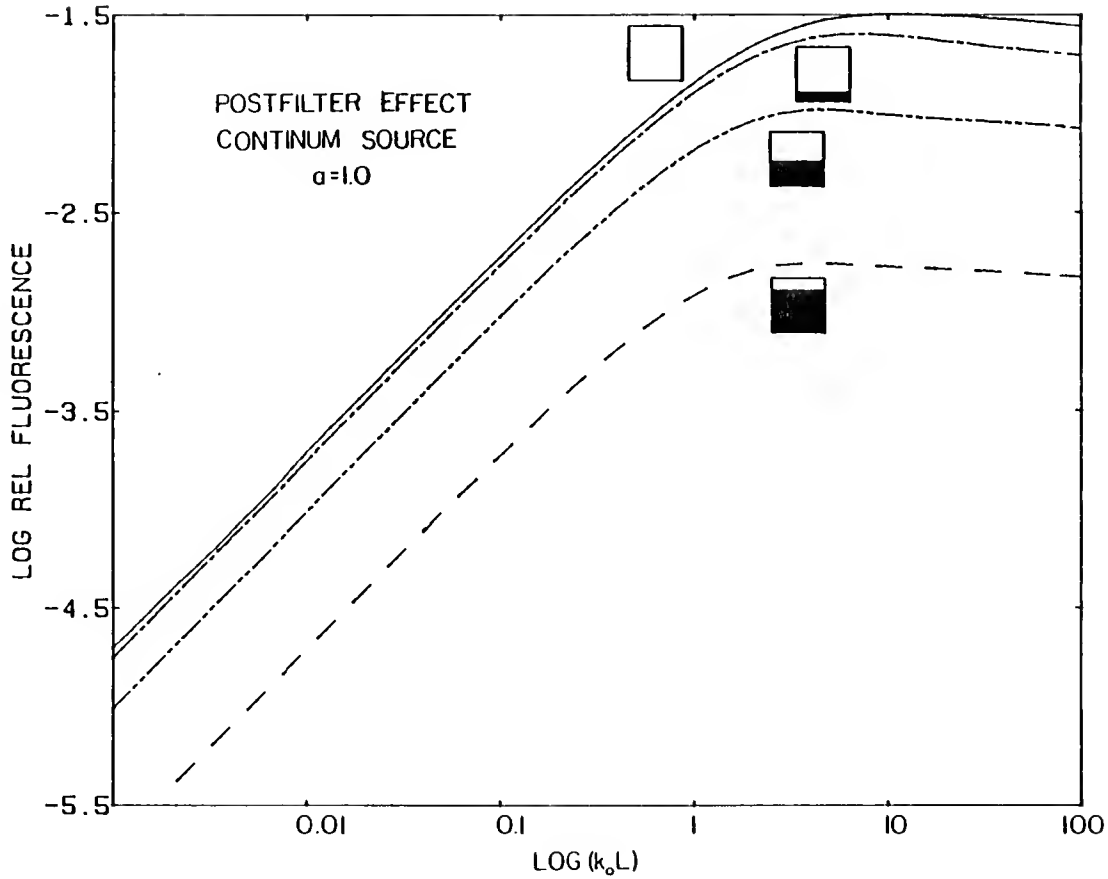

Figure 3-9. Curves of Growth for Mild, Medium, and Severe Postfiltering--Continuum Source, Dark = postfilter region

discussion presented above, it can be seen that it is important to minimize prefilter and postfilter effects (to achieve higher signal-to-noise ratios and maximum linear dynamic range). It is generally possible to do so by simple modification of the optical design.

Experimental Verification of Curves of Growth

Figure 3-10 shows the calculated curve of growth for sodium resonance fluorescence in an air-acetylene flame. The experimental data points are included on this curve also. The curve of growth was calculated for a flame of 2500 K using a Gaussian source of 0.03 nm (FWHM) and a damping parameter of 1.0. These represent the line width of the copper vapor pumped dye laser and resonable parameters for Na in an air-acetylene flame.[40] The fit of the curve of growth to the experimental points is obtained by transposition of the COG until this curve overlaps the experimental points. The overlap of these curves gives a direct relationship between the concentration of the species introduced and the absolute number density present in the flame.

The experimental curve of growth was obtained using the same experimental arrangement as described and diagrammed earlier in Chapter 2 (Figure 2-2). Aqueous solutions of sodium were prepared by dissolving sodium chloride in deionized water. Solutions below 1000 mg/L were prepared by dilution, while solutions above 1000 mg/L were prepared directly by weighing.

The fluorescence results are in good agreement with a calculated estimate of the absolute number density. This estimate is based on

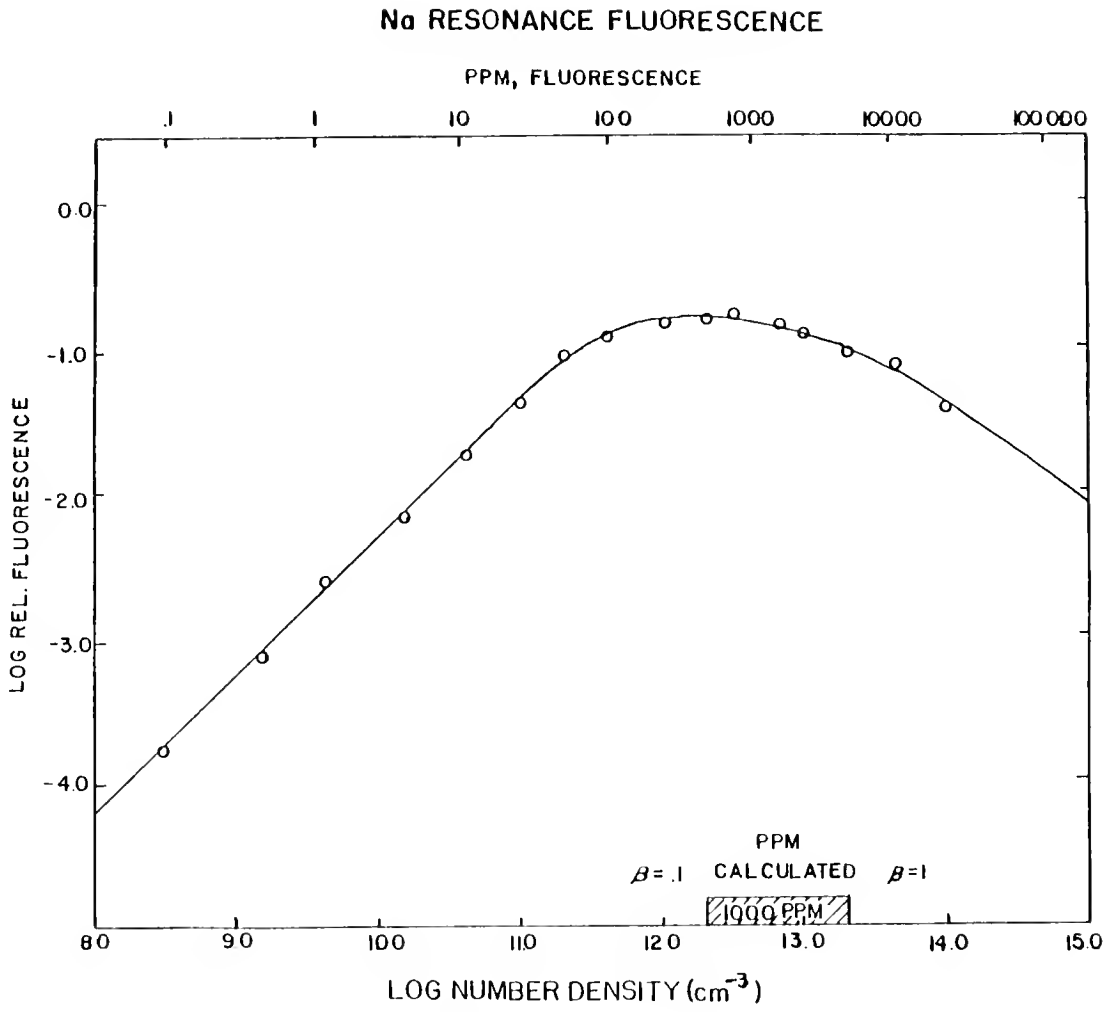

Figure 3-10. Calculated and Experimental Curves of Growth for Na

the solution concentration, the solution uptake rate, the nebulization and atomization efficiencies, and the flow rate and thermal expansion of flame gases. These terms are grouped to form a single term, β, which should be within the range shown in Figure 3-10.

To confirm these experimental results and to extend the curve of growth calculations to direct-line fluorescence, the same experiments were performed using another laser system. Poor doubling efficiencies with the copper vapor laser system (see Chapter 2) make the wavelength used for Pb fluorescence difficult to obtain, at least at a laser intensity level which will provide enough sensitivity for these studies. The COG for lead with 283.3 nm excitation and resonance (283.3 nm) and direct-line (405.7 nm) fluorescence were calculated and measured experimentally. The curves were calculated for a 0.019 nm source spectral line width (FWHM) with a-parameters of 1.0 (283.3 nm) and 1.5 (405.7 nm). These are estimates based on calculations given by Parsons et al.[39] since no known measured values are available. The 0.019 nm source line width is obtained from our Nd:YAG laser pumped frequency doubled dye laser (Quantel, model YG580). The Pb experimental results were measured by Dr. Benjamin Smith. His measurements were performed using an experimental setup similar to that previously described (Figure 2-2). In this experiment, two curves must be transposed to match with two sets of experimental curves. The two experimental curves, shown in Figure 3-11, were found to give reasonable agreement between themselves and are within one order of magnitude agreement with the estimated number

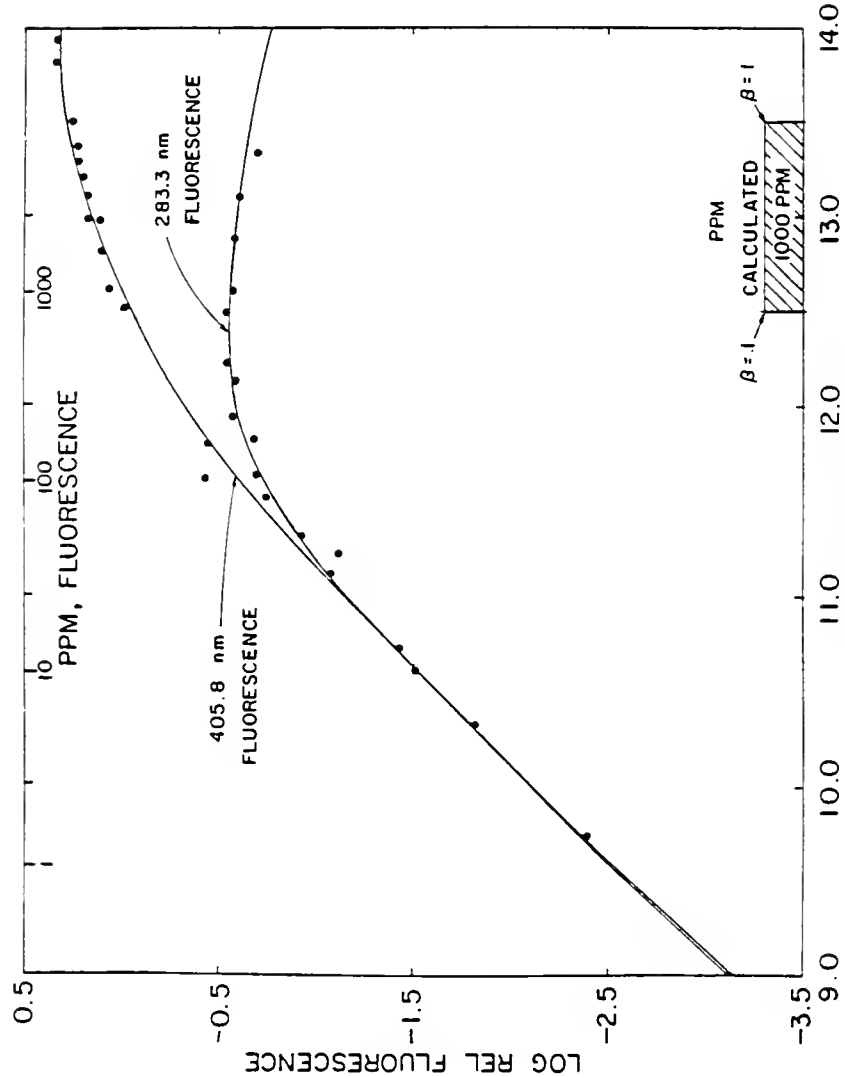

Figure 3-11. Calculated and Experimental Curves of Growth for Pb

density (from the nebulization and atomization efficiencies, etc.). The agreement of these curves with the experimental values demonstrates the accuracy and applicability of these methods.

Saturation and Collisional Effects

A further extension of the curve of growth calculations involves the inclusion of some of the lesser noted effects in atomic fluorescence spectroscopy. The expression for fluorescence presented previously (Figure 3-2) and merely be extended here. The expressions for saturation effects are included in Figure 3-2 but were not previously discussed. The collisional broadening terms have not been discussed yet and will be presented here.

Collisional broadening effects may be considered from two separate aspects: collisional broadening due to analyte collisions with analyte termed self-broadening or resonance broadening and collisional broadening due to collisions with other species. The first will be referred to as self-broadening and the second will be termed collisional broadening. The general expression for collisional broadening is presented in Figure 3-12.[42] The theory of collisional broadening was originally developed by Lorentz and later extended by Lenz and Weisskopf. A complete development is presented by Breene[42] and Mitchell and Zemansky.[10] The general expression for collisional broadening simplifies when only resonance broadening is considered. The summation of all atomic and molecular concentrations simplifies to involve only the analyte concentration. The mass

COLLISIONAL BROADENING

$$\Delta\lambda_c = \frac{2\Sigma N \lambda^2 \sigma^2}{\pi c}\left[2\pi k T N_A\left(\frac{1}{M_a}+\frac{1}{M_q}\right)\right]^{1/2}$$

RESONANCE BROADENING

$$\Delta\lambda_R = \frac{2N\lambda^2\sigma^2}{\pi c}\left[4\pi k T N_A\left(\frac{1}{M_a}\right)\right]^{1/2}$$

Figure 3-12. Expression for Collisional Broadening

term, $1/m_A + 1/m_Q$, simplifies to involve only the mass of the analyte (see Figure 3-12). Worst case collisional broadening effects will be seen for situations of small atomic mass, long wavelength transitions, and large collisional cross sections.

The self-broadening effects for two elemental cases have been included in Table 3-1. The elements evaluated represent the two extremes encountered in atomic spectroscopy: a high mass, low wavelength case and a low mass, high wavelength case. The collisional cross sections used here represent the range of values measured.[40] From curve of growth calculations and the results in Table 3-1, it can be seen that no significant differences due to self-broadening are expected for experimentally realizable situations. No appreciable changes are seen in the a-parameter until number densities of greater than 10^{17} atoms/cm^3 are approached. Based on previous measurements in Chapter 2, this corresponds to an initial atomic concentration of greater than 100 M and an unrealistic aspirated concentration of 10^8 parts-per-million. Additionally, at high number densities where self-broadening effects should become apparent, the primary absorption term will typically have reached absorption saturation and any change in the a-parameter and line shape will not affect the absorption of radiation. Very weak transitions ($k_o/n < 10^{-15}$) may show some small self-broadening effects at high number densities since the absorption terms are very small and allow considerable transmittance at high number densities.

Table 3-1. Broadening Effects on the a-Parameter for Self-Broadening

Best Case (Low Collisional Broadening)		Worst Case (High Collisional Broadening)	
Pb		Li	
λ = 283.3 nm		λ = 670.8 nm	
T = 2500 K		T = 2500 K	
m_A = 207.2 g/Mol		m_A = 6.94 g/Mol	
	a-Parameters		
$n(cm^{-3})$	σ^2 ($Å^2$) 30 / 100	$n(cm^{-3})$	σ^2 ($Å^2$) 30 / 100
10^{16}	1.0007 / 1.0023	10^{16}	1.0035 / 1.0097
10^{17}	1.0068 / 1.0227	10^{17}	1.0350 / 1.0970
10^{18}	1.0680 / 1.2270	10^{18}	1.350 / 1.9700

Collisional broadening effects due to an added matrix species, termed simply collisional broadening effects, are included also. The collisional broadening effects are somewhat different than the self-broadening effect in that these effects are seen over the entire range of analyte concentrations and are due to some constant concentration of an added species. The effect of collisional broadening may or may not be noticeable depending on the spectral width of the source used and the spectral width of the atomic profile. For line sources, the wings of the absorption profile (described by the a-parameter) will not matter since absorption occurs only at the line center. As the source width increases, the wings of the absorption profile may affect the curve of growth. At low atomic concentrations, however, the a-parameter does not affect the curve of growth (see Figures 3-3 to 3-9).

One of the few situations where collisional broadening may need to be considered is the technique of graphite furnace atomic spectroscopy. In many instances, a high concentration of species is added to serve as a matrix modifier. The added species will be vaporized in a small volume of the graphite furnace and result in a high atomic concentration.[43]

In a recent publication, Schlemmer and Welz[44] used an aliquot of Pd and Mg for matrix modification, resulting in an atomic concentration of 10^{16} to 10^{17} in a typical tube furnace atomizer. Collisional broadening effects become barely noticeable at this level. The curves of growth for Li with added Mg matrix modifier are shown in Figure 3-13. These curves are calculated in the same manner

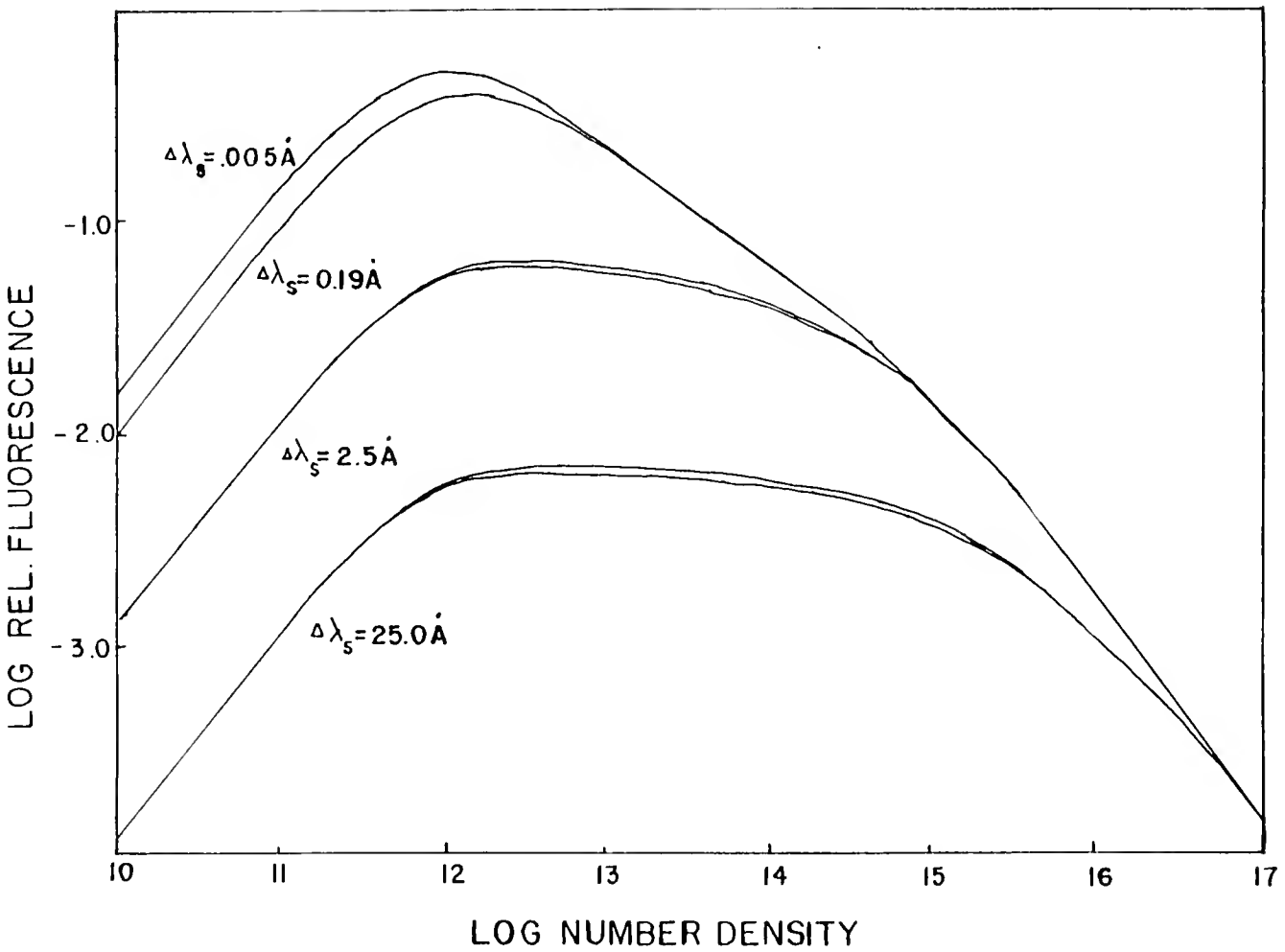

Figure 3-13. Curves of Growth with Added Collisional Broadening

as before (Figures 3-3 to 3-5) but with the added term for collisional broadening. Each of the relationships discussed previously, a-parameter dependence and source width dependence, are shown in this figure. The expected source dependence is seen in the curves of this figure. The differences calculated for the pseudocontinuum ($\Delta\lambda_s$ = 0.19 Å) and the line source ($\Delta\lambda_S$ = 0.005 Å) are too small to be seen here but occur in a region somewhat smaller than that seen in the other pseudocontinuum sources. These results represent an extreme case, not likely to be seen in conventional flame spectroscopy and only infrequently seen in nonflame spectroscopies. Generally, collisional and self-broadening effects will have a very small influence, and in fact may not be apparent at all.

Saturation (optical) effects are dependent on the source spectral irradiance and do not depend upon the analyte of interest, at least not in the same manner as the collisional broadening does. As seen in the expression for right-angle fluorescence (Figure 3-2), an increase of the source spectral irradiance $E(\lambda)$, above the saturation spectral irradiance $E^S(\lambda)$, will result in an effective decrease in the absorption coefficient. This decrease will occur at all wavelengths at which the source irradiance is above the saturation spectral irradiance. Prefilter terms are affected in the same manner as the primary absorption term. The self-absorption term may or may not be affected by saturation, depending upon whether the fluorescence wavelength is within the saturating source spectral profile. A postfilter region will not be affected by a saturating

irradiance since the source does not pass through the postfilter region. A complete discussion of saturation effects and practical measurement of saturation curves is given by Alkemade.[45]

Curves of growth for several source intensities are presented in Figures 3-14 and 3-15 for line and continuum sources, respectively. The general trend seen is an increase in the linear regions of these curves. No change of shape in the COG is seen. Curves of growth were also calculated for the same Pb transitions previously measured (283.3 nm resonance fluorescence and 405.7 nm direct-line fluorescence). These curves are shown in Figure 3-16 and are calculated for the same 0.019 nm source spectral width (FWHM) used previously. As seen in this figure, it is possible to extend the resonance fluorescence COG using a saturating source to equal linear dynamic range and even beyond that of the direct-line fluorescence case.

The source intensity at which equality occurs for the direct-line and resonance fluorescence curves can be shown to be related to the fractional populations of the two lower levels used. The equations relating the source intensity necessary for equality of the direct-line and resonance curves are shown in Figure 3-17. These are derived from the initial curve of growth equation. As seen in Figure 3-16, the equality for the resonance and direct-line curves occurs at a source irradiance approximately 100 times greater than the saturation irradiance for the lead transitions. This agrees with the ratios of the populations of the two levels 98.6% to 1.05%, a ratio of approximately 100 to 1. This is calculated using the continuum

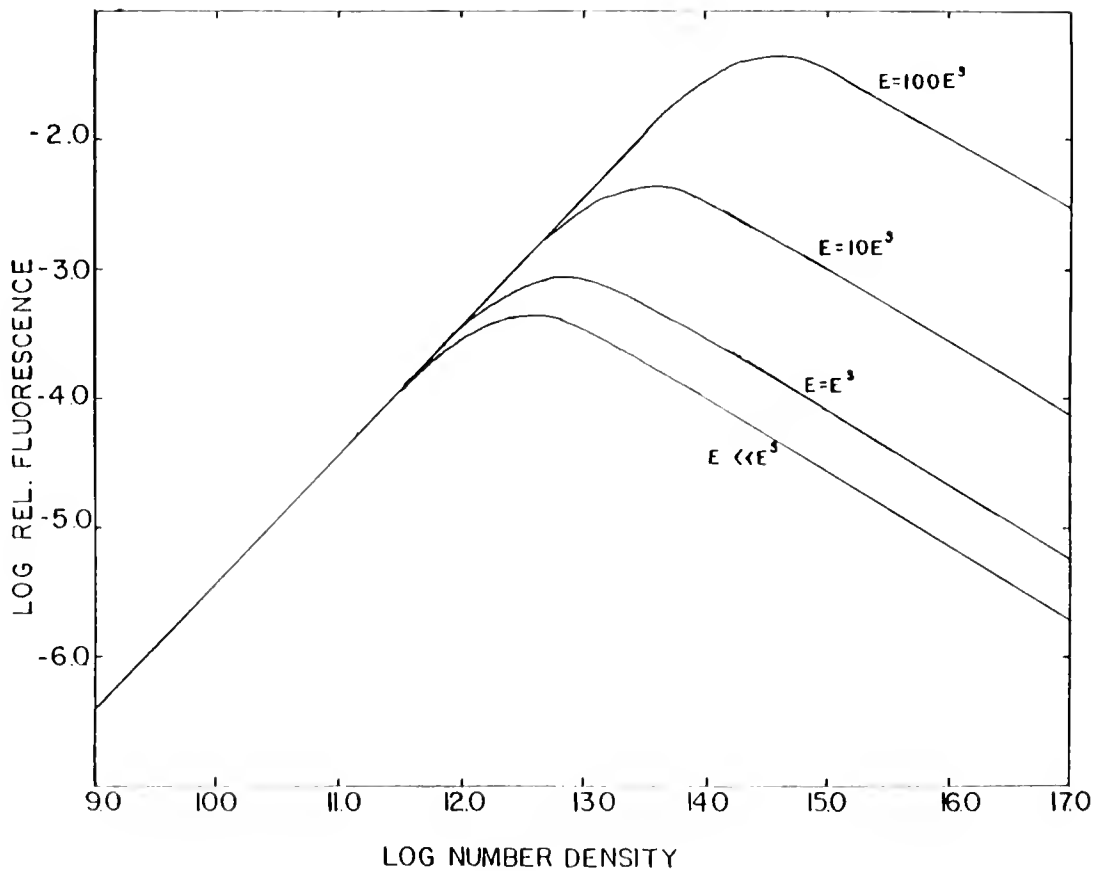

Figure 3-14. Curves of Growth for Several Intensities for a Line Source

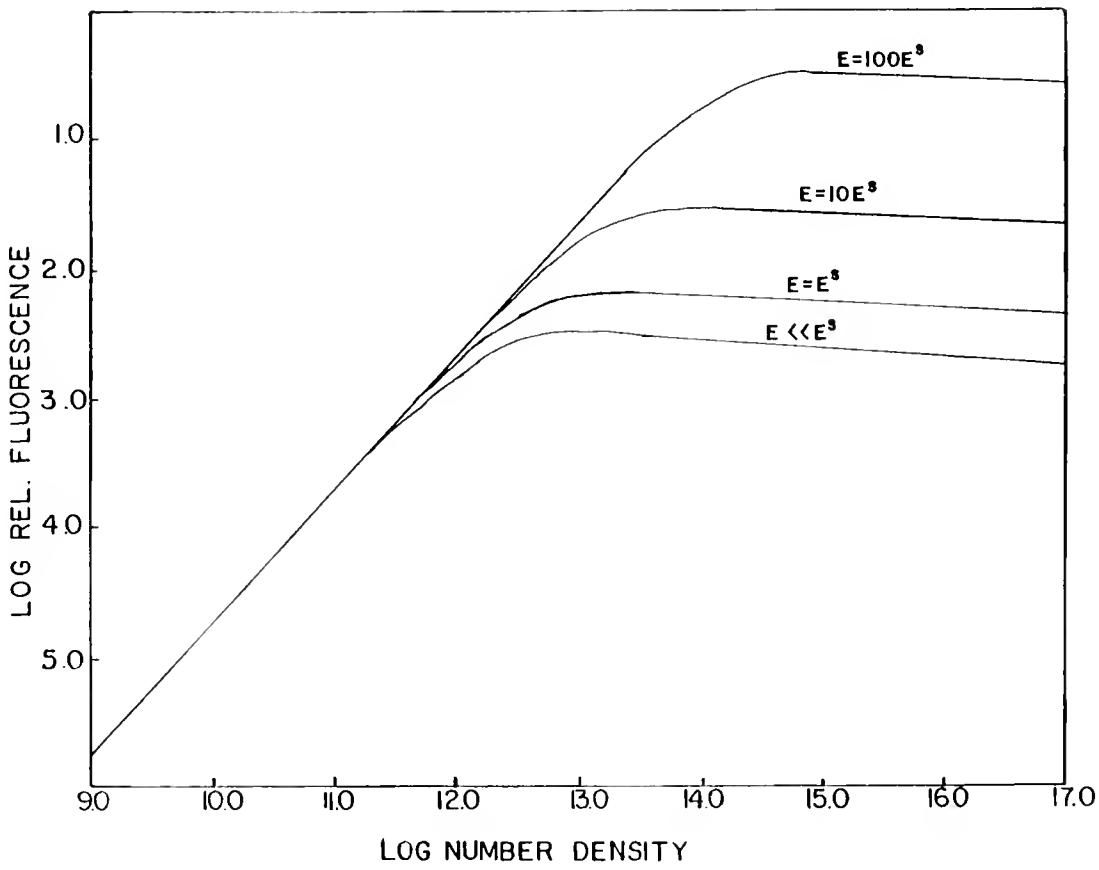

Figure 3-15. Curves of Growth for Several Intensities for a Continuum Source

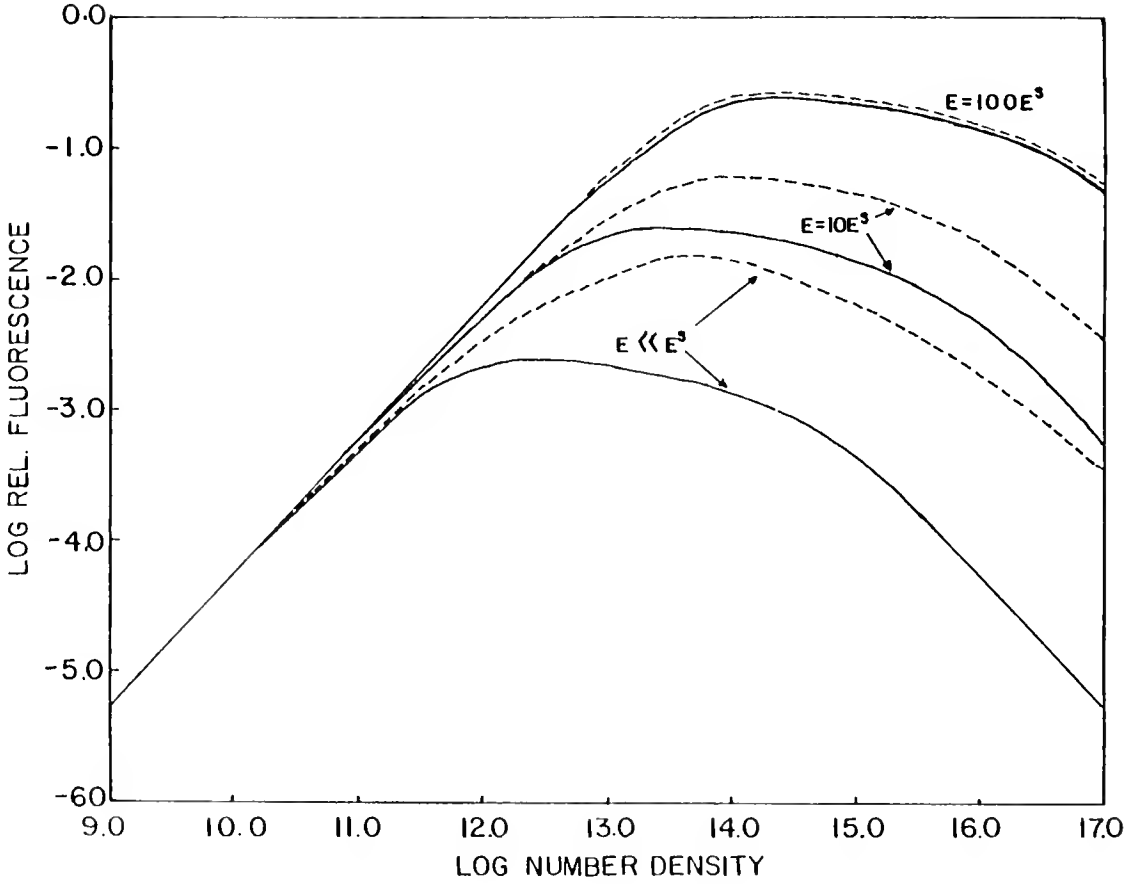

Figure 3-16. Curves of Growth for Pb Direct-Line (----) and Resonance Fluorescence (——) for Several Source Intensities

GENERAL CASE

$$\frac{\int_{-\infty}^{\infty} 1 - e^{-k(\nu)\frac{E_\nu^s}{E_\nu^s + E_\nu} L}\, d\nu}{\int_{-\infty}^{\infty} 1 - e^{-k(\nu')L}\, d\nu} = \frac{k_o}{k_o'}$$

LINE SOURCE CASE

$$\frac{k_o V(a,v) \frac{E^s}{E + E^s}}{k_o' V(a', v')} = \frac{F_1}{F_2}$$

CONTINUUM SOURCE CASE

$$\frac{\delta \nu_D k(\nu) \frac{E_\nu^s}{E_\nu^s + E_\nu}}{\delta \nu_D' k(\nu')} = \frac{F_1}{F_2}$$

Figure 3-17. Equations for Curves of Growth Equalities for Saturating Irradiances

source approximation since the source spectral width (FWHM) is roughly 25 times larger than atom profile and as such closely approximates a continuum.

The prefilter and postfilter effects with a saturating laser source (0.019 nm) are shown in Figures 3-18 and 3-19. A 0.5 cm prefilter length and a 0.5 cm postfilter length were used in the corresponding curves. A 0.5 cm absorption path and a 0.5 cm fluorescence path length are used in all curves here. In both cases, it is possible to extend the calculated curve of growth to some extent. Curves with prefiltering show the greatest extension. This is due to removal of prefilter effects by the saturating laser and an extension of the primary absorption linear region. The constant difference between the curves of growth with and without prefilter is due to the decreased source irradiance passing through the detected volume. This corresponds to an additional primary absorption term with no additional fluorescence. For the postfilter curves of growth in Figure 3-19, the difference between the curves with and without postfilter is seen to increase with increasing source irradiance. The increasing difference between curves is due to the increase in linearity of the curve which does not have postfiltering while the curve with postfilter does not have the same increase in linearity. If the source intensity is increased drastically, the overall curve of growth will become limited by the curvature due to the postfilter region. In no manner is it possible to remove postfilter effects by using a more intense source.

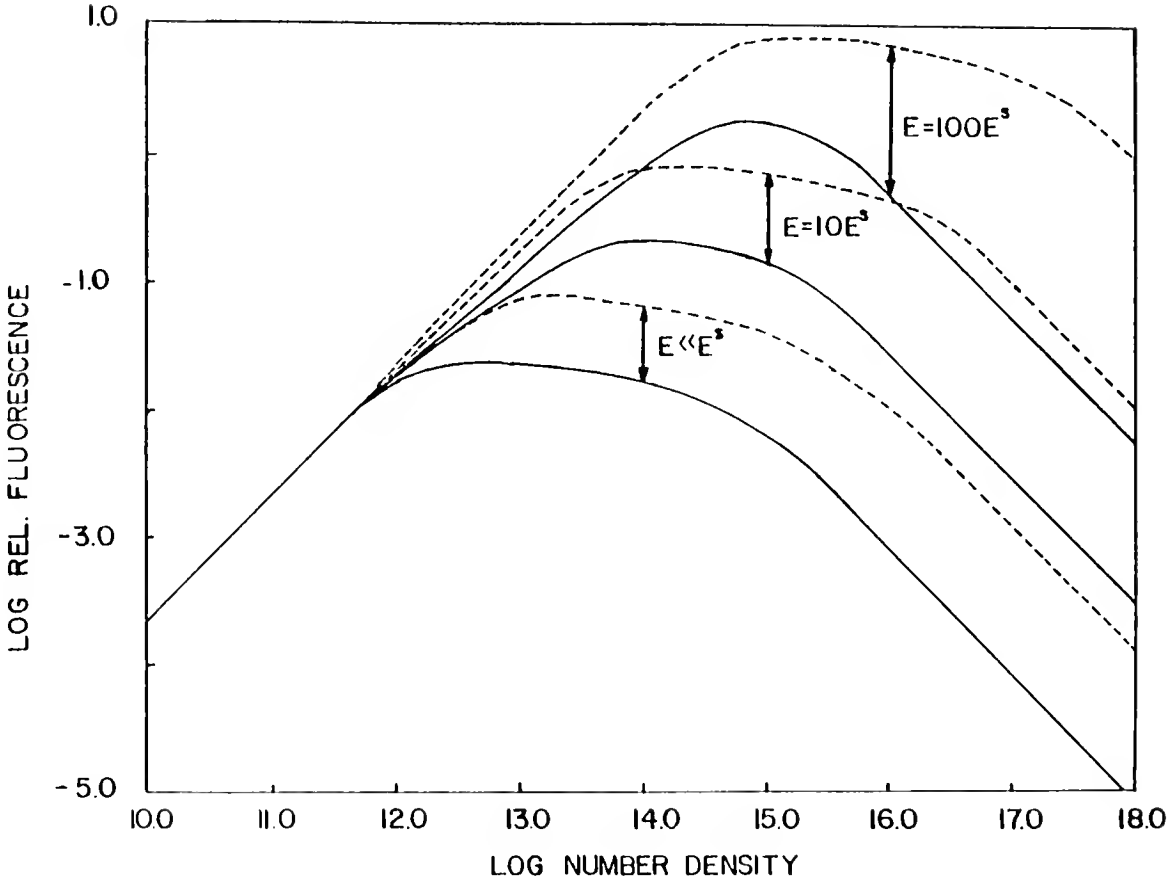

Figure 3-18. Prefilter Removal by a Saturating Source, Resonance (——) and Direct-Line (----)

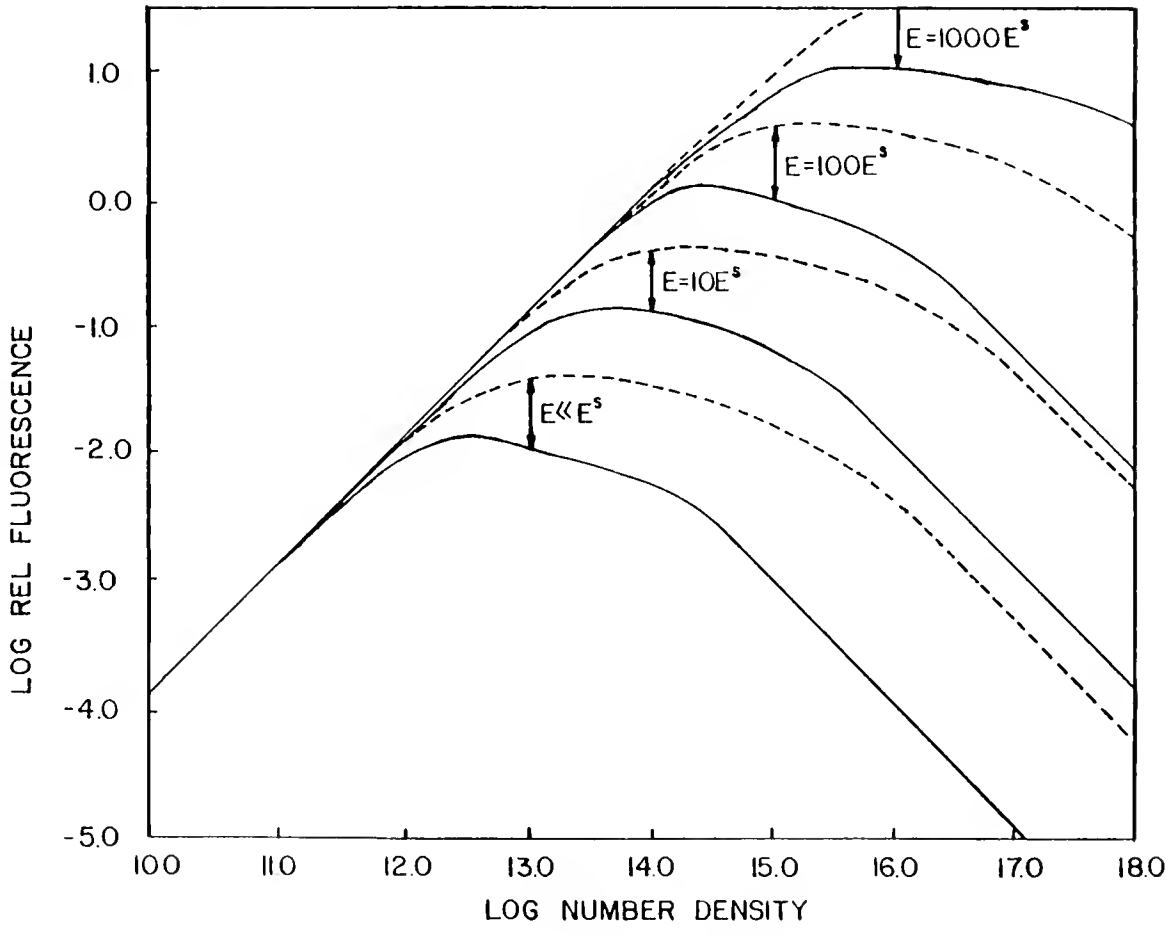

Figure 3-19. Postfilter Effects with Saturation Effects Added, Resonance (——) and Direct-Line (----)

Conclusions

A general purpose computer program has been presented and is investigated for applications to determine the absolute number density of an atomic species. Various aspects of this curve of growth program have been investigated including prefilter and postfilter effects, saturation using various sources and collisional broadening due to resonance broadening and broadening due to quenchers.

It was found that collisional broadening, in all forms, should present very minimal effects if they are seen at all. Prefilter and postfilter regions are shown to cause a premature curvature of the curve of growth. Prefilter and postfilter effects may be accounted for and an absolute number density obtained if the exact geometry is known. The prefilter effect may be removed to a large degree by a saturating excitation source. The use of a saturating source may not be desirable, as it adds another complication to the curve of growth measurement and calculation of the absolute number density. Much of the work of this chapter has been theoretical in nature and some would be difficult to verify experimentally. Nevertheless, the experimental results obtained for two of the simpler cases discussed in this chapter show extremely good agreement between the calculations and the experimentally measured results.

CHAPTER 4
SPATIAL DISTRIBUTIONS OF ATOMS IN INHOMOGENEOUS FLAMES

Concentration Modulated Absorption Spectroscopy

A technique for increased sensitivity in atomic absorption spectroscopy with pulsed lasers was recently introduced by Langley et al.[46] The technique was employed by the authors to yield absolute number densities for atoms in flames and for molecules in solutions. This experiment is based on a pump-probe arrangement of optical beams and relies on a linear relationship between source intensity and fraction absorbed. This technique, along with two other related techniques using pulsed lasers in atomic spectroscopy, are applied for the determination of spatial distributions of atoms in inhomogeneous flames and are described in this chapter.

Many of the techniques presented in Chapter 1 are not applicable to spatial profiling. This is due to the moderate to low sensitivity of those techniques and the small region, and thus the small atomic concentration, probed by these methods. The combination of these two limitations and the limitations presented by pulse-to-pulse instabilities and the spectral bandwidth of some pulsed dye lasers make many techniques unsuitable for spatial diagnostics.

Concentration modulated absorption spectroscopy (COMAS) was initially applied by Langley et al.[46] for absolute number density determination. The development of the COMAS expression follows from

the interaction of two focused Gaussian beams and is based to a large degree on the Beer-Lambert absorption expressions.[47] The beams are assumed to be derived from the same pulsed laser source with a spatially Gaussian electric field amplitude. From the Beer-Lambert absorption expression, the change in the number of laser photons in an incremental length dz will be

$$di_p = \sigma n \Delta i_p dz$$

where i_p is the number of laser photons, Δ is the equilibrium fractional population between levels 1 and 2, and σ is the absorption cross section. This fractional population is equal to the difference of levels 1 and 2 divided by the total analyte concentration $\Delta = (N_1 - N_2)/n$. Based upon expressions for focused Gaussian beams and the interaction volume for these beams, an expression for the modulation of the probe signal is obtained:

$$di_{pr} = (2\pi\sigma^2 n\Delta/\lambda) i_p i_{pr}.$$

Obtaining the fractional change in the number of probe photons or gain gives

$$di_{pr}/i_{pr} = G = (2\pi\sigma^2 n\Delta/\lambda) i_p.$$

Substituting the original Beer-Lambert law $\ln(1/T) = \sigma n \Delta$ and

substituting for σ gives $G = (2\pi i_p/(n\Delta\lambda))(\ln(1/T))^2$. A plot of gain times concentration vs $\ln 1/T^2$ will give straight-line plot, the slope of which is the proportionality factor in the relationship between concentration and analyte number density $C = xN\Delta$ where C is the analyte concentration. Thus, this experiment was viewed as a way of obtaining an absolute number density which required only measuring readily available analytical signals in a relatively simple optical arrangement. Some optical restrictions were applied in the development of the expressions which limit the applicability of these equations.

The development of the COMAS expressions is not questioned here, and in fact extremely good results are obtained by Langley et al.[46] for molecular solution-phase analyses, but the assumption of a true Beer-Lambert relationship for excitation of atoms in flames with a relatively broad spectral width dye laser is not valid. The Beer-Lambert relationship works well for molecular analyses since the molecular absorption band is typically much wider spectrally than the line width of the dye laser excitation source used. The results for molecular analyses by Langley et al.[46] were easily checked assuming no solution phase decomposition and were found to be 7.4×10^{15} molecules/cm^3 experimentally for a solution concentration of 6.0×10^{15} molecules/cm^3. When considering the atomic experiments, the dye laser spectral bandwidth is much wider than the atomic line width. Using the expression in Figure 3-2 for the primary absorption term of the fluorescence curve of growth, a difference in signals of 5 times (for the low-density linear region) is calculated for the signals

expected with a narrow line source and the signal obtained with a source width 10 times greater than the Doppler width of the atom. This will result in a direct error of the absolute number density determined by this factor. A correction for this error may be obtained by evaluating the overlap of the two profiles expected and a correction factor obtained.

The concentration modulated method involves a pump-probe arrangement of optical beams as shown in Figure 4-1. In this arrangement the probe is approximately 5% of total dye laser output. This method was originally investigated for Na in an air-acetylene flame. The same copper vapor laser and dye laser system presented in Chapter 2 were used for this application. The bandwidth limitation approach was used for the absorption measurements.

An initial investigation of the method presented by Langley et al.[46] was carried out. This arrangement of counterpropagating co-linear beams involves modulation of one of the two beams. The COMAS signal is obtained by subtraction of the absorption signal with and without the pump beam present. Subtraction of the two signals is obtained using the active baseline subtraction method employed in Chapter 2. The absorption signals were detected by a fast photodiode (United Detector Technology, model PIN-10DP) and connected to a current-to-voltage converter (Thorn EMI Gencom Inc., model A1). These signals were connected directly to the gated integrator and boxcar averager. The COMAS experiment conducted by Langley et al.[46] was confirmed and a limit of detection of 1 part-per-million (ppm)

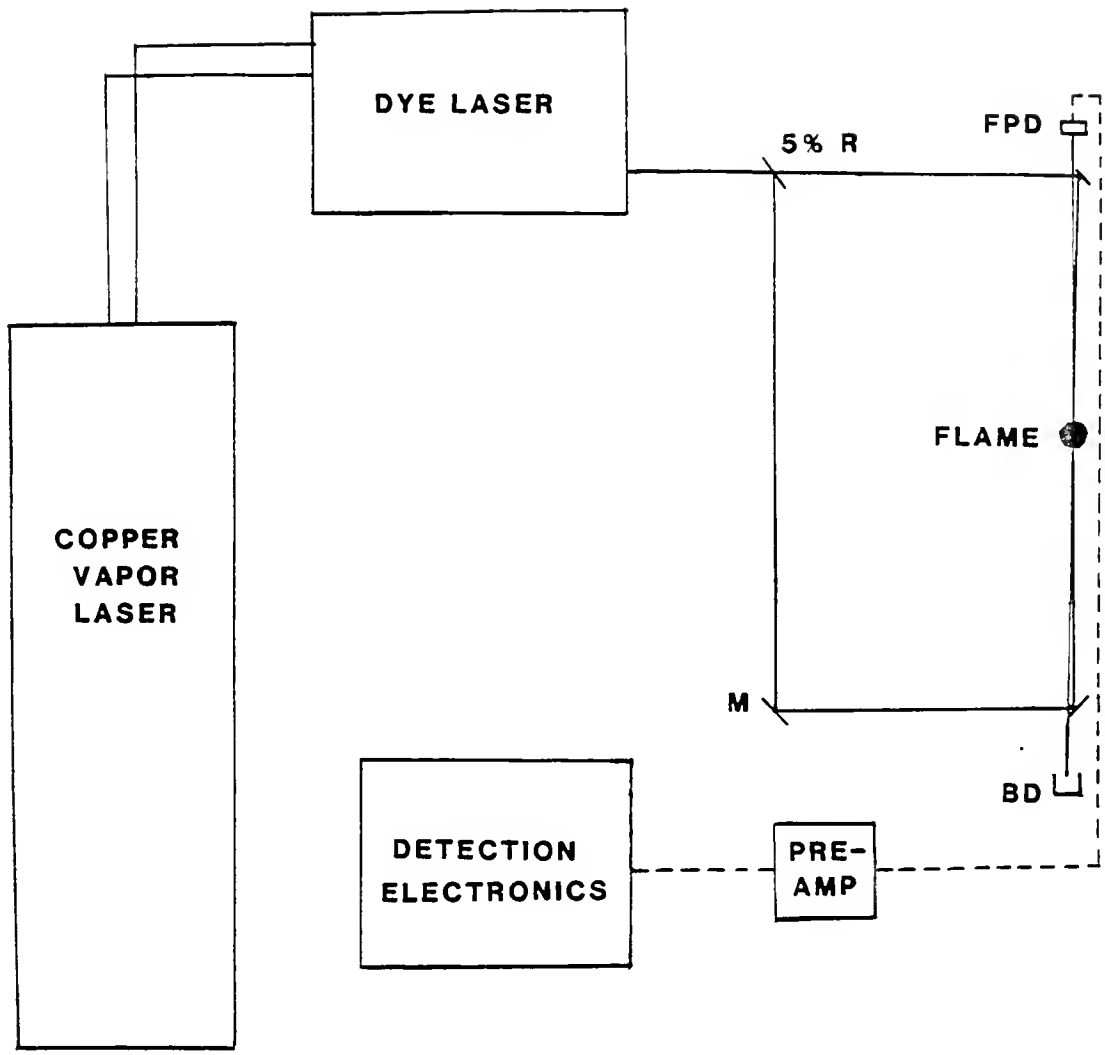

Figure 4-1. Concentration Modulated Absorption Experimental Setup: Co-linear Beams

was found for an interaction volume of approximately 1 cm^3. This agrees closely with previous results found.[46] The COMAS technique relies on the linear interaction of the two beams and allows direct determination of absolute number densities. Better limits of detection are obtainable with simple experiments using hollow cathode lamps.[48]

An extension of COMAS was attempted to determine spatial concentration profiles. The arrangement of optical beams was modified to form a pair of crossing beams (Figure 4-2). A scanning motor (General Scanning Inc., model G3) with a mirror attached and a pair of lenses was added to scan a focused probe beam through the flame. The scanner in conjunction with the first lens serves to position the probe beam within the flame. With the first lens positioned at a distance of one focal length from the scanning mirror, beams from the scanning mirror pass through the flame perpendicular to the pump beam. The second lens served to turn the probe beam and redirect the beams to the photodiode detector. The scanning is controlled by the computer interface (Stanford Research Systems, model 24S) and allowed rapid collection of the entire spatial profile of the flame. For these experiments the computer controlled the scanning of optical beams and collection of all data. For increased spatial resolution several optical elements were added. A small pinhole, diameter 0.5 mm, was used in the optical path of the probe beam to limit the beam size. Additionally, a lens was used in the optical path of the pump beam to produce a smaller beam. Relatively long focal length lenses (200 mm, 2" dia.) were

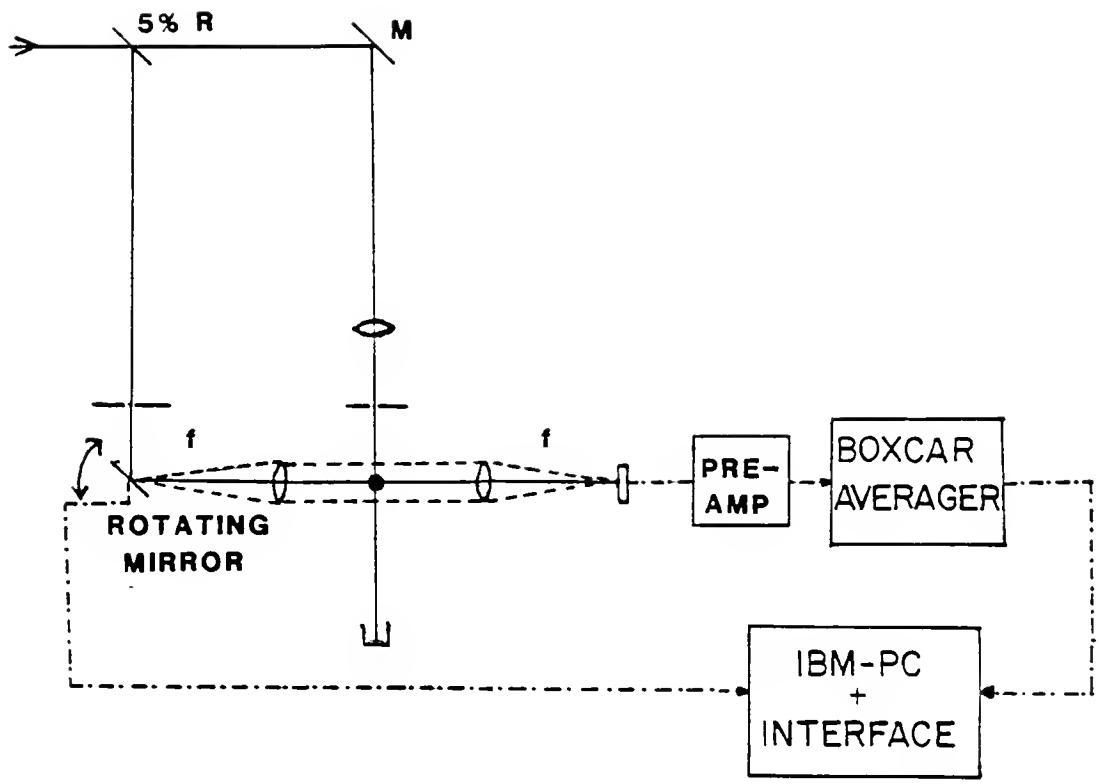

Figure 4-2. Experimental Setup for Spatial Diagnostics for COMAS

used in all cases. These lenses provide a relatively uniform beam waist over the width of the flame.[49] The volume probed by the interaction of these two beams is approximately 0.1 mm^3 (0.4 mm diameter probe by 0.5 mm diameter pump). This interaction volume is calculated using the method of Jackson et al.[50] and relies on the overlap of two spatially Gaussian beams. The beams were measured and closely approximate a Gaussian spatial profile. Additionally, the spectral line profile of a dye laser has been measured here by scanning the dye laser across an atomic transition and elsewhere by this and other[51,52] methods and closely approximates a Gaussian spectral profile. The optical arrangement used allows scanning while maintaining the same optical axes and beam size. Horizontal beam placement was found to be extremely important for a uniform interaction region. The results obtained for scanning the flame produced by an inhomogeneous surface burner[23] are shown in Figure 4-3. The surface burner used in these experiments was provided courtesy of Dr. R.J. Krupa and the construction is shown in Figure 4-4. The COMAS results are shown for an initial solution concentration of approximately 5000 ppm Na. The COMAS results are shown for a single region located above one row of analyte capillaries in both the parallel and diagonal burner orientations. The measurements were taken in a region approximately 6 mm above the surface of the burner head. This corresponded to the top of the flame cones[53] for gas flow rates of 1.6 l/m acetylene, 2.2 l/m oxygen, and 8.3 l/m nitrogen with this type of surface burner. Based on a measured nebulization efficiency of 0.14 and an estimated

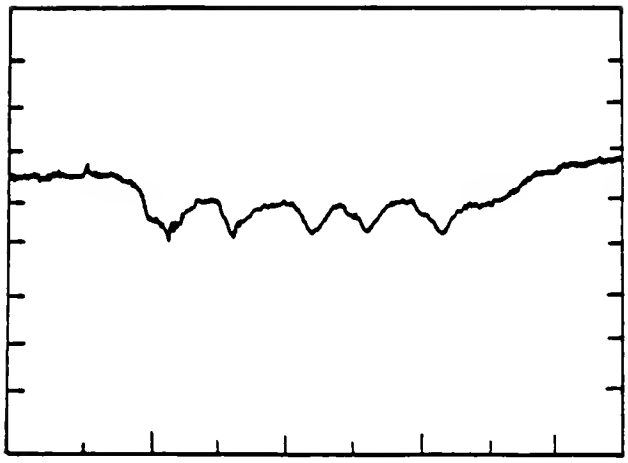

5000 ug/mL Na

PERPENDICULAR BURNER

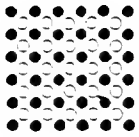

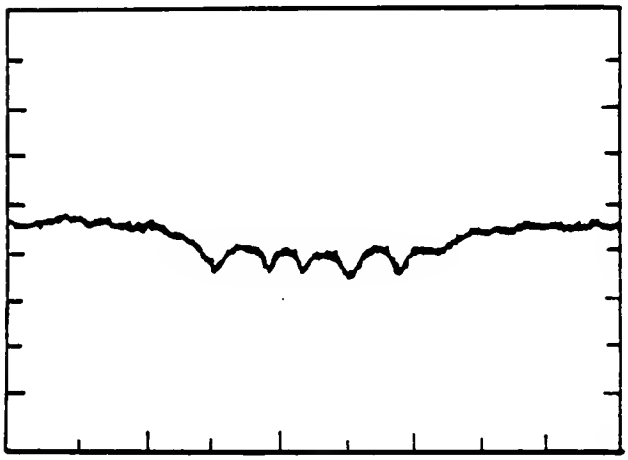

5000 ug/mL Na

DIAGONAL BURNER

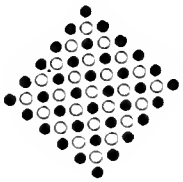

CONCENTRATION MODULATED ABSORPTION

Figure 4-3. Results for Perpendicular and Parallel Burners for COMAS

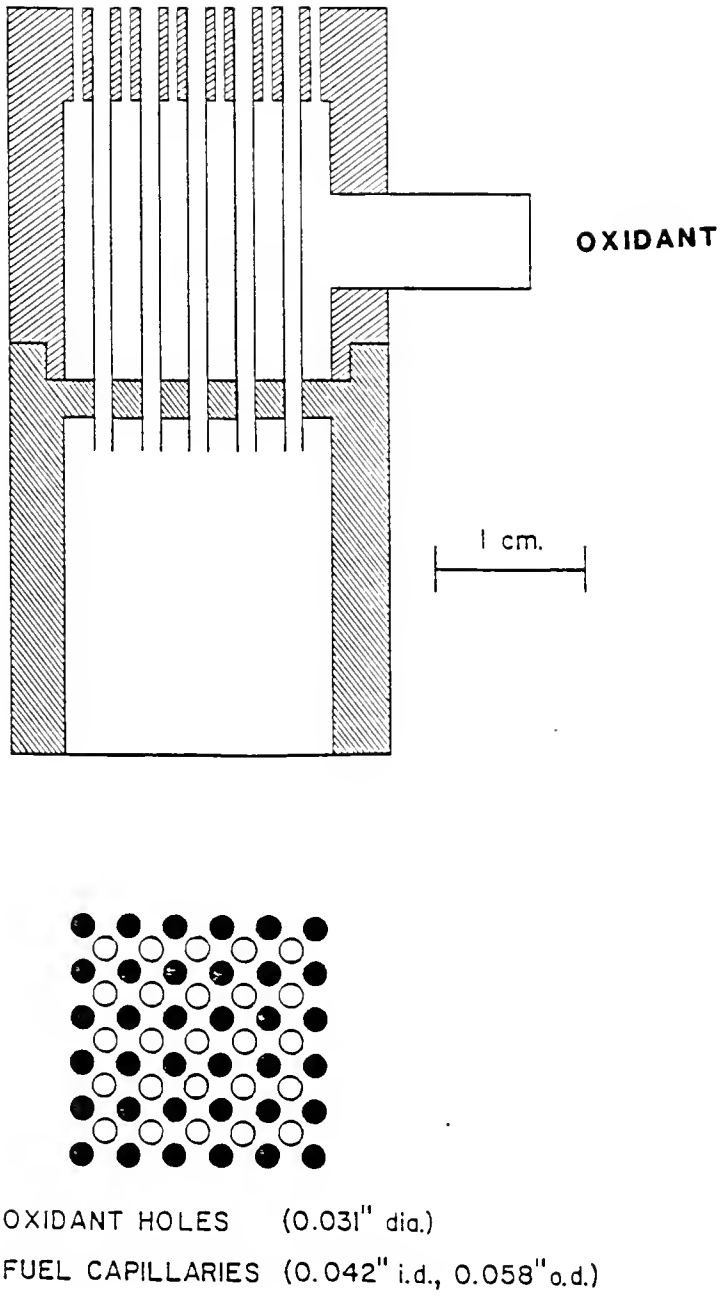

Figure 4-4. Design of Surface Burner Used

atomization efficiency[54] of 0.6, the analytical region of 0.1 mm^3 calculated for the COMAS crossed beam experiments should have ~10^{13} atoms present during each laser pulse. The relative insensitivity of this technique is seen in the high concentration of analyte necessary to obtain any analytical signal. This low sensitivity is due to several experimental problems. The relatively large spectral bandwidth of the dye laser (0.3 A) is approximately 6 times greater than the Doppler-width (FWHM) of Na in an air-acetylene flame with an estimated temperature of 2500°C. This large bandwidth results in unabsorbed source irradiation reaching the detector and increased background shot noise. The peak-to-peak fluctuation of the dye laser intensity also limits the minimum absorption measurable.[55] Radio-frequency noise is also thought to contribute to some degree (see Chapter 2). At any rate, COMAS has been found to be too insensitive for applications in spatial profiling.

The minimum detectable signal may also be calculated based upon the spectral bandwidth of the laser, the parameters for Na in an air-acetylene flame, the region probed in the interaction volume and the minimum detectable absorbance which may be typically measured.[56] The same curve of growth program used in Chapter 3 is used for this calculation with only the primary absorption term calculated (see Figure 3-2). The minimal concentration detectable based on this calculation and a minimum detectable absorbance was found to be approximately 1000 ppm Na. This does not consider the effect of pulse-to-pulse fluctuations of the laser or any shot noise or radio-frequency (RF) noise added by the laser.

Results were also obtained for a simple atomic absorption experiment with only the relatively weak probe beam and optical scanning system (no pump beam). Results for the parallel and diagonal burner configuration are shown in Figure 4-5. Again a solution concentration of 10 ppm Na was used for these experiments. The increased sensitivity of this technique is seen immediately since these results are for an initial atomic concentration 50 times lower than the COMAS results. This increase in sensitivity is accomplished at a loss in spatial information since the analytical signal is obtained for the entire absorption path length (1 cm or greater for the burner used) and are not obtained for a much smaller interaction region. The interaction volume is approximately 1.3 mm^3 (0.4 mm diameter by 10 mm (or greater in the diagonal burner case)), approximately 13 times greater than in the COMAS case. This accounts for a significant portion of the increased sensitivity. The spatial information obtainable with this system is still somewhat remarkable. Since the laser beam is coherent and has an extremely low degree of divergence, good spatial resolution may be obtained. An attempt was made to perform the same series of experiments with a hollow cathode lamp. The hollow cathode lamp, with its much narrower spectral bandwidth (compared to the dye laser), should have had a higher sensitivity. No suitable optical arrangement could be found to give a tightly focused beam within the flame volume. With the high repetition rate of this laser and the fast optical beam scanning method employed, entire spatial profiles of the atom cell may be obtained in a very short period of time.

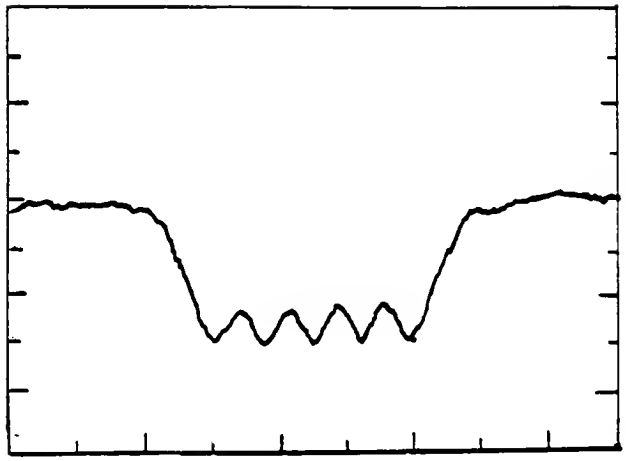

10 ug/mL Na

PERPENDICULAR BURNER

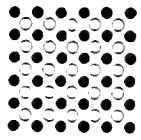

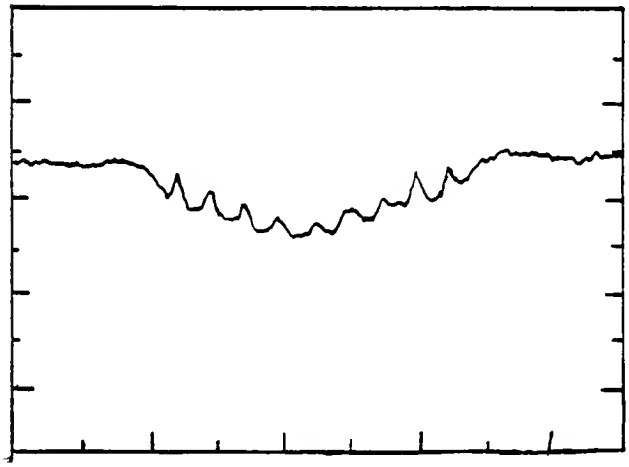

10 ug/mL Na

DIAGONAL BURNER

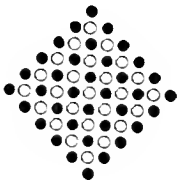

SIMPLE ABSORPTION

Figure 4-5. Simple Absorption Results for Perpendicular and Parallel Burners

In an attempt to decrease the spectral bandwidth of the dye laser, an etalon was added within the oscillator cavity of the dye laser.[57] The decreased spectral bandwidth would have resulted in an increased sensitivity in all absorption results. The etalon was found to reduce the oscillator cavity gains to such an extent that lasing would not occur. The dye laser was then switched to an oscillator-only configuration with 100% of the copper vapor laser output used to pump a single dye laser cell. The etalon was found to increase cavity losses[58] and decrease the stability of the dye laser (in terms of pulse-to-pulse fluctuations) and gave only a slight reduction in the spectral bandwidth (0.3 Å to 0.18 Å). The only slight reduction in the spectral bandwidth of the dye laser is due to the relatively poor quality of the etalon used.

Concentration modulated absorption spectroscopy was initially investigated by us as a means of performing spatial profiling and determining absolute number densities. The low sensitivity of the technique prevented this application; in addition, complications far beyond those expected were present. As a result of these complications, other methods were investigated for increased sensitivity in spatial profiling applications.

Two-Wavelength Laser Enhanced Ionization and Fluorescence: Spatial Distributions

In several recent articles,[18-20] the use of laser excited fluorescence for spatial distribution measurement has been studied

using a planar laser beam and a 2-dimensional image detector. The spatial resolution element for this technique was found to be ≈1 mm^3 with concentrations between 1 and 20 ppm being used for spatial profiling results. In other studies, spatial profiles have been measured in inductively coupled plasmas[59] and in flames[60] with a lens and image detector or lenses and monochromators used to obtain the spatial profiles. One advantage of image detection has been pointed out in a recent publication where spatial information was obtained in an entire plane within the flame volume on a single laser pulse.[61] Other studies have included probing of local electrical fields in flames using LEIS which involved measurement of the atomic line widths.[62] The electrically-broadened atomic line width is a measure of the strength of the local electrical field. Several of these methods are applied later in this chapter for similar applications with some modifications.

Two of the most sensitive methods for atomic species determinations in flames are laser excited atomic fluorescence spectrometry (LEAFS) and laser enhanced ionization spectrometry (LEIS). The sensitivity of these techniques has been discussed previously in Chapters 2 and 3 and the discussion is extended here. Recent results presented by Magnusson et al.[63,64] and Axner et al.[65] in graphite furnaces and flames, respectively, show limits of detection which approach 1 part-per-trillion (ppt) for single wavelength excitation. For two-wavelength excitation in a graphite furnace, results approaching 1 pg absolute limits of detection have been obtained. Two-wavelength excitation was found to give an

ionization signal enhancement of up to 6000 times over single wavelength excitation.[64] With the high temperatures present in an inductively coupled plasma (ICP) and the hazards of arcing of the high power radio-frequency field, an optical method of detection of laser induced ionization was presented by Turk et al.[66,67] This is instead of an electrode placed within the atom cell. As yet, no one has applied two-wavelength LEIS and LEAFS for spatial measurements.

Experimental Setup and Discussion

The experimental arrangement of optical beams for two-wavelength LEIS and LEAFS for spatial diagnostics is shown in Figure 4-6. This is an extension of the technique presented previously for COMAS with an additional wavelength of excitation and fluorescence and ionization detection instead of an absorption detection method. The same copper vapor laser used earlier was also used here. The beam from this laser was used to pump two dye lasers. The dye lasers used (Hansch-design) were pumped in the oscillator-only configuration.[58] That is, only one flowing dye cell in each dye laser was excited by the copper vapor beam. This was found to be a more efficient method for pumping the dye lasers since the power per pulse of the copper vapor laser is relatively low. Approximately 40% of the copper vapor beam was used to pump the first dye laser with the remainder used in the second. A fast photodiode placed at the end of the second dye laser received the small fraction of the copper vapor beam which was not reflected by the 99% reflector in the second dye laser. The signal from this photodiode was used to trigger the boxcar detection

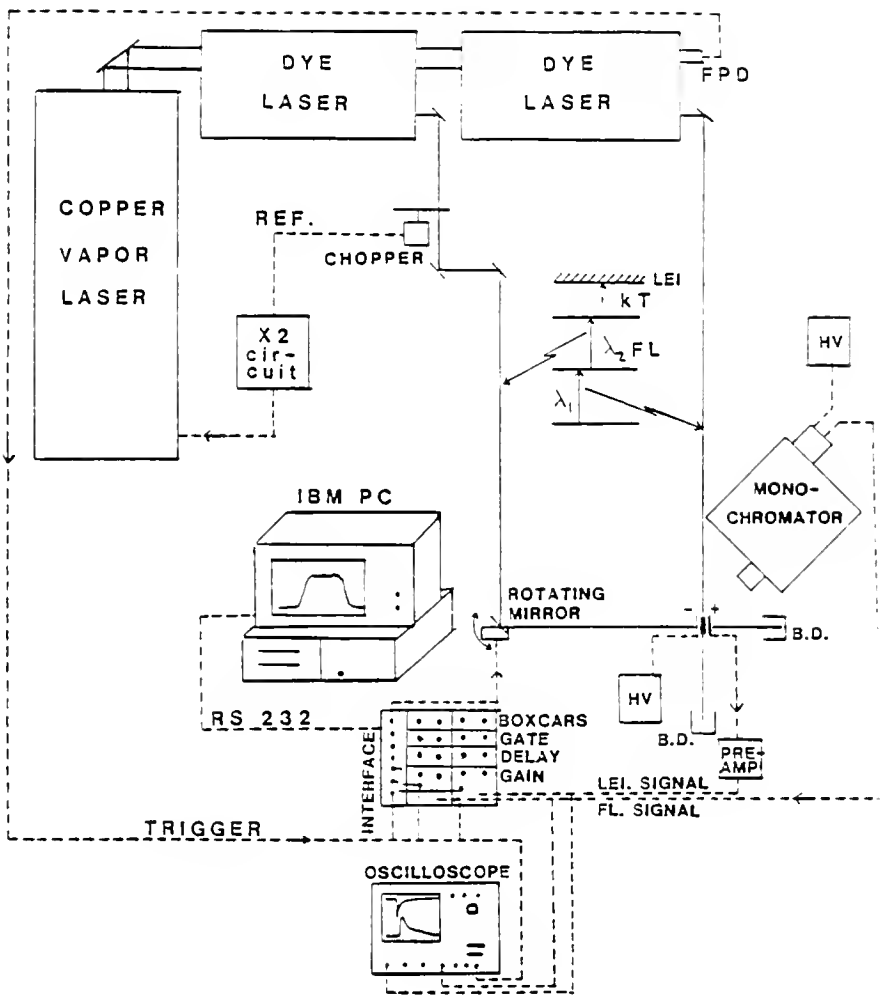

Figure 4-6. Experimental Setup for Two-Wavelength LEIS and LAFS

electronics and the oscilloscope. The same signal, used to trigger the boxcars, was divided by multiples of 10 to trigger the computer interface. This division was necessary in many instances since the computer interface was only capable of transferring data to the computer at a rate of 960 samples per second. The necessity of division was dependent on the number of data points taken since the computer interface contained a buffer memory which accumulated untransferred data points. Scans across the burner in one direction were obtained using the rotating mirror. To obtain the total profile across the burner, the burner itself was translated using a micrometer stage, with profiles obtained at several positions using the rotating mirror. An initial attempt to obtain profiles by positioning the λ_1 beam at different places within the flame volume was investigated. Voltage field variances and voltage field collection effects were found which complicated all spatial results obtained. With a water-cooled bias electrode (-1500 V) placed directly in the flame, spatial profiles were obtained. When the λ_1 laser beam was positioned directly under and parallel to the electrode, signals were found to reach a maximum. Translation of the laser beam, while maintaining the same burner and electrode position, to a horizontal distance of approximately 0.5 cm from directly under the electrode, but still at approximately the same atomic concentration (see COMAS and absorption results), the analyte signal was found to drop by more than one order of magnitude. This is due to field collection effects and voltage field differences. Other field collection effects have been investigated by other

authors.[62,68] To minimize voltage field effects, the burner head was translated and was found to give no appreciable voltage field effects when measured by the method of Axner and Berglind.[62] The placement of a large electrode within the flame volume does disturb the laminarity and shape of the flame and may result in somewhat distorted profiles. For these reasons, fluorescence was investigated as an alternate means of detection.

In the course of these investigations, several important factors were discovered. To obtain a uniform interaction volume and an equal sensitivity over the entire optical path probed, the two optical beams had to be horizontal and intersect or remain a fixed distance apart, over the entire distance probed. Additionally, the burner and electrode also had to be horizontal to maintain a constant distance between the laser beam and the electrode and to reduce voltage field effects.

A typical profile obtained in a single scan is shown in Figure 4-7. This profile was obtained approximately 7 mm above the surface of the burner at the tips of the flame cones. This profile was obtained for an initial atomic concentration of 1 ppm Na with excitation at 588.9 nm and 568.8 nm. From the signal-to-noise ratio apparent in this figure, the atomic concentration produced by 1 ppm Na is well above the limit of detection. These results were obtained for a 1000 point scan, each point representing an average of 10 laser shots (for reasons discussed earlier). With the high repetition rate of the laser and the data acquisition system, these results required only 1.67 s to obtain. Thus, the speed, ease, and high capacity for

information gathering is shown. The slightly irregular profile obtained for this case is due to a slight flow constriction in one of the analyte capillaries. This only served to illustrate the analytical usefulness of this technique, as it was possible to correct this flow restriction in later studies. Two arrangements of optical beams were investigated for these studies. These arrangements involved swapping the positions of the two laser beams. Each arrangement had its own advantages. When the first wavelength laser (λ_1) was positioned directly under the electrode, a large pulsed ionization current was created by λ_1. The ionization current created by λ_2 occurs only in the interaction region. Thus the current produced by λ_1 had to be subtracted from that due to $\lambda_2+\lambda_1$ to obtain the interaction volume. The current due to λ_1 produced a background shot noise which could not be corrected for. An additional consideration was the thermal population of the lowest excited state. Thermally excited atoms are excited by λ_2 and collected.

In the first configuration with λ_1 directly under the electrode, the collection of thermally excited and optically excited (λ_2) atoms was limited by the electric field decrease with distance away from the electrode. In the second configuration with λ_2 directly under the electrode, there was a lower background current produced due to λ_1 but a higher current which could not be corrected for due to thermal excitation of atoms. The best analytical scheme would be that one which gives the lowest background signals. It would seem

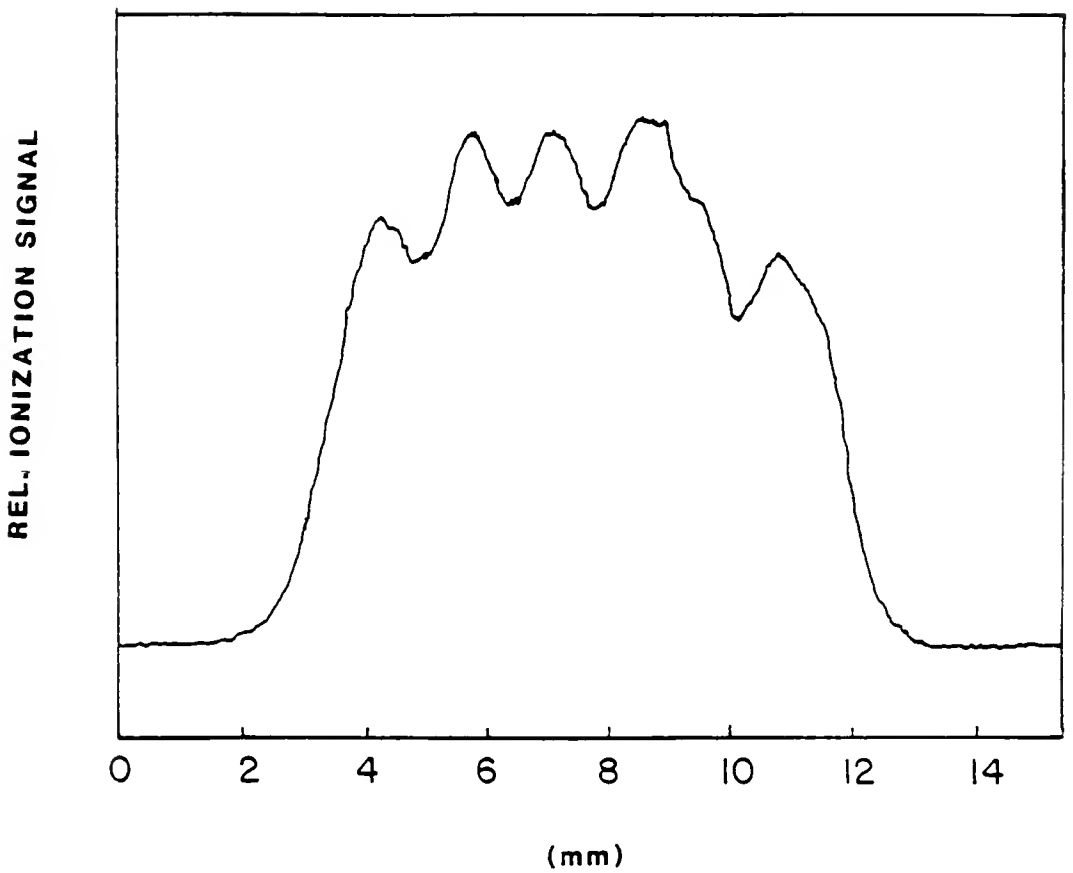

Figure 4-7. Spatial Profile Result for LEIS

that as long as λ_1 is of higher energy than kT, the first scheme would be best but this is complicated by the electric field effects and the intensities of the lasers employed. For these experiments, the first configuration was found to give better signal-to-noise ratio. The contributions of the thermal, electric field, and optical arrangement effects to signals obtained, corrections obtainable and noises for each ionization process are summarized in Table 4-1.

The best arrangement for subtraction of signals due to ionization outside the interaction region would involve modulation of both λ_1 and λ_2. A modulation scheme which would give equivalent results for both optical arrangements would be to sequentially excite the analyte with λ_1, then λ_2, and then the combined beams, $\lambda_1+\lambda_2$. The analytical signal would be obtained by subtracting the single wavelength signals from the combined signals $\lambda_1+\lambda_2$. Such a modulation scheme would involve custom design of the optical choppers or the use of acousto-optic deflectors and electronic circuits to form the modulation pulses. Demodulation of the signals obtained would be complicated also and would require a custom design lock-in amplifier. Considering the complications expected from the discussion above and the minimal improvement expected, this method of correction was not attempted. This method of modulation would also use three pump laser pulses for each data point and shift the effective data taking rate to 2 kHz for this laser system. For any pulsed laser system other than copper vapor (or mode-locked cavity-dumped lasers), this modulation scheme would result in a shift in the data taking rate back into a flicker noise dominated region (i.e.,

Table 4-1. Ionization Processes, Optical Arrangements, Signals and Noises for Two-Wavelength Laser Enhanced Ionization Spectroscopy

PROCESSES	SIGNALS
1	Nonspecific thermal ionization of atoms and molecules
2	Ionization due to λ_1 and thermal processes
3	Ionization due to thermal processes and λ_2
4	Ionization due to $\lambda_1+\lambda_2$ in interaction region

OPTICAL ARRANGEMENTS	
1	λ_1 directly beneath electrode, λ_2 perpendicular
2	λ_2 directly beneath electrode, λ_1 perpendicular

PROCESSES	1	2	3	4
CORRECTION METHODS	D.C. signals blocked by boxcar input capacitor.	Modulation of λ_2	Modulation of λ_1	Analytical signal. No correction necessary.
NOISES	Shot noise due to D.C. signal. Equivalent noises for both optical arrangements. Magnitude will vary for different elements. Analyte & background fluctuations corrected for by modulating λ_1 or λ_2.	Signal magnitude and noise greater for arrangement 1. Shot noise uncorrectable.	Signal magnitude and noise greater for arrangement 2 but smaller than that due to process 2 in arrangement 1 (due to lower population of excited state).	Noises and signal are the same for both optical arrangements.

$\tilde{<}$100 Hz). The only laser system which comes close to the high-repetition rate needed is a 500 Hz excimer system, with an effective data taking rate of approximately 160 Hz. This is still within the flicker noise region for a typical analytical flame.

Similar results were obtained for two-wavelength laser excited atomic fluorescence spectrometry (LEAFS). A lower sensitivity is obtained for this technique compared to LEIS due to several reasons. The detector in this instance is placed a significant distance from the region excited by the two beams. Since the fluorescence is isotropic, this detector will only receive a small fraction of the fluorescence emitted. Using two-wavelength excitation, atoms are excited to levels within several kT of the ionization continuum. Losses of these atoms to the ionization continuum are likely and make the fluorescence from the second excited level to the first excited level less sensitive. Monitoring the fluorescence from the first excited level to the ground state is possible and the change in this fluorescence, when λ_2 is added, is referred to as fluorescence dip spectroscopy.[69] Monitoring fluorescence from the first excited state to the ground state is somewhat complicated by shot noise from analyte emission and noise due to analyte and laser flicker. Fluorescence from the second excited state to the first excited state is limited by shot noise of the scatter of λ_2 and losses to the ionization continuum. For monitoring fluorescence, the best method would primarily depend upon the proximity of the second excited level to the ionization continuum. For these results, the fluorescence from the second level

to the first was found to yield the best results. Omenetto et al.[70] have investigated two-wavelength fluorescence of ions produced in an inductively coupled plasma. The results approach low part-per-trillion levels and benefit from the lower losses to the ionization continuum (the doubly ionized species is especially difficult to form in most instances) compared to the two-wavelength atomic fluorescence case.

A typical result for two-wavelength excitation and fluorescence detection is shown in Figure 4-8 for 10 ppm Na at a height of approximately 4 mm in the same burner used previously. The increased separation of the spatial distribution for each capillary within the burner are evident in this figure. Approximately the same representation was obtained at a height of 7 mm as shown for ionization results in Figure 4-7. These two figures demonstrate that this burner has very good laminarity low in the flame which deteriorates rapidly. The fluorescence was monitored at λ_2. The presence of fluorescence was confirmed (versus scatter) by detuning λ_2. One major advantage of the fluorescence method is that it is not necessary to place an electrode within the flame volume, which makes it possible to detect signals without disturbing the flame. This also makes the fluorescence method more applicable, especially in situations where it is not possible to place an electrode within the cell volume.

As a direct result of these techniques, it was possible to spatially map the entire combustion zone. By translating the burner and obtaining successive profiles across the burner, it was possible

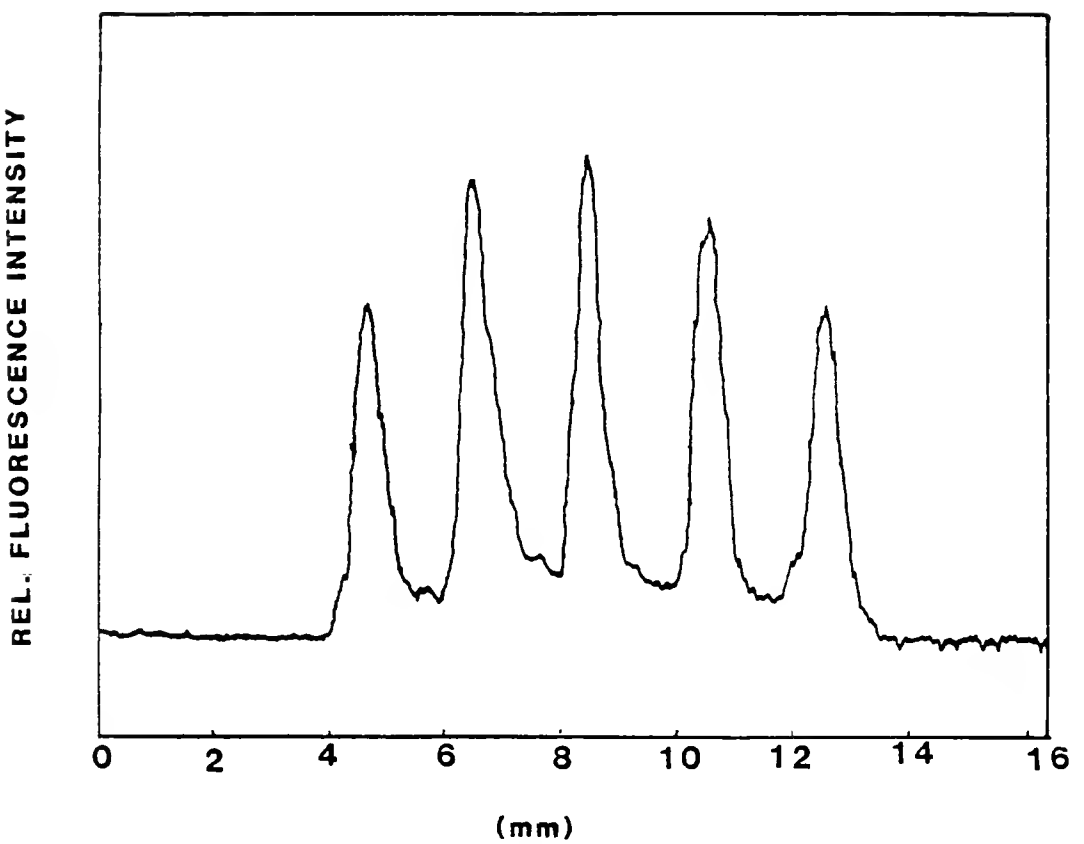

Figure 4-8. Spatial Profile Result for LAFS

to map a horizontal plane within the flame volume. If multiple horizontal planes are obtained a four-dimensional structure may be developed, three spatial dimensions and a concentration dimension. A single horizontal plane located at approximately the top of the flame cones is shown in Figure 4-9 using ionization detection for a 1 ppm solution of Na.

Conclusions

Single-wavelength and two-wavelength methods for obtaining spatial information within inhomogeneous flames have been presented. While the single wavelength concentration-modulated absorption results were not particularly sensitive or useful, the two-wavelength LEIS and LEAFS results demonstrated exceptional spatial resolution and very good sensitivity. The spatial results shown here represent the first application of two-wavelength LEIS and LAFS to this area. The high-repetitive rate laser used and an optical method of scanning the beams through the flame were shown to allow rapid determination of spatial profiles of analyte concentrations. While the applications here are limited in scope, it is felt that these techniques will find many applications.

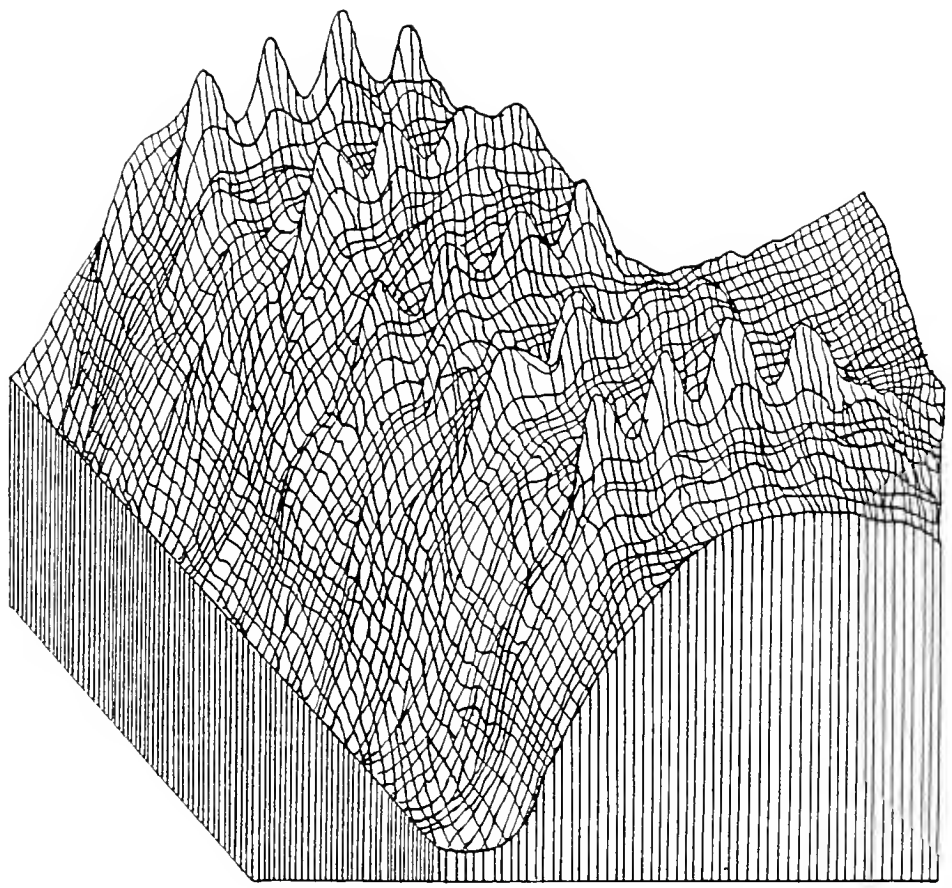

Figure 4-9. Three-Dimensional Spatial Profile for LEIS

CHAPTER 5
FINAL COMMENTS AND FURTHER STUDIES

Several new applications for laser atomic fluorescence and laser enhanced ionization spectroscopies have been presented. Several electrical signal processing methods which were especially applicable to a copper vapor laser system were presented. These results show that it is possible to obtain a significant improvement in detection power by electrical bandwidth limitation and subtraction of slowly varying noises. Further studies which could provide some degree of detection power improvement include more bandwidth limitation to extend the preliminary results obtained here and optimization of the photomultiplier tube voltage to increases with the sensitivity. The noise of the photomultipler also increased voltage but since this noise from the photomultiplier tube was not the limiting noise source, improvement of the detection power should be possible. This work is currently being studied at the National Bureau of Standards by Epstein et al.[33]

A general-purpose computer program was written and evaluated for determination of absolute number densities of atomic species in flames via fluorescence. This method was found to agree well with other previously developed methods within one order of magnitude for both resonance and direct-line fluorescence. Computer-based

investigations were conducted into the effects of collisions with other atoms or molecules and the effect of saturation by a high intensity laser source. Studies into the development of a general purpose program for similar investigations using LEIS should be one of the first methods available for absolute number densities.

Several new and novel methods were developed and evaluated for obtaining spatial information within flames. A recently introduced technique for absolute number density termed concentration modulated absorption spectroscopy, COMAS, was investigated for spatial profiling applications. Absorption measurements obtained with a pulsed fluctuating relatively broadband dye laser were found to be too insensitive for any analytical applicability even at high analyte concentrations (5000 ppm). Other studies involving ionization and fluorescence were shown to be quite sensitive with high resolution spatial profiles being obtained for both methods. Other studies by the J.D. Winefordner research group and others using these spatial profiling results with two-wavelength excitation are varied. Two-wavelength excitation has been applied in many instances to measure ionization processes and wavelength dependencies, but only in a gross spatial manner with no consideration given to inhomogeneous profiles. These two-wavelength spatial results may be used to measure lifetimes of species in very localized regions, to measure concentrations of analyte and flame radicals in small zones, and to determine mixing rates of close lying excited states in small regions by the use of a delayed second laser. Many other results which have only been obtained for an average value within the entire atom cell

can now be determined accurately and rapidly with extremely good sensitivity. Further studies which should be well-suited to these techniques include investigation of different types of flames and burners, especially measuring the laminarity of flow within various flame types.

APPENDIX A
DEFINITION OF TERMS AND SYMBOLS

ABS	Active Baseline Subtraction Method
BLIA	Boxcar Plus Lock-In Amplifier Method
BW or BLSQ	Bandwidth Limited Signal Processing
COMAS	Concentration Modulated Absorption Spectroscopy
FWHM	full width of an analytical signal measured at the half maximum
a	a-parameter for absorption transition, dimensionless
a'	a-parameter for fluorescence transition, dimensionless
BD	beam dump
c	speed of light ms^{-1}
e	charge of an electron, esu
E_λ	source spectral irradiance, $Jm^{-2}s^{-1}Hz^{-1}$
E_λ^s	saturation spectral irradiance, $Jm^{-2}s^{-1}Hz^{-1}$
FPD	fast photodiode
f	oscillator strength of absorption transition, dimensionless
f'	oscillator strength of fluorescence transition, dimensionless
HV	high voltage
Δh	height of volume element detected, cm
k	Boltzmann constant, $J°K^{-1}$

k_o	$\sqrt{4\ln 2}\ e^2\lambda Nf/(mc^2\Delta\lambda_D)$ = peak absorption coefficient, cm^{-1}
$k(\lambda)$	$k_o V(a,v)$
l	fluorescence path length, cm
Δl	width of volume element detected, cm
L	absorption path length, cm
ΔL	depth of volume element detected, cm
lpo	fluorescence postfilter length, cm
Lpr	absorption prefilter length, cm
$\Delta\lambda_C$	collisional halfwidth, cm
$\Delta\lambda_D$	Doppler halfwidth, cm
$\Delta\lambda_S$	source spectral halfwidth, cm
M	mirror
m	mass of an electron, g
m_a	mass of the analyte, g
m_b	mass of the majority quenching species present, g
m_H, m_L	magnification in the height and length dimensions induced by the source collection optics
N_A	Avagadro's number, mol^{-1}
n	analyte number density, $atoms/cm^3$
Φ	fluorescence radiance detected, $Js^{-1}cm^{-2}$
Ω	solid angle of fluorescence collected, sr
PM	photomultiplier tube
PR	partial reflector
R	universal gas constant, $J°K^{-1}mol^{-1}$
REF	reference pulse
T	temperature of flame cell, °K

T_e	transmission of optics used for fluorescence detection, dimensionless
μ	index of refraction of flame, dimensionless
V(a,v)	Voigt profile factor, dimensionless
v	$4\ln 2(\lambda-\lambda_o)/\Delta\lambda_D$, dimensionless
ν	central frequency of absorption transition, s^{-1}
ν'	central frequency of fluorescence transition, s^{-1}
Y_p	spectral luminescence power efficiency, dimensionless

APPENDIX B

COMPUTER PROGRAM LISTING FOR CALCULATION OF FLUORESCENCE CURVES OF GROWTH INCLUDING SATURATION, COLLISIONAL AND PREFILTER AND POSTFILTER EFFECTS

```
$STORAGE:2
$NOFLOATCALLS
C  CALCULATION OF FLUORESCENCE CURVE OF GROWTH
C  USES HUIS APPROXIMATION OF VOIGT FUNCTION
C  IN COMPLEX NUMBER ROUTINE FOR PREFILTER AND POSTFILTER IN
C  DIRECT OR RESONANCE FLUORESCENCE COG
C  PROGRAM WAS ORIGINALLY WRITTEN TO CALCULATE ONLY RESONANCE CASES
C  THEN LATER EXPANDED TO INCLUDE DIRECT-LINE FLUORESCENCE
C
C  FOR DEFINITION OF TERMS AND GEOMETRIES SEE SMITH, B.W., RUTLEDGE, M.J.
C  AND WINEFORDNER, J.D.  APPLIED SPECTROSCOPY 1987
      IMPLICIT REAL*8 (Q-R)
       COMMON /VOIGT/ DOPPLR,APARAM,SOURCE,ABSP,CONC1,FPATH,APATH
       COMMON /DUMMY/ FRAC1,ABS2,FRAC2,APARM2,DOPPL2,APOST,APRE
       COMMON Q(7),R(8)
C  OPEN DATA STORATE ARRAYS
       REAL ALPHA(70), BETA(70), GAMMA(70), NPDEC
       REAL DELTA(70),ZETA(70),THETA(70),LAMBDA(70)
       REAL CONC1,LOW,SIZ,ITMAX,KS1,K1,LIMIT
       REAL KLINE,K02
C  OPEN FILES FOR DATA STORAGE "2" IS FOR ALL DATA, "3" IS FOR ONLY
C  FLUORESCENCE VALUES AND CAN BE USED FOR PLOTTING PURPOSES
       OPEN (2,FILE=' ',STATUS='NEW')
       OPEN (3,FILE=' ',STATUS='NEW')
       DATA LOW,ITMAX/0.0,40.0/
       WRITE(*,3)
 3     FORMAT(' CALC OF COG FOR A SINGLE LINE N PTS/DEC')
       WRITE(*,10)
 10    FORMAT(' INPUT A PARAMETER FOR EXC (REAL)')
       READ(*,150)APARAM
       WRITE(*,20)
 20    FORMAT(' INPUT DOPPLER LINE WIDTH FOR EXC. (A,REAL)')
       READ(*,150)DOPPLR
       WRITE(*,30)
 30    FORMAT(' INPUT SOURCE PROFILE (A,REAL)')
       READ(*,150)SOURCE
```

```
C  SET INTEGRATION LIMIT TO 5 x SOURCE WIDTH
       LIMIT=5.0*SOURCE
       WRITE(*,40)
 40    FORMAT(' INPUT ABS Ko/N FIRST LEVEL (EXPONENTIAL)')
       READ(*,200)KLINE
       WRITE(*,45)
 45    FORMAT(' INPUT ABS PATH LENGTH (CM,REAL)')
       READ(*,150)APATH
       WRITE(*,50)
 50    FORMAT(' INPUT SOURCE IRRADIANCE W/CM/CM/NM/NM/S (EXP)')
       READ(*,200)ESRC
       WRITE(*,55)
 55    FORMAT(' INPUT SATURATION SPECTRAL IRRADIANCE (EXPONENTIAL)')
       READ(*,200)ESAT
       KLINE=KLINE*ESAT/(ESRC+ESAT)
       WRITE(*,58)
 58    FORMAT(' INPUT TEMPERATURE OF ATOM CELL K (REAL)')
       READ(*,150)TEM
       WRITE(*,60)
 60    FORMAT(' INPUT MASS OF ATOM G/MOLE (REAL)')
       READ(*,150)AM
       WRITE(*,62)
 62    FORMAT(' INPUT COLLISIONAL CROSS SECTION ANGSTROMS (REAL)')
       READ(*,150)SIG
       WRITE(*,65)
 65    FORMAT('INPUT ABSORPTION WAVELENGTH ANGSTROMS (REAL)')
       READ(*,150)LO
       WRITE(*,70)
C  INTEGRATION LIMIT IS A CONVERGENCE TOLERANCE LIMIT FOR INTEGRATION
C  10**-6 IS USUALLY A GOOD START.  THIS VALUE IS INCREMENTED LATER TO
C  PRODUCE CONVERGENCE WITHIN 0.1%-0.001%
C
 70    FORMAT(' INPUT TOLERANCE LIMIT (EXPONENTIAL)')
       READ(*,200)TOL1
       WRITE(*,80)
 80    FORMAT(' INPUT NUMBER OF POINTS PER DECADE (REAL)')
       READ(*,150)NPDEC
 150   FORMAT(F10.4)
 200   FORMAT(E12.4)
       WRITE(*,210)
 210   FORMAT(' INPUT Ko/N SECOND LEVEL (REAL)')
       READ(*,900)K02
       WRITE(*,220)
 220   FORMAT(' INPUT FRACTIONAL POP.OF FIRST LEVEL (REAL)')
       READ(*,900)FRAC1
       WRITE(*,230)
 230   FORMAT(' INPUT FRACTIONAL POP OF LAST LEVEL (REAL)')
       READ(*,900)FRAC2
       WRITE(*,240)
 240   FORMAT(' INPUT a-PARAMETER OF SECOND TRANSITION (REAL)')
       READ(*,900)APARM2
```

```
      WRITE(*,250)
 250  FORMAT(' INPUT ABS. PREFILTER LENGTH (CM,REAL)')
      READ(*,900)APRE
      WRITE(*,260)
 260  FORMAT(' INPUT POST FILTER LENGTH (CM,REAL)')
      READ(*,900)APOST
      WRITE(*,350)
 350  FORMAT(' INPUT DOPPLER LINE WIDTH OF SECOND TRANSITION (A,REAL)')
      READ(*,900)DOPPL2
      DLC=APARM2*DOPPL2*1.20112
 900  FORMAT(F10.4)
      ABSP=KLINE*APATH
      ABS2=K02*APATH
      WRITE(*,1902)
C  CALCULATION IS DONE OVER THE RANGE FROM LOWER TO HIGHER ABSOLUTE NUMBER
C  DENSITY WITH N POINTS SPACED EVENTLY ON A LOGARITHMIC SCALE
C
 1902 FORMAT(' INPUT UPPER NUMBER DENSITY (EXPONENTIAL)')
      READ(*,1906)CHIGH
      WRITE(*,1905)
 1905 FORMAT(' INPUT LOWER NUMBER DENSITY (EXPONENTIAL)')
      READ(*,1906)CONC1
 1906 FORMAT(E12.4)
      V=LOG10(CONC1)
C  WRITE PARAMETERS TO FILE
      WRITE(2,1910)APARAM,APARM2
      WRITE(2,1920)DOPPLR,DOPPL2
      WRITE(2,1925)APATH,FPATH
      WRITE(2,1930)SOURCE
      WRITE(2,1940)ABSP,ABS2
      WRITE(2,1950)LIMIT,TOL1
      WRITE(2,1960)FRAC1,FRAC2
      WRITE(2,1970)APRE,APOST
 1910 FORMAT(' APARAMETER FOR EXC AND FLUOR =',F10.4,F10.4)
 1920 FORMAT('DOPPLER LINEWIDTH FOR EXC AND FLUOR=',F12.6,F12.6)
 1925 FORMAT(' ABS AND FLUOR PATH LENGTH=',F10.4,F10.4)
 1930 FORMAT(' SOURCE HALFWIDTH=',F10.4)
 1940 FORMAT(' ABS FACTOR KoL/N FOR EXC AND FLUOR',E12.4,E12.4)
 1950 FORMAT(' INTEGR LIMIT',F12.4, 'INTEGRATION TOLERANCE',E12.4)
 1960 FORMAT(' FRAC. POP OF LEVELS 1 AND 2 ',F12.6,F12.6)
 1970 FORMAT(' PRE AND POSTFILTER LENGTHS',F12.6,F12.6)
      WRITE(2,2000)
 2000 FORMAT(5X,'ALPHA',5X,'SLF ABS',2X,'PRFLTR',4X,'PSTFLTR',5X,
     'LOG 1PHI',5X,'NUM DENS')
C  CALCULATION OF FRACTION ABSORBED USING REAL FUNCTION FAB AND
C  HUI'S APPROXIMATION FOR VOIGT PROFILE
      UP=LIMIT
      DLUP=50.0*DOPPLR
C  DIRECT LINE INTEGRATION OCCURS OVER 50 TIMES THE DOPPLER WIDTH NOT
C  ASSOCIATED WITH RESONANCE INTEGRATION LIMITS.  THIS WORKS WELL IF
C  APARAMETER DOES NOT GET TOO LARGE OTHERWISE THE INTEGRATION LIMIT
```

```
C  MUST BE INCREASED.
       K1=0.797884561
       N=1
       PI=3.1415926
       C=2.997E10
 2060  DNT=0.0
       ALPHA(0)=0.0
       VAR1=(1.0449E9*TEM/AM)**0.5
       VAR2=L0*L0*SIG/PI/C*VAR1*2*1.0E-16
       DLCP=DLC+CONC1*VAR2*1.0E-8
       APARAM=0.83255*DLCP/DOPPLR
       APARM2=(DLC2+CONC1*VAR2*1.0E-8)*0.83255/DOPPL2
       WRITE(*,2065)APHARM,APARM2
 2065  FORMAT(' '),f10.4)
       I=0
C  NORMALIZE FOR GAUSSIAN SOURCE
       KS1=2.35482/SOURCE
C  IF PREVIOUS RESULT CA.  1.0 SKIP CALCULATION:CHECK FOR OPTICAL
C  SATURATION
       IF (ALPHA(N-1).GT.0.9995) THEN
       ALPHA(N)=1.0
       GOTO 2510
       ENDIF
       I=0
       FRST=1
       X=LOW
       Y=FAB(X)
       DNT=DNT+Y
       X=UP
       Y=FAB(X)
       TEMP=DNT+Y
C  SIMPSONS RULE INTEGRATION
 2080  I=I+1
 2160  Z=2**(real(i))
       SIZ=(UP-LOW)/Z
       X=SIZ+LOW
       Y=FAB(X)
       DNT=DNT+4*Y
       DARG=LOW
 2190  DARG=DARG+2*SIZ
       IF (DARG.LT.UP) GOTO 2340
       DNT=SIZ*DNT/3
       IF (FRST.EQ.0) GOTO 2290
       FRST=0
       GOTO 2310
 2290  IF (I.LE.3) GOTO 2310
       IF (ABS(DNTOLD-DNT).GE.TOL1) GOTO 2310
       GOTO 2500
 2310  DNTOLD=DNT
       DNT=TEMP
       GOTO 2080
```

```
 2340  X=DARG
       Y=FAB(X)
       DNT=DNT+2*Y
       X=DARG+SIZ
       Y=FAB(X)
       DNT=DNT+4*Y
       GOTO 2190
 2500  ALPHA(N)=1-DNT*K1*KS1
C  CALCULATION OF SELF ABSORPTION FACTOR IN THIS AND NEXT PART
C  FACTOR = BETA/GAMMA
 2510  DNT=0.0
       I=0
       FRST=1.0
       X=LOW
       Y=BPART(X)
       DNT=DNT+Y
       X=DLUP
       Y=BPART(X)
       TEMP=DNT+Y
       DNT=DNT+Y
 2580  I=I+1
 2660  Z=2**(REAL(I))
       SIZ=(DLUP-LOW)/Z
       X=SIZ+LOW
       Y=BPART(X)
       DNT=DNT+4*Y
       DARG=LOW
 2690  DARG=DARG+2*SIZ
       IF (DARG.LT.DLUP) GOTO 2840
       DNT=SIZ*DNT/3
       IF (FRST.EQ.0) GOTO 2790
       FRST=0
       GOTO 2810
 2790  IF (I.LE.3) GOTO 2810
       T=DNTOLD-DNT
       IF (ABS(T).GE.TOL1) GOTO 2810
       GOTO 3000
 2810  DNTOLD=DNT
       DNT=TEMP
       GOTO 2580
 2840  X=DARG
       Y=BPART(X)
       DNT=DNT+2*Y
       X=DARG+SIZ
       Y=BPART(X)
       DNT=DNT+4*Y
       GOTO 2690
 3000  BETA(N)=DNT
 3510  DNT=0.0
       I=0
       FRST=1.0
```

```
      X=LOW
      Y=CPART(X)
      DNT=DNT+Y
      X=DLUP
      Y=CPART(X)
      TEMP=DNT+Y
      DNT=DNT+Y
 3580 I=I+1
 3660 Z=2**(REAL(I))
      SIZ=(DLUP-LOW)/Z
      X=SIZ+LOW
      Y=CPART(X)
      DNT=DNT+4*Y
      DARG=LOW
 3690 DARG=DARG+2*SIZ
      IF (DARG.LT.DLUP) GOTO 3840
      DNT=SIZ*DNT/3
      IF (FRST.EQ.0) GOTO 3790
      FRST=0
      GOTO 2810
 3790 IF (I.LE.3) GOTO 3810
      T=DNTOLD-DNT
      IF (ABS(T).GE.TOL1) GOTO 3810
      GOTO 3990
 3810 DNTOLD=DNT
      DNT=TEMP
      GOTO 3580
 3840 X=DARG
      Y=CPART(X)
      DNT=DNT+2*Y
      X=DARG+SIZ
      Y=CPART(X)
      DNT=DNT+4*Y
      GOTO 3690
 3990 GREEK=DNT
 4000 GAMMA(N)=1.7527576*1.064467*DOPPL2*K02*CONC1*FRAC2*FPATH
 4060 DNT=0.0
C  PREFILTER TERM CALCULATION
      I=0
      FRST=1
      X=LOW
      Y=FPART(X)
      DNT=DNT+Y
      X=UP
      Y=FPART(X)
      TEMP=DNT+Y
      DNT=DNT+Y
 4080 I=I+1
 4160 Z=2**(REAL(I))
      SIZ=(UP-LOW)/Z
      X=SIZ+LOW
```

```
      Y=FPART(X)
      DNT=DNT+4*Y
      DARG=LOW
 4190 DARG=DARG+2*SIZ
      IF (DARG.LT.UP) GOTO 4340
      DNT=SIZ*DNT/3
      IF (FRST.EQ.0) GOTO 4290
      FRST=0
      GOTO 4310
 4290 IF (I.LE.3) GOTO 4310
      IF (ABS(DNTOLD-DNT).GE.TOL1) GOTO 4310
      GOTO 4500
 4310 DNTOLD=DNT
      DNT=TEMP
      GOTO 4080
 4340 X=DARG
      Y=FPART(X)
      DNT=DNT+2*Y
      X=DARG+SIZ
      Y=FPART(X)
      DNT=DNT+4*Y
      GOTO 4190
 4500 LAMBDA(N)=1-DNT*K1*KS1
 4510 DNT=0.0
C  POSTFILTER TERM CALCULATION
      I=0
      FRST=1
      X=LOW
      Y=DPART(X)
      DNT=DNT+Y
      X=DLUP
      Y=DPART(X)
      TEMP=DNT+Y
      DNT=DNT+Y
 4580 I=I+1
 4660 Z=2**(real(i))
      SIZ=(DLUP-LOW)/Z
      X=SIZ+LOW
      Y=DPART(X)
      DNT=DNT+4*Y
      DARG=LOW
 4690 DARG=DARG+2*SIZ
      IF (DARG.LT.DLUP) GOTO 4840
      DNT=SIZ*DNT/3
      IF (FRST.EQ.0) GOTO 4790
      FRST=0
      GOTO 4810
 4790 IF (I.LE.3) GOTO 4810
      IF (ABS(DNTOLD-DNT).GE.TOL1) GOTO 4810
      GOTO 5000
 4810 DNTOLD=DNT
```

```
      DNT=TEMP
      GOTO 4580
 4840 X=DARG
      Y=DPART(X)
      DNT=DNT+2*Y
      X=DARG+SIZ
      Y=DPART(X)
      DNT=DNT+4*Y
      GOTO 4690
 5000 DELTA(N)=DNT
 5060 DNT=0.0
      FRST=1
C  PREFILTER TERM CALCULATION
      X=LOW
      Y=GPART(X)
      DNT=DNT+Y
      X=UP
      Y=GPART(X)
      TEMP=DNT+Y
      DNT=DNT+Y
 5080 I=I+1
 5160 Z=2**(REAL(I))
      SIZ=(UP-LOW)/Z
      X=SIZ+LOW
      Y=GPART(X)
      DNT=DNT+4*Y
      DARG=LOW
 5190 DARG=DARG+2*SIZ
      IF (DARG.LT.UP) GOTO 5340
      DNT=SIZ*DNT/3
      IF (FRST.EQ.0) GOTO 5290
      FRST=0
      GOTO 5310
 5290 IF (I.LE.3) GOTO 5310
      IF (ABS(DNTOLD-DNT).GE.TOL1) GOTO 5310
      GOTO 5500
 5310 DNTOLD=DNT
      DNT=TEMP
      GOTO 5080
 5340 X=DARG
      Y=GPART(X)
      DNT=DNT+2*Y
      X=DARG+SIZ
      Y=GPART(X)
      DNT=DNT+4*Y
      GOTO 5190
 5500 THETA(N)=1-DNT*K1*KS1
 5510 DNT=0.0
C  POSTFILTER TERM CALCULATION
      I=0
      FRST=1
```

```
      X=LOW
      Y=EPART(X)
      DNT=DNT+Y
      X=DLUP
      Y=EPART(X)
      TEMP=DNT+Y
      DNT=DNT+Y
 5580 I=I+1
 5660 Z=2**(REAL(I))
      SIZ=(DLUP-LOW)/Z
      X=SIZ+LOW
      Y=EPART(X)
      DNT=DNT+4*Y
      DARG=LOW
 5690 DARG=DARG+2*SIZ
      IF (DARG.LT.DLUP) GOTO 5840
      DNT=SIZ*DNT/3
      IF (FRST.EQ.0) GOTO 5790
      FRST=0
      GOTO 5810
 5790 IF (I.LE.3) GOTO 5810
      IF (ABS(DNTOLD-DNT).GE.TOL1) GOTO 5810
      GOTO 6000
 5810 DNTOLD=DNT
      DNT=TEMP
      GOTO 5580
 5840 X=DARG
      Y=EPART(X)
      DNT=DNT+2*Y
      X=DARG+SIZ
      Y=EPART(X)
      DNT=DNT+4*Y
      GOTO 5690
 6000 ZETA(N)=DNT
      FPO=2.0*(DELTA(N)-ZETA(N))/GREEK
      FPRE=(LAMBDA(N)-THETA(N))/ALPHA(N)
      SLFABS=BETA(N)/GAMMA(N)
 6010 PHI=LOG10(ALPHA(N)*SLFABS*FPATH*APATH*FPRE*FPO)
C  ALPHA=FRACTION ABSORBED, SLFABS=SELF ABSORPTION TERM, FPRE=PREFILTER
C  TERM, FPOST=POSTFILTER TERM
      WRITE(2,6100),ALPHA(N),SLFABS,FPRE,FPO,PHI,CONC1
      WRITE(3,6101)PHI
      WRITE(*,6100)ALPHA(N),SLFABS,FPRE,FPO,PHI,CONC1
 6100 FORMAT(' ',F10.6,F10.6,F10.6,F10.6,E12.4,E12.4)
 6101 FORMAT(F12.4)
      V=V+1.0/NPDEC
      TOL=10.0**ANINT(LOG10(ALPHA(N))=3.0)
C  TEST FOR INCREMENTATION OF TOLERANCE
      IF (TOL.GT.TOL1) THEN
      TOL1=TOL
      ENDIF
```

```
      N=N+1
      CONC1=10**(V)
C  INCREMENT CONCENTRATION TO BE CALCULATED ON NEXT DATA PT.
      IF (CONC1,GT.CHIGH) GOTO 6110
      GOTO 2060
 6110 STOP
      END
C
C  BLOCK DATA FOR HUI'S APPROXIMATION
      BLOCK DATA
C  COEFFICIENTS FOR EVALUATION OF VOIGT FUNCTION USING HUI'S APPROX.
      IMPLICIT REAL*8 (Q-R)
      COMMON Q(7),R(8)
      DATA Q(1),R(1)/122.607931777104326, 122.60793177387535/
      DATA Q(2),R(2)/214.382388694706425, 352.730625110963558/
      DATA Q(3),R(3)/181.928533092181549, 457.334478783897737/
      DATA Q(4),R(4)/93.155580458138441, 348.703917719495792/
      DATA Q(5),R(5)/30.180142196210589, 170.354001821091472/
      DATA Q(6),R(6)/5.912626209773153, 53.992906912940207/
      DATA Q(7),R(7)/0.564189583562615, 10.479857114260399/
      DATA R(8)/1.0/
      END
      REAL FUNCTION FAB(X)
      IMPLICIT REAL*8 (Q-R)
C  EVALUATION OF VOIGT FUNCTION FOR PRIMARY ABSORPTION
      REAL*8 C,D
      REAL KS2,KK,RESR
      COMMON /VOIGT/DOPPLR,APARAM,SOURCE,ABSP,CONC1,FPATH,APATH
      COMMON /DUMMY/ FRAC1,ABS2,FRAC2,APARM2,DOPPL2,APOST,APRE
      COMMON Q(7),R(8)
      COMPLEX*16 F,BTM,TOP,RATIO
      D=1.66511/DOPPLR*X
      C=APARAM
      F=DCMPLX(C,D)
      TOP=(((((Q(7)*F+Q(6))*F+Q(5))*F+Q(4))*F+Q(3))*F+Q(2))*F+Q(1)
      BTM=((((((F+R(7))*F+R(6))*F+R(5))*F+R(4))*F+R(3))*F+R(2))*F+R(1)
      RATIO=TOM/BTM
      RESR=REAL(RATIO)
      KK=ABSP*CONC1*FRAC1
      KS2=5.54518/SOURCE/SOURCE
      FACTOR=REAL(-1.0*(X*X*KS2/2)-KK*RESR)
      IF (FACTOR.LT.-50.) THEN
      FAB=0
      ELSE
      FAB=EXP(FACTOR)
      ENDIF
      RETURN
      END
C
      REAL FUNCTION BPART(X)
      IMPLICIT REAL*8 (Q-R)
```

```
      REAL*8 C,D
C  EVALUATION OF VOIGT FUNCTION FOR SELF ABSORPTION TERM
      REAL RESR
      COMMON /VOIGT/DOPPLR, APARAM, SOURCE, ABSP,CONC1,FPATH,APATH
      COMMON /DUMMY/ FRAC1,ABS2,FRAC2,APARM2,DOPPL2,APOST,APRE
      COMMON Q(7),R(8)
      COMPLEX*16 F,BTM,TOP,RATIO
      D=1.66511/DOPPL2*X
      C=APARM2
      F=DCMPLX(C,D)
      TOP=(((((Q(7)*F+Q(6))*F+Q(5))*F+Q(4))*F+Q(3))*F+Q(2))*F+Q(1)
      BTM=((((((F+R(7))*F+R(6))*F+R(5))*F+R(4))*F+R(3))*F+R(2))*F+R(1)
      RATIO=TOP/BTM
      RESR=REAL(RATIO)
      TEMP1=(CONC1*ABS2*(-1.772454)*RESR*FPATH/APATH*FRAC2)
      IF (TEMP1.LT.-50.) THEN
      BPART=2.0
      ELSE
      BPART=2*(1-EXP(TEMP1))
      ENDIF
      RETURN
      END
C
      REAL FUNCTION CPART(X)
      IMPLICIT REAL*8 (Q-R)
      REAL*8 C,D
      REAL RESR
      COMMON /VOIGT/DOPPLR,APARAM,SOURCE,ABSP,CONC1,FPATH,APATH
      COMMON Q(7),R(8)
      COMPLEX*16 F,8TM,TOP,RATIO
      D=2.0*SQRT(LOG(2.0))/DOPPLR*X
      C=APARAM
      F=DCMPLX(C,D)
      TOP=(((((Q(7)*F+Q(6))*F+Q(5))*F+Q(4))*F+Q(3))*F+Q(2))*F+Q(1)
      BTM=((((((F+R(7))*F+R(6))*F+R(5))*F+R(4))*F+R(3))*F+R(2))*F+R(1)
      RATIO=TOP/BTM
      RESR=REAL(RATIO)
      IF (RESR.LT.1.0E-12) THEN
      CPART=2.0
      ELSE
      CPART=2.0*(1.0-EXP(1.7724*CONC1*ABSP*RESR*FPATH/APATH*FRAC2))
      ENDIF
      RETURN
      END
C
      REAL FUNCTION DPART(X)
      IMPLICIT REAL*8 (Q-R)
      REAL*8 C,D
      REAL KS2,KK,RESR
      COMMON /VOIGT/DOPPLR,APARAM,SOURCE,ABSP,CONC1,FPATH,APATH
      COMMON /DUMMY/ FRAC1,ABS2,FRAC2,APARM2,DOPPL2,APOST,APRE
```

```
      COMMON Q(7),R(8)
      COMPLEX*18 F,BTM,TOP,RATIO
      D=1.66511/DOPPL2*X
      C=APARM2
      F=DCMPLX(C,D)
      TOP=(((((Q(7)*F+Q(6))*F+Q(5))*F+Q(4))*F+Q(3))*F+Q(2))*F+Q(1)
      BTM=((((((F+R(7))*F+R(6))*F+R(5))*F+R(4))*F+R(3))*F+R(2))*F+R(1)
      RATIO=TOP/BTM
      RESR=REAL(RATIO)
      TEMP1=(CONC1*ABS2*(-1.772454)*RESR*FPATH/APATH)
      TEMP1=TEMP1*FRAC2*(1+APOST/FPATH)
      IF (TEMP1.LT.-50.) THEN
      DPART=1.0
      ELSE
      DPART=(1-EXP(TEMP1))
      ENDIF
      RETURN
      END
C
      REAL FUNCTION EPART(X)
      IMPLICIT REAL*8 (Q-R)
      REAL*8 C,D
      REAL KS2,KK,RESR
      COMMON /VOIGT/DOPPLR,APARAM,SOURCE,ABSP,CONC1,FPATH,APATH
      COMMON /DUMMY/ FRAC1,ABS2,FRAC2,APARM2,DOPPL2,APOST,APRE
      COMMON Q(7),R(8)
      COMPLEX*16 F,BTM,TOP,RATIO
      D=1.66511/DOPPL2*X
      C=APARM2
      F=DCMPLX(C,D)
      TOP=(((((Q(7)*F+Q(6))*F+Q(5))*F+Q(4))*F+Q(3))*F+Q(2))*F+Q(1)
      BTM=((((((F+R(7))*F+R(6))*F+R(5))*F+R(4))*F+R(3))*F+R(2))*F+R(1)
      RATIO=TOP/BTM
      RESR=REAL(RATIO)
      TEMP1=(-1.77245*CONC1*ABS2*RESR*FPATH/APATH*FRAC2*APOST/FPATH)
      IF (TEMP1.LT.-50.) THEN
      EPART=1.0
      ELSE
      EPART=(1-EXP(TEMP1))
      ENDIF
      RETURN
      END
C
      REAL FUNCTION FPART(X)
      IMPLICIT REAL*8 (Q-R)
      REAL*8 C,D
      REAL KS2,KK,RESR
      COMMON /VOIGT/DOPPLR,APARAM,SOURCE,ABSP,CONC1,FPATH,APATH
      COMMON /DUMMY/ FRAC2,ABS2,FRAC2,APARM2,DOPPL2,APOST,APRE
      COMMON Q(7),R(8)
      COMPLEX*16 F,BTM,TOP,RATIO
```

```
      D=1.66511/DOPPLR*X
      C=APARAM
      F=DCMPLX(C,D)
      TOP=(((((Q(7)*F+Q(6))*F+Q(5))*F+Q(4))*F+Q(3))*F+Q(2))*F+Q(1)
      BTM=((((((F+R(7))*F+R(6))*F+R(5))*F+R(4))*F+R(3))*F+R(2))*F+R(1)
      RATIO=TOP/BTM
      RESR=REAL(RATIO)
      KK=ABSP*CONC1*FRAC1*(1+APRE/APATH)
      KS2=5.54518/SOURCE/SOURCE
      FACTOR=REAL(-1.0*(X*X*KS2/2)-KK*RESR)
      IF (FATOR.LT.-50.) THEN
      FPART=0.0
      ELSE
      FPART=EXP(FACTOR)
      ENDIF
      RETURN
      END
C
      REAL FUNCTION GPART(X)
      IMPLICIT REAL*8 (Q-R)
      REAL*8 C,D
      REAL KS2,KK,RESR
      COMMON /VOIGT/COPPLR,APARAM,SOURCE,ABSP,CONC1,FPATH,APATH
      COMMON /DUMMY/ FRAC1,ABS2,FRAC2,APARM2,DOPPL2,APOST,APRE
      COMMON Q(7),R(8)
      COMPLEX*16 F,BTM,TOP,RATIO
      D=1.66511/DOPPLR*X
      C=APARAM
      F=DCMPLX(C,D)
      TOP=(((((Q(7)*F+Q(6))*F+Q(5))*F+Q(4))*F+Q(3))*F+Q(2))*F+Q(1)
      BTM=((((((F+R(7))*F+R(6))*F+R(5))*F+R(4))*F+R(3))*F+R(2))*F+R(1)
      RATIO=TOP/BTM
      RESR=REAL(RATIO)
      KK=ABSP*CONC1*FRAC2*APRE/APATH
      KS2=5.54518/SOURCE/SOURCE
      FACTOR=REAL(-1.0*(X*X*KS2/2)-KK*RESR)
      IF (FACTOR.LT.-50.) THEN
      GPART=0.0
      ELSE
      GPART=EXP(FACTOR)
      ENDIF
      RETURN
      END
```

REFERENCES

1. J.C. Travis, J. Chem. Ed. 59, 909 (1982).

2. G.S. Hurst, M.G. Payne, S.D. Kramer, and J.P. Young, Rev. Mod. Phys. 51, 767 (1979).

3. J.D. Winefordner and N. Omenetto in "Analytical Applications of Lasers," E.H. Piepmeier, Ed., Wiley Interscience, New York (1986), Chapter 2.

4. M. Broyer, J. Chevalyre, G. Delacretaz, and L. Woste, Appl. Phys. B35, 31 (1984).

5. D.B. McDonald and C.D. Jonah, Rev. Sci. Instrum. 55, 1166 (1984).

6. R.E. Grove, Laser Focus Magazine, July (1982).

7. K. Doerffel, A. Wundrack, and S. Tarigopula, Fresenius Z. Anal. Chem. 324, 507 (1986).

8. C.Th.J. Alkemade, Ph.D. Thesis, Utrecht, Netherlands (1954).

9. H.C. Meng, and H.J. Kunze, Phys. Fluids 22, 1082 (1979).

10. A.C.G. Mitchell and M.W. Zemansky, "Resonance Radiation and Excited Atoms," Cambridge University Press, New York (1971).

11. L. Pasternack, A.P. Baronavski, and J.R. McDonald, J. Chem. Phys. 69, 4830 (1979).

12. P.W.J.M. Boumans, "Theory of Spectrochemical Excitation," Plenum Press, New York (1966).

13. C.Th.J. Alkemade, T. Hollander, W. Snelleman, and P.J.Th. Zeegers, "Metal Vapors in Flames," Pergamon Press, New York (1982), Chapter 5.

14. W.W. McGee and J.D. Winefordner, J. Quant. Spectrosc. Radiat. Transfer. 7, 261 (1967).

15. C.L. Pan, J.V. Prodan, W.M. Fairbank, Jr., and C.Y. She, Opt. Lett. 5, 459 (1980).

16. M.A. Bolshov, A.V. Zybin, V.G. Koloshnikov, and M.V. Vasnetsov, Spectrochim. Acta 36B, 345 (1981).

17. C.Th.J. Alkemade in "Analytical Applications of Lasers," E.H. Piepmeier, Ed., Wiley-Interscience, New York (1986), Chapter 4.

18. J.E.M. Goldsmith and R.J.M. Anderson, Appl. Opt. 24, 607 (1985).

19. M.J. Dyer and D.R. Crosley, Optics Lett. 7, 381 (1982).

20. G. Kychakoff, R.D. Howe, and R.K. Hanson, Appl. Opt. 23, 704 (1984).

21. G.C. Turk, F.C. Ruegg, J.C. Travis, and J.R. Devoe, Appl. Spectrosc. 40, 1146 (1986).

22. W.T. Walter, M. Piltch, N. Solimene, and G. Gould, Bull. Am. Phys. Soc. 11, 113 (1966).

23. R.J. Krupa, T.F. Culbreth, B.W. Smith, and J.D. Winefordner, Appl. Spectrosc. 40, 729 (1986).

24. J.C. Travis, G.C. Turk, and R.B. Green, Anal. Chem. 54, 1007A (1982).

25. C.Th.J. Alkemade, W. Snelleman, G.D. Boutilier, B.D. Pollard, J.D. Winefordner, T.L. Chester, and N. Omenetto, Spectrochim. Acta 33B, 383 (1978).

26. "IUPAC, Nomenclature, Symbols, Units and Their Usage in Spectrochemical Analysis," Revision 1975 Part II Spectrochim. Acta 33B, 248 (1978).

27. G.L. Long and J.D. Winefordner, Anal. Chem. 55, 712A (1983).

28. C.Th.J. Alkemade, Tj. Hollander, W. Snelleman, and P.J.Th. Zeegers, "Metal Vapors in Flames," Pergamon Press, Elmsford, New York (1982), Chapter 3.

29. G.F. Kirkbright and M. Sargent, "Atomic Absorption and Fluorescence Spectrometry," Academic Press, New York (1974), Chapter 10.

30. E. Voigtman and J.D. Winefordner, Prog. Analyt. Atom. Spectrosc. 9, 7 (1986).

31. S. Cova and A. Longini in "Analytical Laser Spectroscopy," N. Omenetto, Ed., J. Wiley and Sons, New York (1979), Chapter 7.

32. A. Yariv, "Quantum Electronics," John Wiley and Sons, New York (1975), Chapter 16.

33. M.S. Epstein and J.C. Travis, Appl. Spectrosc. (in press).

34. P.J.Th. Zeegers, R. Smith, and J.D. Winefordner, Anal. Chem. 40, 26A (1968).

35. H.P. Hoomayers, Spectrochim. Acta 23B, 567 (1968).

36. P.J.Th. Zeegers and J.D. Winefordner, Spectrochim. Acta 26B, 161 (1971).

37. V. Svoboda, R.F. Browner, and J.D. Winefordner, Appl. Spectrosc. 26, 505 (1972).

38. A.K. Hui, B.H. Armstrong, and A.A. Wray, J. Quant. Spectrosc. Radiat. Transfer 19, 509 (1978).

39. M.L. Parsons, W.J. McCarthy, and J.D. Winefordner, Appl. Spectrosc. 20, 223 (1966).

40. M.L. Parsons, B.W. Smith, and G.W. Bentley, "Handbook of Flame Spectroscopy," Plenum Press, New York (1975).

41. H.C. Wagenaar and L. DeGalen, Spectrochim. Acta 28B, 157 (1973).

42. R.G. Breene, Jr., "The Shift and Shape of Spectral Lines," Pergamon Press, New York (1961).

43. B.V. L'vov, V.G. Nikolaev, E.A. Norman, L.K. Polzik and M. Mojica, Spectrochim. Acta 41B, 1043 (1986).

44. G. Schlemmer and B. Welz, Spectrochim. Acta 41B, 1157 (1986).

45. C.Th.J. Alkemade, Spectrochim. Acta 40B, 1331 (1985).

46. A.J. Langley, R.A. Beamon, A.N. Davies, W.J. Jones, and J. Baran, Chemical Physics 101, 117 (1986).

47. C.Th.J. Alkemade and R. Hermann, "Fundamentals of Analytical Flame Spectroscopy," Adam Hilger Ltd., Bristol, England (1979), Chapter 2.

48. J.D. Messman, M.S. Epstein, T.C. Rains, and T.C. O'Haver, Anal. Chem. 55, 1055 (1983).

49. W. Demtroder, "Laser Spectroscopy," Springer Verlag, New York (1982), Chapter 5.

50. W.B. Jackson, N.M. Amer, A.C. Boccarra, and D. Fournier, Appl. Opt. 20, 1333 (1981).

51. A. Rose, Y.X. Nie, and R. Gupta, Appl. Opt. 25, 1738 (1986).

52. T.W. Hansch, Appl. Opt. 11, 895 (1972).

53. A.G. Gaydon and H.G. Wolfhard, "Flames: Their Structure, Radiation, and Temperature," John Wiley and Sons, New York (1960), Chapter 2.

54. L. deGalan and J.D. Winefordner, Spectrochim. Acta 25B, 245 (1970).

55. M.S. Epstein and J.D. Winefordner, Prog. Analyt. Atom Spectrosc. 7, 67 (1984).

56. T.C. O'Haver in "Trace Analysis: Spectroscopic Methods for Elements," J.D. Winefordner, Ed., Wiley-Interscience, New York (1976), Chapter 2.

57. E.H. Piepmeier in "Analytical Laser Spectroscopy," E.H. Piepmeier, Ed., Wiley Interscience, New York (1986), Chapter 1.

58. F.P. Schafer in "Dye Lasers," F.P. Schafer, Ed., Springer Verlag, New York (1973), Chapter 1.

59. G. Gilson and G. Horlick, Spectrochim. Acta 41B, 1299 (1986).

60. N. Omenetto and H. Human, Spectrochim. Acta 39B, 1333 (1984).

61. M. Alden, H. Edner, G. Holmstedt, S.S. Vanberg, and T. Hogberg, Appl. Opt. 21, 1236 (1982).

62. O. Axner and T. Berglind, Appl. Spectrosc. 40, 1224 (1986).

63. I. Magnusson, O. Axner, I. Lindgren, and H. Rubinsztein-Dunlop, Appl. Spectrosc. 40, 968 (1986).

64. I. Magnusson, S. Sjostrom, M. Lejon, and H. Rubinsztein-Dunlop, Spectrochim. Acta B (in press).

65. O. Axner, I. Magnusson, J. Petersson, and S. Sjostrom, Appl. Spectrosc. 41, 19 (1987).

66. G.C. Turk, O. Axner, and N. Omenetto, Spectrochim. Acta B (in press).

67. G.C. Turk and N. Omenetto, Appl. Spectrosc. 40, 1085 (1986).

68. G.J. Havrilla and R.B. Green, Anal. Chem. 52, 2376 (1980).

69. N. Omenetto, G.C. Turk, M.J. Rutledge, and J.D. Winefordner, Spectrochim. Acta B (in press).

70. N. Omenetto, B.W. Smith, L.P. Hart, P. Cavelli, and G. Rossi, Spectrochim. Acta 40B, 1411 (1985).

BIOGRAPHICAL SKETCH

Michael James Rutledge was born in Auburn, Alabama, on June 27, 1960. He attended Woodham High School in Pensacola, Florida, where he learned the value of a good tan and the beach scenery. He graduated with a B.S. in chemistry from Auburn University in 1983. Since that time he has attended the University of Florida where he received his Ph.D. in chemistry in 1987 under the direction of Dr. James D. Winefordner.

I certify that I have read this study and that in my opinion it conforms to acceptable standards of scholarly presentation and is fully adequate, in scope and quality, as a dissertation for the degree of Doctor of Philosophy.

James D. Winefordner, Chairman
Graduate Research Professor of
Chemistry

I certify that I have read this study and that in my opinion it conforms to acceptable standards of scholarly presentation and is fully adequate, in scope and quality, as a dissertation for the degree of Doctor of Philosophy.

John G. Dorsey
Associate Professor of Chemistry

I certify that I have read this study and that in my opinion it conforms to acceptable standards of scholarly presentation and is fully adequate, in scope and quality, as a dissertation for the degree of Doctor of Philosophy.

Robert Gould
Professor of Materials Science

This dissertation was submitted to the Graduate Faculty of the Department of Chemistry in the College of Liberal Arts and Sciences and to the Graduate School and was accepted as partial fulfillment of the requirements for the degree of Doctor of Philosophy.

May, 1987

Dean, Graduate School